CALIFORNIA INSTITUTE OF TECHNOLOGY

ELECTRON TUBE AND MICROWAVE LABORATORY

SURFACE IMPEDANCE OF THIN SUPERCONDUCTING FILMS

by

Peter V. Mason

Technical Report No. 17

October 1961

A REPORT ON RESEARCH CONDUCTED UNDER

CONTRACT WITH THE OFFICE OF NAVAL RESEARCH

SURFACE IMPEDANCE
OF
THIN SUPERCONDUCTING FILMS

by

Peter V. Mason

Technical Report No. 17
CALIFORNIA INSTITUTE OF TECHNOLOGY
Pasadena, California

A Technical Report to the Office of Naval Research

Contract Nonr 220(13)

October 1961

TABLE OF CONTENTS

ABSTRACT

Theoretical analysis and experimental measurements have been made of the propagation of electromagnetic waves in a structure consisting of two planar superconductors which are of the order of a penetration depth apart. One superconductor is tantalum and is much thicker than a penetration depth; the other is a vacuum evaporated indium film and may be as thin as a penetration depth.

It is shown that such a structure will propagate waves at a phase velocity less than the speed of light in the medium separating the superconductors, a phenomenon that is the result of an inductive component in the surface impedance of the superconductors. The exact velocity is shown to be a function of the thickness parameters in a manner which depends on the law relating the vector potential and the supercurrent in the indium.

Experimental measurements indicate that the relationship between vector potential and current in the vacuum evaporated indium is characterized by a coherence distance which is considerably smaller than that found for pure metals by the measurements of Pippard and the theory of Bardeen, Cooper and Schrieffer.

The penetration depth at zero temperature is deduced from dependence of phase velocity on the thicknesses of the indium and dielectric. For indium λ is found to be 650 ± 75Å, in good agreement with Lock's value of 640Å and Toxen's range from 625 to 725Å. For tantalum λ is found to be 500 ± 175Å. This is believed to be the first measurement. The value of λ for indium is also deduced from the dependence of phase velocity on temperature. It is found to be 704 ± 120Å.

Surface resistance of the two superconductors is found to increase as ω^2, in good agreement with theory, and to depend on temperature according to an empirical law proposed by Pippard.

ACKNOWLEDGEMENT

I should like to thank Dr. Roy W. Gould for his constant encouragement and advice during the progress of the research reported herein. I should also like to thank Dr. Carver Mead for much useful advice on experimental techniques, and Richard Carrouche for construction of much of the apparatus. And last, but not least, my thanks to Mrs. Ruth Stratton who did an excellent job of preparing the manuscript in a very short time.

I. INTRODUCTION

In 1947 Pippard (1) noted that the surface impedance of a superconductor is inductive, and that therefore a transmission line constructed of superconducting metals would exhibit a velocity of propagation less than that of light. He also mentioned that for transmission lines of macroscopic dimensions the difference would be so small as to be immeasurable by a direct velocity measurement; he therefore proposed and used a resonant frequency technique which measured the change in velocity between the normal and superconducting state.

In 1959 Young et al (2) measured the slowing in a strip transmission line in which each of the metallic elements was a vacuum deposited thin film. Pulse techniques were used to observe a slowing to about 90% of the velocity of light in the dielectric medium.

At about the same time that Young was proposing his experiments, we independently deduced the slowing based on the analogy between the London model of a superconductor (3) and the ideal collisionless gaseous plasma. In the London model the superelectrons are free to move within the metal influenced only by electric and magnetic forces, since they do not interact with the lattice; in a collisionless plasma the electrons are free to move, and again only electric and magnetic forces influence them, since the positive ions are so massive that they do not move nor do the electrons lose energy by collisions. Thus in both cases application of Newton's laws and Maxwell's equations leads to a complete description of the motions of the particles. The principal experimental difference is in the density of particles, for one can perform experiments at the plasma frequency of a gaseous plasma (defined by $\omega_p^2 = \frac{\rho e}{m\epsilon_o}$), but for the

superconductor the plasma frequency lies in the optical region where metals no longer behave as superconductors.

Here we seemed to be at an impasse, for nearly all plasma effects are exhibited in the region of the plasma frequency.

However, at this time Trivelpiece was studying a mode of propagation in a plasma which exhibited plasma effects at frequencies far below the plasma frequency as described by Trivelpiece and Gould (4). This mode depended on the fact that the plasma was bounded rather than unbounded in some dimension*. If this dimension was small compared to the penetration depth of the plasma (the depth below the surface at which an external DC magnetic field would be reduced to $1/e$ in intensity), then the phase velocity would be very much smaller than the speed of light.

While the analogy cited above is a rough one, it is shown in Chapter II that an analysis using the London phenomenological equations (which should be approximately valid for macroscopic phenomena) does indeed yield these slow plasma guide modes. Further, an exact analysis using the Bardeen-Cooper-Schrieffer (BCS) theory (5) yields nearly the same results, but with some interesting and experimentally verifiable differences.

When Gould pointed out the applicability of Trivelpiece's work to superconductors, we proposed to verify the existence of these slow waves. In the middle of our experimental work we learned of Young's discovery of these waves (2), so we broadened our objectives to include

*In Trivelpiece's case the radius of a cylindrical plasma; in a planar case, the finite thickness of a plasma of infinite extent in the other two dimensions.

a detailed investigation of the dependence of the phase velocity on such factors as temperature, physical dimensions, and magnetic field. We also were interested in trying to verify the effects which a non-local theory such as the BCS or the Pippard (6) theories* would produce.

We give a brief description of our experiment here in order to clarify the theoretical discussion of Chapter II. A more detailed discussion of experimental procedures is given in Chapter III.

An insulating film of tantalum oxide was formed on a tantalum sheet by an electrical anodization process. Its thickness ranged in different experiments from 300Å to 3000Å . Over this was vacuum deposited a strip of indium about 3.5 mm. wide by 65 mm. long, with thickness ranging from 400Å to 11,500Å . This formed a strip transmission line of very low characteristic impedance, of the order of fractions of a milliohm. A cross section of this line along the long axis is shown in Figure 1, which also defines the coordinate system and geometrical parameters**. A signal generator of 50 ohm source impedance is connected to one end, while a detector also of 50 ohm impedance is connected to the other. Since the source and load are very badly mismatched to the line, we have the necessary conditions for the line to act as a resonant transmission cavity. Transmission will take place only when the line is very nearly an integral number of half wavelengths long, for at these frequencies the load impedance will simply be referred to the input and perfect matching of load to

*The Pippard theory proposed a non-local relationship between the vector potential and the current on a phenomenological basis. The BCS theory gave a theoretical justification for this relationship.

**The tantalum sheet substrate is so thick that it may be considered infinite; hence no thickness parameter is shown.

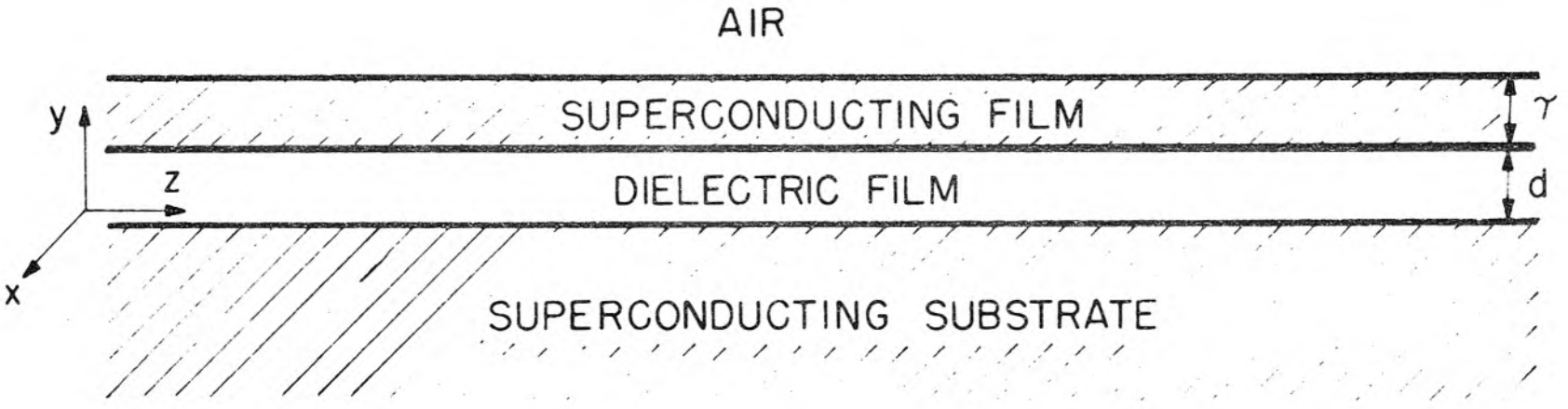

Figure 1. Superconducting Transmission Line

source will exist. Since the physical length of the line is known, a calculation of phase velocity is readily made. Since essentially all of the energy is transmitted between the planes, this phase velocity would be $v_K = c/\sqrt{K}$, where c is the free space velocity of light, and K is the dielectric constant of the tantalum oxide, if the metal films were simply perfect conductors rather than superconductors. The ratio of the actual phase velocity v to v_K is a measure of the effect of the superconductors.

It is also possible to calculate the Q which the resonant transmission peak should have, considering the losses in both the 50 ohm loads and in the superconductors. Measurement of Q thus enables us to estimate the losses on the superconductor, or if we use the Gorter-Casimir two-fluid model (7), we can calculate the normal current.

The absolute gain through the transmission line is also easily measured, but the theoretical calculation here is almost impossible, since the transition from the coaxial cable, which is used to connect to the signal source and load, is very imperfect and furthermore varies from experiment to experiment.

During the measurement of each film, the temperature is readily varied by pumping on the helium bath in which the film is immersed. In these experiments the temperature ranged from $4.2^{\circ}K$ to about $1.35^{\circ}K$ in some cases. The critical temperature of tantalum is $4.38^{\circ}K$; that of bulk indium is $3.41^{\circ}K$, but that of the films was found to be a few hundredths of a degree higher, probably due to impurities and thermal stresses.

For a few of the films a longitudinal (z-directed) magnetic field was used. But for several reasons discussed later, accurate determination of magnetic field dependence had to be postponed.

The experimental results are best interpreted by assuming a coherence length considerably shorter than that predicted by the Pippard and BCS theories for pure metals. (In the limit of zero coherence length these theories reduce to the London local theory). Dependence on the thickness parameters follows fairly well the theoretical form if we assume that the penetration depth of indium at zero temperature is 650Å, and that of the tantalum is 580Å. Slowing of the wave, extrapolated to zero temperature, ranged from $v/v_K = 0.807$ for the thickest films, to 0.388 for the thinnest.

The velocity was also strongly temperature dependent, approaching zero rapidly as the temperature was raised to the critical temperature of indium. For the thinnest film v/v_K was 0.388 at $0^\circ K$ (extrapolated) while at $3.449^\circ K$ it was 0.113 .

Losses in the indium were also strongly dependent on temperature. Q's ranged from 13 near the critical temperature of indium to 1670 at the lowest temperature ($1.35^\circ K$).

Phase velocity was found to depend on magnetic field. In one case a field of 300 gauss caused a decrease of 30% in v/c . Q also dropped as the field was increased.

II. THEORY OF SLOW WAVES IN THIN SUPERCONDUCTORS

A. Phase Velocity

1. London Theory. The basic equations which London (3) proposed as describing the relation between the supercurrent and fields in a superconductor were

$$\nabla \times (\Lambda \bar{J}_s) = - \mu_o \bar{H} \tag{II.1a}$$

$$\frac{\partial}{\partial t} (\Lambda \bar{J}_s) = \bar{E} \tag{II.1b}$$

where $\bar{J}_s$ is the supercurrent; $\Lambda = m_s/\rho_s e_s$ is a constant; m_s, ρ_s and e_s are the mass, density, and charge of the superelectrons respectively, and $\bar{H}$ and $\bar{E}$ are the usual magnetic and electric field intensity vectors*. Equations 1a and 1b** may be restated as

$$- \Lambda \bar{J}_s = \bar{A} \tag{II.2}$$

in a gauge in which $\nabla \cdot A = 0$.

An elementary phenomenological derivation of the London equations may be given in a manner which shows the analogy between superconductors and plasmas.

Consider a collisionless gas of particles of mass m_s, charge e_s, and density ρ_s. D'Alembert's principle requires that the force on the particle equal the time rate of change of momentum. We consider only low velocities so that mass is constant and $\bar{v} \times \bar{B}$ forces may be neglected. We have

$$e_s E = m_s dv_s/dt \tag{II.3}$$

---

*We restate the equations here in rationalized MKS units, which are used throughout; London uses Gaussian units.

**Equations referred to in the text without chapter numbers are in the same chapter.

We can also identify the supercurrent as

$$J_s = \rho_s v_s \tag{II.4}$$

Then if the density ρ_s is a constant we eliminate v_s

$$E = \frac{d}{dt}\left\{\left(\frac{m_s}{e_s \rho_s}\right) J_s\right\} = \frac{d}{dt}(\Lambda J_s) \tag{II.5}$$

Using Faraday's law we have

$$\nabla \times \frac{d}{dt}(\Lambda J_s) = -\mu_o \frac{d}{dt} H \tag{II.6}$$

If we integrate this we have

$$\nabla \times (\Lambda J_s) = -\mu_o [H(t) + H_o] \tag{II.7}$$

Equation 7 allows a solution which is not found in a superconductor, i.e., $H = H_o$. This would imply that if normal metal is changed to a superconductor (as by lowering the temperature through the critical value) in a magnetic field, the magnetic field would still enter the superconductor. However, Meissner and Ochsenfeld (8) discovered that the superconductor ejects the field so that inside $H = 0$, except for a very thin layer at the surface. To account for this London proposed to set $H_o = 0$. In doing this he abandoned any pretense at a microscopic description, i.e., the resulting equations 1a and 1b are simply phenomenological descriptions of superconductivity. They are surprisingly successful in describing the phenomenon, however. As we shall see, the non-local theory which is based on a macroscopic quantum mechanical model gives results which differ little in most respects from the London theory.

In addition to the London equations discussed above, we make use of Maxwell's equations relating the total current $\bar{J}$ to $\bar{E}$ and $\bar{H}$,

$$\nabla \times \bar{H} = \bar{J} + \epsilon_o \frac{\partial \bar{E}}{\partial t} \qquad \text{(II.8a)}$$

$$\nabla \times \bar{E} = - \mu_o \frac{\partial \bar{H}}{\partial t} \qquad \text{(II.8b)}$$

$$\nabla \cdot \bar{H} = 0 \qquad \text{(II.8c)}$$

$$\nabla \cdot \bar{E} = \frac{\rho}{\epsilon_o} \quad ; \qquad \text{(II.8d)}$$

the equation of continuity

$$\nabla \cdot \bar{J} + \frac{\partial \rho}{\partial t} = 0 \quad ; \qquad \text{(II.9)}$$

the assumption that total current is composed of the supercurrent plus a normal current

$$\bar{J} = \bar{J}_s + \bar{J}_n \quad ; \qquad \text{(II.10)}$$

and finally, Ohm's law for the normal current

$$\bar{J}_n = \bar{\sigma}\, \bar{E} \quad . \qquad \text{(II.11)}$$

We now take the curl of equation 8a and using the vector identity $\nabla \times \nabla \times H = \nabla(\nabla \cdot H) - \nabla^2 H$ and equation 8c, we modify the left hand side to $-\nabla^2 H$. On the right we use equations 1a, 8b, 10 and 11 to eliminate J, J_s, J_n and E, leaving

$$\nabla^2 \bar{H} = \frac{\mu_o}{\Lambda} \bar{H} + \mu_o \sigma \frac{\partial \bar{H}}{\partial t} + \mu_o \epsilon_o \frac{\partial^2 \bar{H}}{\partial t^2} \qquad \text{(II.12)}$$

which would be the usual damped wave equation for H if the term

$\frac{\mu_o}{\Lambda} \bar{H}$, due to the superelectrons, were not present.

We now wish to obtain a similar equation from equation 8b, but we find that $\nabla \cdot \bar{E} = \rho/\epsilon_o$. Hence we use equations 1b, 10 and 11 to eliminate $\bar{J}$ from equation 9, obtaining

$$\ddot{\rho} + \frac{\sigma}{\epsilon_o} \dot{\rho} + \frac{\rho}{\Lambda \epsilon_o} = 0 \quad . \tag{II.13}$$

This has solutions of the form

$$\rho = Ae^{-\gamma_1 t} + Be^{-\gamma_2 t} \tag{II.14}$$

where $\gamma_1 = \sigma/\epsilon_o \left(1 + \sqrt{1 - \frac{4\epsilon_o}{\Lambda\sigma^2}} \right) \approx \frac{\sigma}{\epsilon_o} \approx 10^{19}/\text{sec}$,

and $\gamma_2 = \sigma/\epsilon_o \left(1 - \sqrt{1 - \frac{4\epsilon_o}{\Lambda\sigma^2}} \right) \approx \frac{2}{\Lambda\sigma} \approx 10^{12}/\text{sec}$. *

Any free charge will decay to zero in 10^{-12} sec. Therefore, $\nabla \cdot \bar{E} = 0$ and we can obtain an equation for $\bar{E}$ of the same form as equation 12.

$$\nabla^2 \bar{E} = \frac{\mu_o}{\Lambda} \bar{E} + \mu_o \sigma \frac{\partial \bar{E}}{\partial t} + \mu_o \epsilon_o \frac{\partial^2 \bar{E}}{\partial t^2} \quad . \tag{II.15}$$

We ask now which terms of equations 15 and 12 are of interest to us. If we assume sinusoidal time dependence, i.e., $E = Ee^{j\omega t}$ we have

$$\nabla^2 \bar{E} = -\omega^2 \mu_o \epsilon_o \left(1 - j \frac{\sigma}{\omega \epsilon_o} - \frac{1}{\omega^2 \Lambda \epsilon_o} \right) \bar{E} \quad . \tag{II.16}$$

Hence if $\omega = \frac{1}{\Lambda\sigma} \approx 10^{12}$, the first two terms will be equal, while if

---

* $\sigma \approx 10^8$ mho/meter, $\epsilon_o = 8.85 \cdot 10^{-12}$, and Λ may be deduced from measured values of the penetration depth; $\lambda = \sqrt{\Lambda/\mu_o} \approx 500\text{Å}$ for most materials. From this $\Lambda = 3 \cdot 10^{32}$.

$\omega = \sqrt{\frac{1}{\Lambda \epsilon_o}} \approx 10^{16}$, the first and last will be equal. It is clear then that the first may be omitted, but the losses due to the second may be important above frequencies of perhaps 10 gigacycles/sec (10^{10} cps).

Actually, however, the losses are primarily a quantum mechanical effect and according to the BCS theory should start to appear relatively abruptly at about $\frac{3.5\ kT_c}{h}$ (about 250 gc for indium). Glover and Tinkam (9) by measuring transmission of infrared through films about 20Å thick, found that resistive losses first appeared at about $2kT_c$, and reached the value for the normal metal at about 10 kT_c. Further discussion is given in Section II-B.

A fundamental parameter of a superconductor is the penetration depth λ. To show how this arises we consider the solution of equation 12 for the static case, in which the last two terms vanish. We consider a superconducting sheet filling the half plane $y < 0$ as in Figure 2. A magnetic field H_o is tangential to the plane at $y = 0+$, say in the x direction. Since there is no x or z dependence, equation 12 becomes

$$\frac{\partial^2 H_x}{\partial y^2} = \frac{\mu_o}{\Lambda} H_x \qquad y < 0 \qquad \text{(II.17)}$$

whose solution is

$$H_x = Ae^{y/\lambda} + Be^{-y/\lambda} \qquad y < 0 \qquad \text{(II.18)}$$

where

$$\lambda = \sqrt{\Lambda/\mu_o} = \sqrt{\frac{m_s}{\mu_o e_s \rho_s}} \quad . \qquad \text{(II.19)}$$

For $y < 0$ we must set $B = 0$, since H_x would become infinite at $y = -\infty$ otherwise. Hence our final solution is

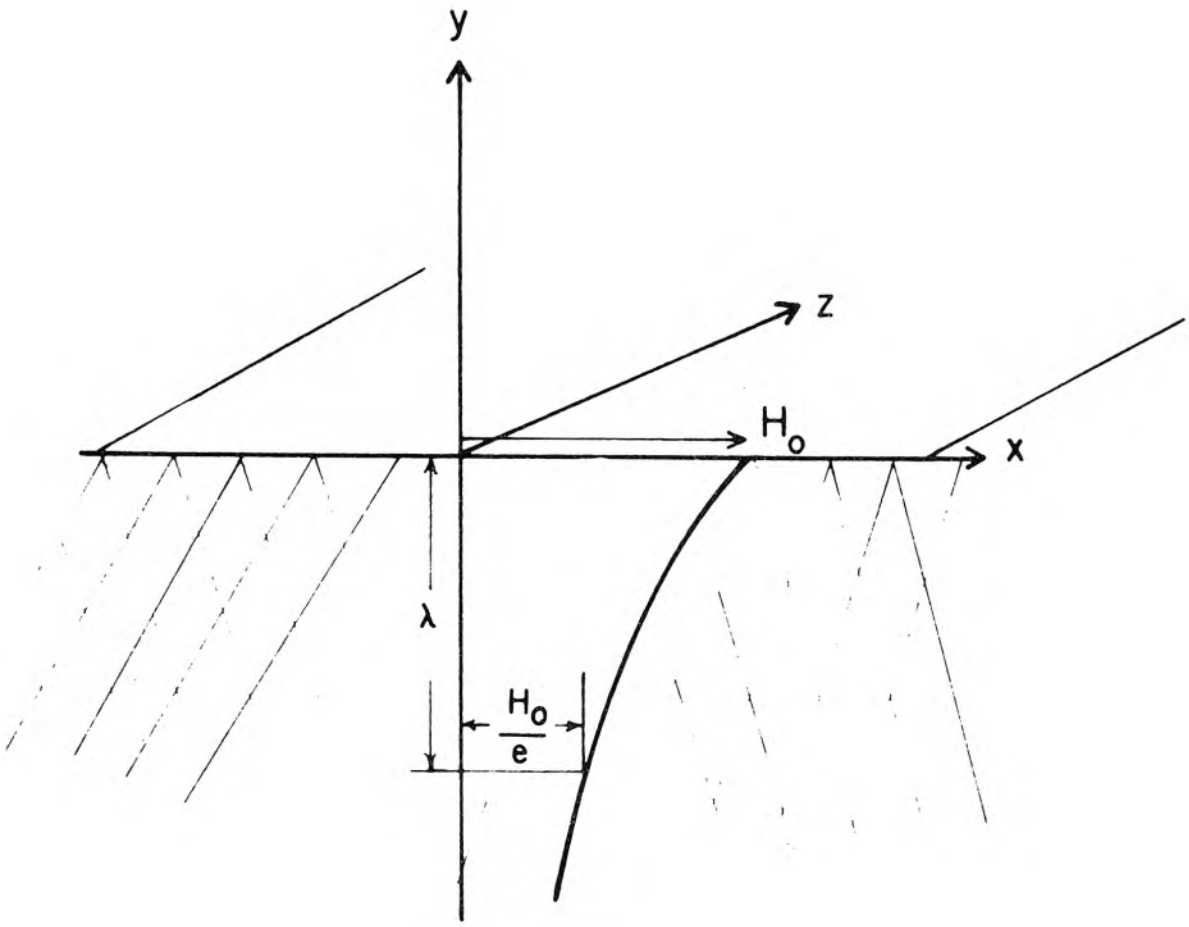

Figure 2. Decay of a Magnetic Field in a Superconductor

$$H_x = H_o e^{y/\lambda} \qquad y < 0 \quad . \tag{II.20}$$

Thus the field decays to $1/e$ of its surface value in a distance λ into the metal. Equation 1a becomes

$$\bar{e}_x \frac{\partial(\Lambda J_{sz})}{\partial y} = - \bar{e}_x \mu_o H_o e^{y/\lambda} \tag{II.21}$$

or

$$J_{sz} = - \frac{1}{\lambda} H_o e^{y/\lambda} \tag{II.22}$$

Hence supercurrents flow in the z direction, acting to shield the magnetic field from the interior. The value of E for the static case is zero from equation 1b.

When we consider other theories of superconductivity we will use a generalized definition of λ which reduces to 19 for the London case

$$\lambda = \int_0^\infty \frac{H_{tan}(y)}{H_{tan}(0)} \, dy \quad . \tag{II.23}$$

Having obtained electrodynamic equations for the superconductor we now wish to solve the boundary value problem of transmission along the strip line of Figure 1. Since our interest in the problem has been inspired by plasma devices in which slow waves are a fundamental part of the operation and by a theory which finds slow waves well below the plasma frequency, we shall attempt to find solutions of this type. We cannot exclude the possibility of fast wave solutions, but in all probability they would exist at such high frequencies that the metal would no longer behave as a superconductor.

In Appendix A we consider the solution in detail. We show that for two-dimensional geometry (infinite extent in the x-direction and hence no x-dependence) and assuming wave motion in the z-direction, an E mode solution can be found whose form in a dielectric is

$$E_z = (A \sinh \gamma_D y + B \cosh \gamma_D y)\, e^{j(\omega t - \beta z)} \qquad \text{(II.24)}$$

(where $\gamma_D^2 = \beta^2 - \omega^2 \mu_o \epsilon_o K$, K being the relative permittivity of the dielectric) and whose form in a superconductor is

$$E_z = (C \sinh \frac{y}{\lambda} + D \cosh \frac{y}{\lambda})\, e^{j(\omega t - \beta z)} \qquad \text{(II.25)}$$

where λ is the London penetration depth.

We solve the boundary value problem, obtaining as a result γ_D^2 , from which β^2 and therefore $(c/v)^2 = \frac{c^2}{\omega^2/\beta^2}$ can be found. (v is the phase velocity ω/β of the wave.) The final solution for a London material is (see equation A.26)

$$(\frac{c}{v})^2 = \frac{K}{d}\left[d + \lambda_{Ta} + \lambda_{In} \coth \tau/\lambda_{In}\right] \qquad \text{(II.26)}$$

Here we write K/d outside the bracketed expression, since K/d and d are the experimentally measured parameters. d and τ are defined in Fig. 1. We can understand the import of this equation best by considering some of the limiting cases. If d is very large compared to λ_{Ta} and λ_{In} , and if τ is not so small as to make coth τ/λ_{In} large (it approaches λ_{In}/τ for small τ), then we have simply

$$(\frac{c}{v})^2 = K \qquad \text{(II.27)}$$

that is, the wave moves with the velocity of light in the dielectric just as in a strip line made with perfect conductors.

If d is not large, but if $\tau \gg \lambda_{In}$, i.e., we have two infinitely thick sheets of superconductor spaced the order of a penetration depth apart, then

$$\left(\frac{c}{v}\right)^2 = \frac{K}{d}\left[d + \lambda_{Ta} + \lambda_{In}\right] \quad . \tag{II.28}$$

Since the factor multiplying K can be much larger than 1, slow waves are possible here. Also in theory at least, if K/d, d, and one of the λ's is known, the other can be found. We know λ_{In} fairly well, for example, so we should be able to deduce λ_{Ta}. Thus the method might be useful in finding the λ's of metals such as tantalum which cannot easily be made into thin films.

In the limit of very small τ, coth τ/λ_{In} approaches λ_{In}/τ which dominates the other terms so we have

$$\left(\frac{c}{v}\right)^2 = K\frac{\lambda_{In}^2}{d\tau} \tag{II.29}$$

For the general case we show in Figure 3 a family of plots of $\left(\frac{c}{v}\right)^2$ for a number of values of d. Also shown are the results for the nonlocal theory discussed in the next section. The values for the important parameters are values deduced from our experimental work as discussed in Chapter IV. It would perhaps be better in theory to show $\left(\frac{c\sqrt{K}}{v}\right)^2$, the ratio of the speed of light in the dielectric to the wave velocity, but since K is an experimentally measured parameter with considerable uncertainty we preferred to plot $(c/v)^2$.

It is also useful to plot $(c/v)^2$ versus $\frac{1}{d}$ with τ as a parameter. This is simply a straight line with zero intercept at K and slope $\lambda_{Ta} + \lambda_{In}$ coth (τ/λ_{In}). Such a plot is shown in Figure 4.

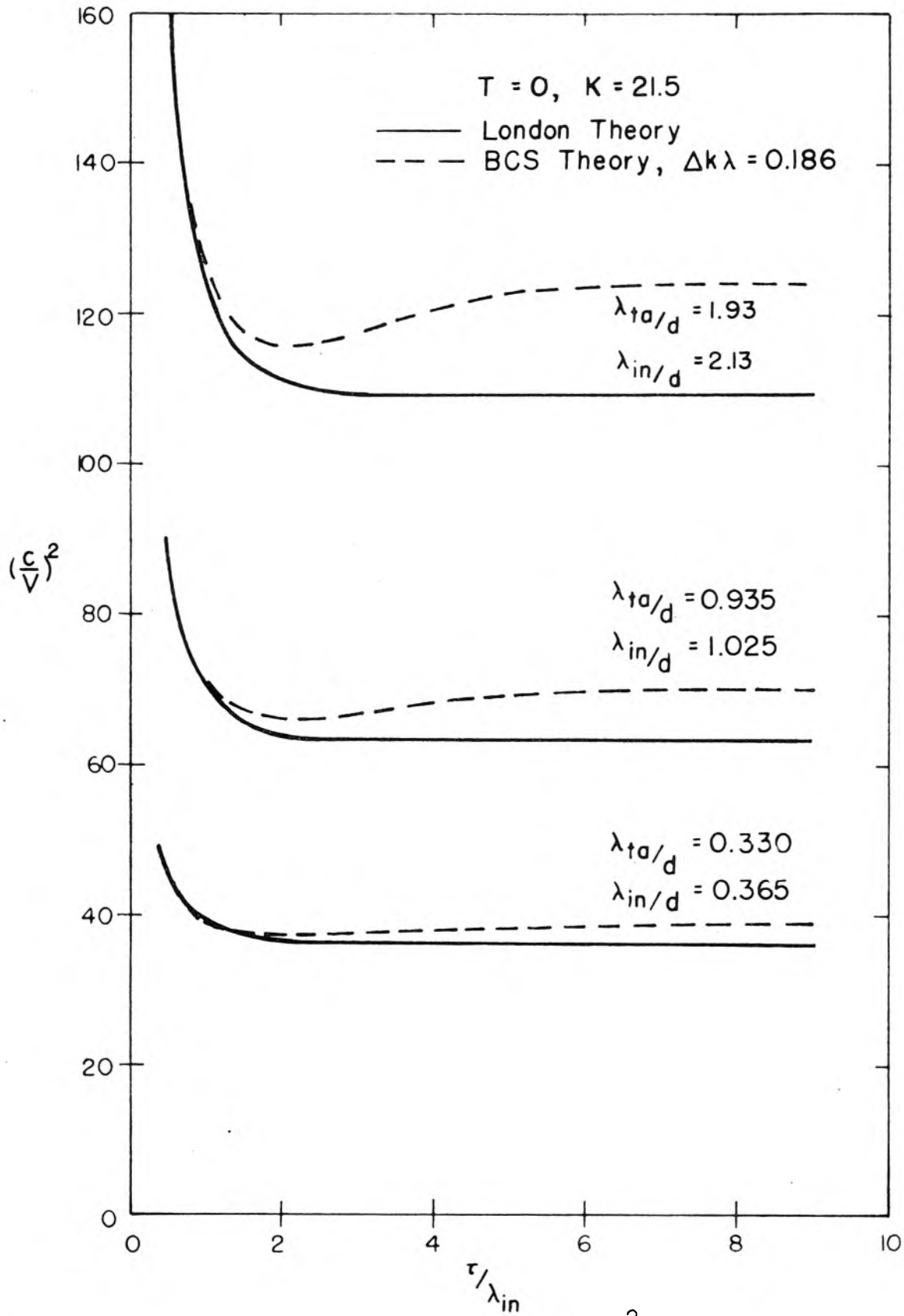

Figure 3. Theoretical Velocity Function $(c/v)^2$ versus Film Thickness with Dielectric Thickness as a Parameter

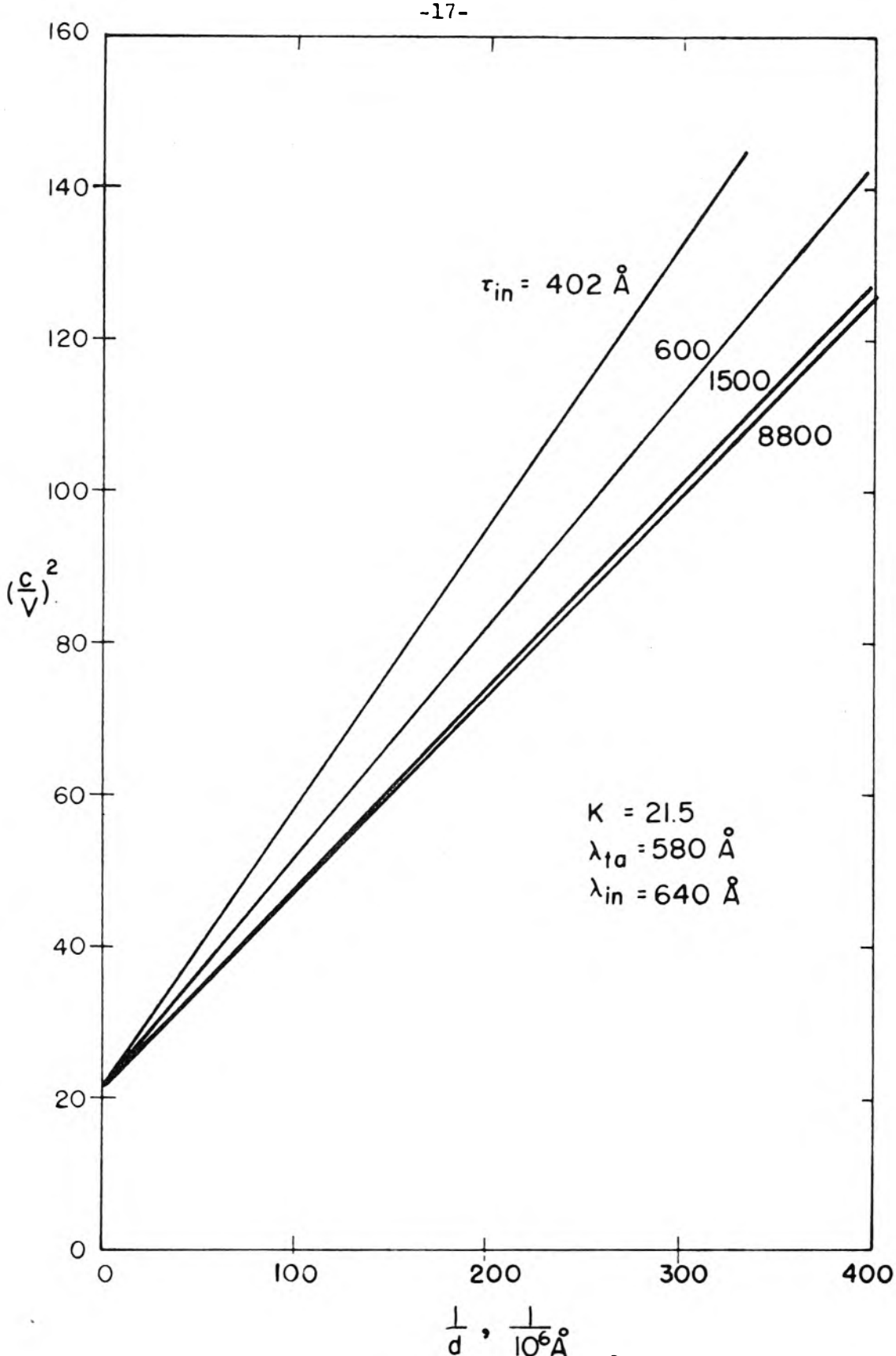

Figure 4. Theoretical Velocity Function $(c/v)^2$ versus Inverse Dielectric Thickness with Film Thickness as Parameter

2. Non-Local Theories. As first proposed on empirical grounds by Pippard (6), and later put on sound theoretical foundation by Bardeen, Cooper and Schrieffer (5), it is necessary to modify the relationship between $\bar{J}_s$ and $\bar{A}$ in such a way that the current at a point is a weighted integral of $\bar{A}$ over a sphere of radius roughly ξ, the coherence length. From his measurements Pippard deduced a value of ξ of the order of 10^{-4} cm. This means that in general we do not expect $\bar{J}_s$ to change much in distances ξ. Clearly interesting properties should appear as we investigate the penetration depth in films of the order of ξ or less. In particular we might expect the phase velocity to depend upon thickness of the films in a manner dependent upon the exact penetration law.

Schrieffer (10), in an evaluation of the magnetic susceptibility of thin superconducting films according to various theories, gives the following expressions for the relationships between $\bar{J}_s(\bar{r})$ and $\bar{A}(\bar{r})$ where $\bar{r}$ is the radius vector, and also between their Fourier transforms $\bar{J}_s(\bar{k})$ and $\bar{A}(\bar{k})$, where $\bar{k}$ is the wave vector, i.e., the Fourier transform variable. The former are, except for the London theory, integral relationships, while the latter are algebraic.

London:

$$\bar{J}_s(\bar{r}) = -\frac{\bar{A}(\bar{r})}{\Lambda} \tag{II.30a}$$

$$\bar{J}_s(\bar{k}) = -\frac{\bar{A}(\bar{k})}{\Lambda} \tag{II.30b}$$

Pippard:

$$\bar{J}_s(\bar{r}) = -\frac{3}{4\pi\xi_o\Lambda} \int \frac{\bar{R}\left[\bar{R}\cdot\bar{A}(\bar{r}')\right]e^{-R/\xi}}{R^4}\, d\tau' \tag{II.31a}$$

$$\bar{J}_s(\bar{k}) = -\left[\frac{3\pi^2}{\xi_o \Lambda k}\right] \frac{2}{\pi(\xi k)^2}\left\{\left[1+(\xi k)^2\right]\tan^{-1}\xi k - \xi k\right\} \bar{A}(\bar{k}) \quad . \qquad \text{(II.31b)}$$

Here $\bar{R} \equiv \bar{r} - \bar{r}'$, $d\tau'$ is the element of volume, ξ is the coherence length which is equal to ξ_o for pure metals and decreases for impure metals, and light face values are the lengths of the corresponding bold face vectors. We note that the factor $e^{-R/\xi}$ in the expression for $\bar{J}_s(\bar{r})$ indicates that the major contributions to the integral come from a sphere of radius roughly ξ around the tip of $\bar{r}$.

BCS:

$$\bar{J}_s(\bar{r}) = -\int \bar{R}\left[\bar{R} \cdot \bar{A}(r')\right] f_{BCS}(R)\, d\tau' \qquad \text{(II.32a)}$$

$$\bar{J}_s(\bar{k}) = -\frac{3}{4\Lambda}\left(\frac{\Delta k}{k}\right) \ell n \left(1 + \frac{k}{\Delta k}\right) \bar{A}(\bar{k}) \quad . \qquad \text{(II.32b)}$$

Here Δk is the reciprocal of the range of the BCS integral and

$$f_{BCS}(R) \equiv -\frac{1}{32\pi^4 \mu_o}\int \left\{\int k' K_{BCS}(k')dk'\right\} e^{i\bar{k}\cdot\bar{R}}\, d^3k \, . \qquad \text{(II.33)}$$

K, the kernel, is defined for all three cases by

$$\bar{A}(\bar{k})\, K(\bar{k}) = -\mu_o \bar{J}_s(\bar{k}) \qquad \text{(II.34)}$$

so that

London:

$$K_L = \mu_o/\Lambda = 1/\lambda_L^2 \qquad \text{(II.35)}$$

Pippard:

$$K_p = \frac{1}{\lambda_L^2}\left[\frac{6\pi}{\xi_o k}\right]\frac{1}{(\xi k)^2}\left\{\left[1+(\xi k)^2\right]\tan^{-1}\xi k - \xi k\right\} \qquad \text{(II.36)}$$

BCS:

$$K_{BCS} = \frac{3}{4}\frac{1}{\lambda_L^2}\left(\frac{\Delta k}{k}\right) \ell n\left(1 + \frac{k}{\Delta k}\right) \qquad (II.37)$$

Another non-local theory, that of Schafroth and Blatt (11) has the kernel

$$K = - \frac{k}{\mu_o \Lambda (k + \mu)} \qquad (II.38)$$

but the penetration depth calculated from it increases indefinitely for increasing thickness, in direct contradiction to our experiment, so we have not included it.

We now wish to solve for the dependence of $(c/v)^2$ on film thickness for various theories. The details of the calculation are given in Appendix A . The results may be summarized as follows:

$$(c/v)^2 = \frac{K}{d}\left(d + \lambda_{Ta} + L_{In}\right) \qquad (II.39)$$

where L_{In}, which is a length associated with the indium film and which is proportional to its surface impedance, is given in the three cases by:

$$\frac{L_{LONDON}}{\lambda_L} = \coth \frac{\tau}{\lambda_L} \qquad (II.40)$$

$$\frac{L_{PIPPARD}}{\ell_p} = \frac{\ell_p}{\tau}\left[1 + 2\sum_{n=1}^{\infty} \frac{1}{(k_n \ell_p)^2 + \frac{3}{2}\left[\frac{(1+\xi k_n)^2 \tan^{-1}\xi k_n - \xi k_n}{\xi k_n}\right]}\right] \qquad (II.41)$$

$$\frac{L_{BCS}}{\ell_B} = \frac{\ell_B}{\tau}\left[1 + 2\sum_{n=1}^{\infty} \frac{1}{(k_n \ell_B)^2 + \frac{3}{2}\frac{\Delta k}{k_n}\ell n\left(1 + \frac{k_n}{\Delta k}\right)}\right]. \qquad (II.42)$$

Here λ_L is the London penetration depth and

$$k_n \ell \equiv \frac{n\pi\ell}{\tau} \tag{II.43}$$

$$\ell_p \equiv \sqrt{\frac{\xi_o}{4\pi\xi}}\,\lambda_L = \lambda_L/\sqrt{4\pi} \qquad \text{for pure metals} \tag{II.44}$$

$$\ell_B \equiv \sqrt{\frac{4}{3}}\;\lambda_L \tag{II.45}$$

It is convenient to write these expressions as functions of dimensionless parameters. Since ξk_n may be written in the form $(\frac{\xi}{\ell_p})(n\pi\,\frac{\ell_p}{\tau})$ and since $k_n\,\ell_p = n\pi\,\ell_p/\tau$, the expression for $L_{PIPPARD}/\ell_p$ is a function only of the dimensionless parameters ξ/ℓ_p, a measure of the range of integration, and τ/ℓ_p, the dimensionless thickness.

Similarly, since $\Delta k/k_n$ may be written in the form $\Delta k\ell_B/n\pi\,\frac{\ell_B}{\tau}$, L_{BCS}/ℓ_B is a function only of an inverse range parameter $\Delta k\;\ell_B$ and a dimensionless thickness τ/ℓ_B.

We have left ℓ_p and ℓ_B in the equations since their values are actually not found from equations 44 and 45, but are adjusted to fit the observed curve of L_{In} versus τ.

Figures 5 and 6 show plots of $L_{PIPPARD}/\ell_p$ versus τ/ℓ_p and L_{BCS}/ℓ_B versus τ/ℓ_B, respectively. For very short range (small ξ, large Δk) both expressions reduce to the London expression $\coth \tau/\ell$.

The most striking feature of both the non-local theories is the minimum in the value of L_{In} as compared with the monotonic decrease of I_{In} in the London theory. For data with sufficiently small scatter one should be able to make a good estimate of the range parameters ξ or Δk. Even with considerable scatter, one might be able to observe the minimum qualitatively and hence be able to say that a non-local theory should be used. In attempting to fit a theoretical curve to the

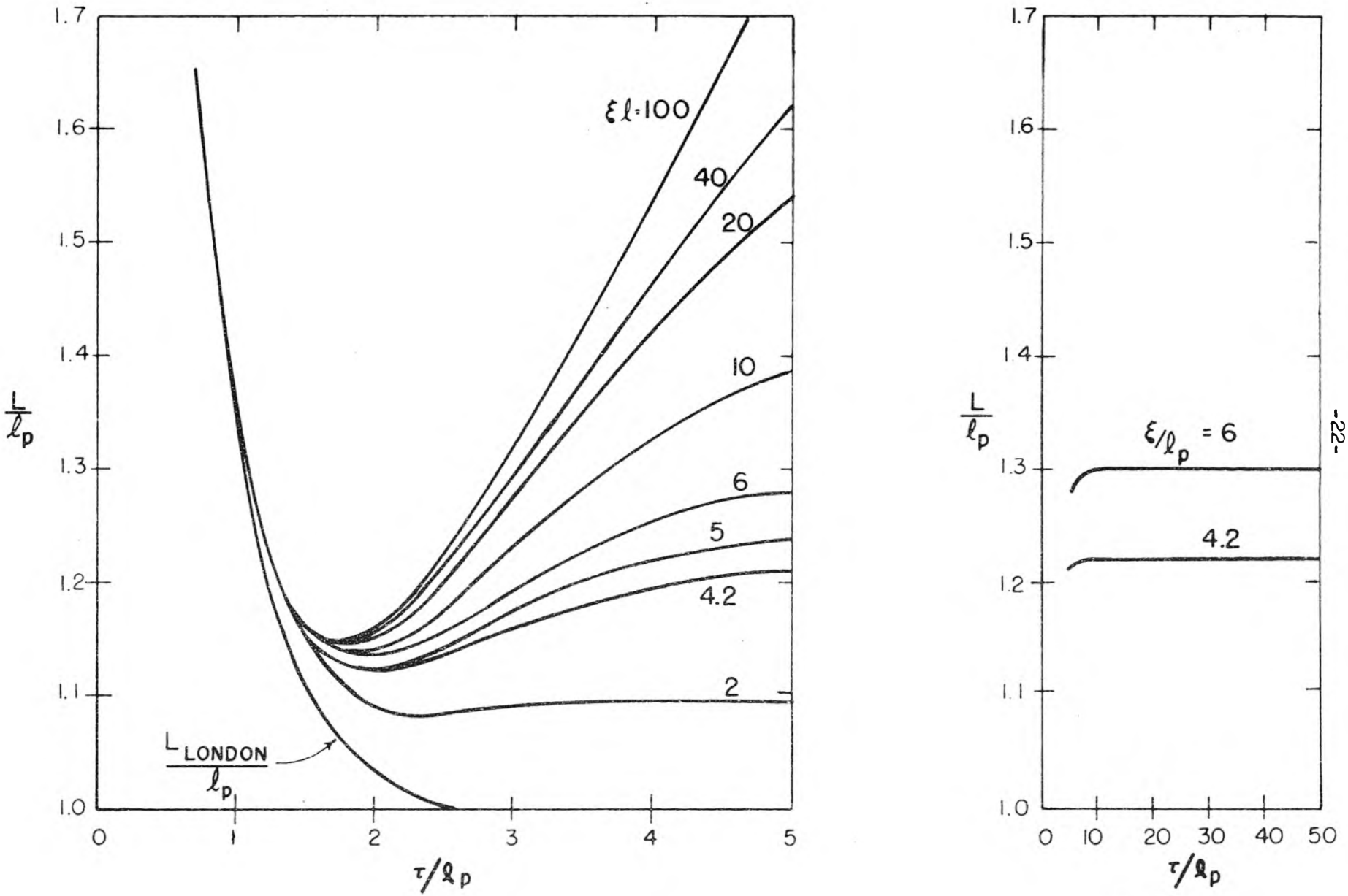

Figure 5. Pippard Length versus Film Thickness with Coherence Length ξ as Parameter

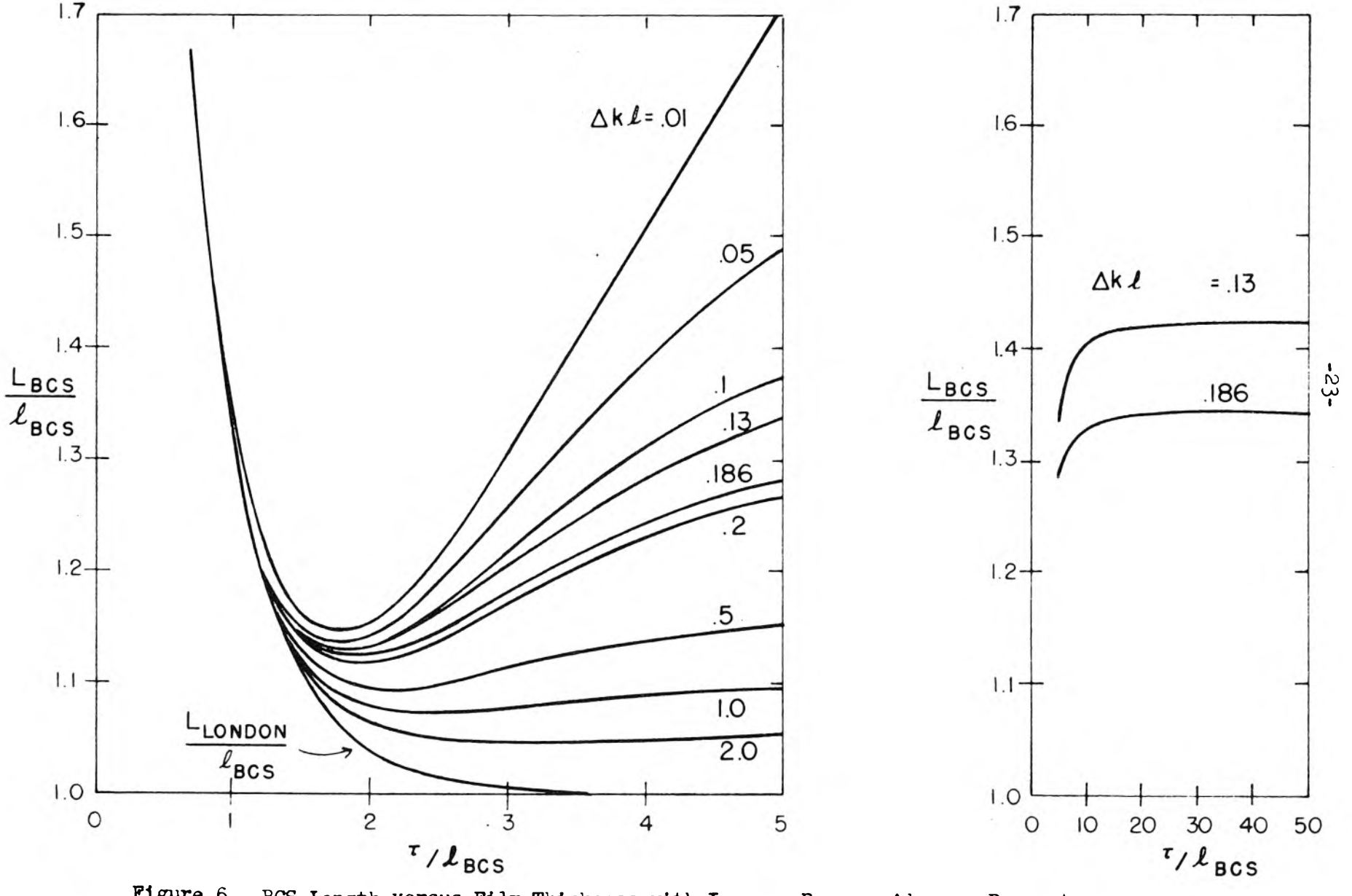

Figure 6. BCS Length versus Film Thickness with Inverse Range, Δk , as Parameter

experimental data, one would probably choose ℓ to give the best fit for small τ, on the steeply falling part of the curve. Then the other free parameter ξ or Δk would be chosen to give the best fit at large τ, where L_{In} is nearly constant. This might not fit precisely in the region of the minimum so that some compromise might be necessary.

As it happens, our data appear to fit best with the range equal to zero, i.e., the London or local theory seems to be most valid. In this case a fairly straightforward fitting procedure may be used as discussed in Chapter IV.

In order to compare the Pippard and BCS lengths we have plotted two curves together in Figure 7. We have chosen $\Delta k\ell = 0.186$ for the BCS theory, then found a value $\xi/\ell = 7.0$ for the Pippard theory which gave the same large τ limit. As may be seen, the major difference occurs in the region between $\tau/\ell = 2$ and $\tau/\ell = 10$ and is at most 2-1/2%. Since these values are so close compared to the uncertainties of our data, and since the Pippard theory is phenomenological, while the BCS theory is based on a fundamental model, we shall usually omit separate discussion of the former. In any case, our films appear to obey the London theory.

The choice of $\Delta k\ell$ of the BCS theory is somewhat difficult since there are no very well agreed-on data. Toxen (12) discusses this point at some length and finally concludes that $1/\Delta k$ (or in his notation, ξ_o) lies somewhere between 2600Å and 4400Å. For Lock's value for λ of 640Å (which agrees fairly well with our data), this corresponds to $0.145 < \Delta k\lambda < 0.246$. Schrieffer used a value (for tin) of 0.186, in his discussion of the magnetic properties of thin films (10). We will

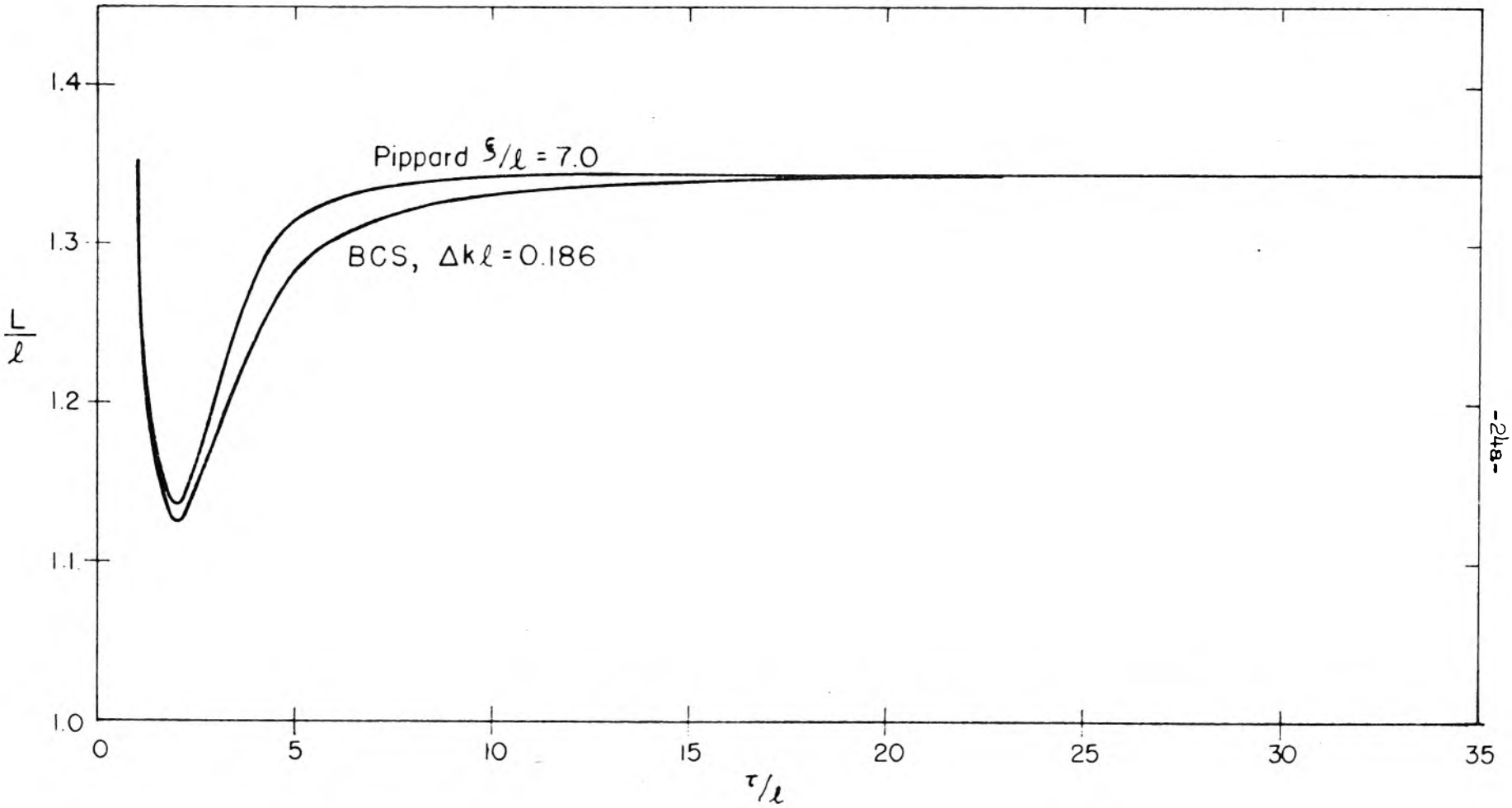

Figure 7. Comparison of BCS and Pippard Lengths

use this value in most of our discussion.

We have also plotted in Figure 2 $(c/v)^2$ versus τ for the BCS theory with $d = 300$, 625, and 1755Å. We take $K = 21.5$, $\lambda_{Ta} = 580$Å, and $\lambda_{In} = 640$Å, yielding the values of λ_{Ta}/d and λ_{In}/d given on the figure. These values are taken from our data, as discussed in Chapter IV. The minimum associated with the non-local theory is most pronounced for the smallest value of d, the dielectric thickness.

3. Temperature Dependence of Phase Velocity. Our basic expression for phase velocity

$$(c/v)^2 = \frac{K}{d}\left[d + \lambda_{Ta} + L_{In}\right] \tag{II.46}$$

contains two terms which are temperature dependent; λ_{Ta} and L_{In}. The exact form of L_{In} will depend upon the theory used, but we have shown in Figure 3 that it is fairly close to the London dependence,

$$L_{In} = \lambda_{In} \coth \tau/\lambda_{In} . \tag{II.47}$$

In the non-local theories we have also shown that L_{In}/ℓ is a function of the dimensionless parameters τ/ℓ_p and $\xi\ell_p$ for Pippard theory, or $\Delta k/\ell_B$ for the BCS theory. Since ℓ_p and ℓ_B are simply proportional to λ_L the whole problem of temperature dependence of $(c/v)^2$ reduces to the problem of the temperature dependence of λ_L for indium and tantalum.

If one combines the two-fluid theory of Gorter and Casimir (7) with the London electrodynamic equations one obtains a dependence of the form

$$\lambda(T) = \frac{\lambda_o}{\sqrt{1 - (T/T_{crit})^4}} \quad . \qquad \text{(II.48)}$$

If we define $T/T_{crit} \equiv t$ we may also express this in the form

$$(\frac{\lambda_o}{\lambda})^2 = 1 - t^4 \qquad \text{(II.49)}$$

where λ_o is the zero temperature value and T_{crit} is the critical temperature of the metal.

Experimental measurements verify this quite well. In particular, Daunt, Miller, Pippard and Shoenberg (13) show that the exponent is quite close to 4 . Their discussion is based primarily on earlier measurements on mercury and tin cylinders of radius 10^{-3} cm by Desirant and Shoenberg (14), and on mercury colloids by Shoenberg (15). Both these investigators measured the normalized magnetic susceptibility of a specimen in a uniform field by measuring the voltage generated in a coil when the specimen is suddenly displaced. For a cylinder of radius r this is related to λ by

$$\chi/\chi_o = 1 - 2\lambda/r \qquad \text{(II.50)}$$

where χ_o is the value of χ for infinite radius.

This same method was applied in 1951 by Lock (16) to vacuum evaporated thin films. He determined χ/χ_o for films of tin, indium and lead for films ranging from 1000 to 8000Å. He found excellent agreement with the following relationship based on equation 48 and the London theory.

$$\frac{\chi}{\chi_o} = k\left[1 - \frac{\lambda_o y}{a}\tanh\frac{a}{\lambda_o y}\right] \qquad \text{(II.51)}$$

where $2a$ is the thickness, $y \equiv 1/\sqrt{1-t^4}$, and k is a factor near unity which is necessary to adjust for the fact that the film is not quite parallel to the applied magnetic field. From his data, Lock was able to obtain values of the universal constant λ_o and of k and T_{crit}, both of which varied from film to film. He finds $\lambda_o = 500 \pm 10$Å for tin, 640 ± 30Å for indium, and 390 ± 30Å for lead*.

In 1958 Schieffer (10) carried out an analysis of χ/χ_o for thin films according to the London theory, the Bardeen-Cooper-Schrieffer theory (5), the Pippard theory (6) and the Schafroth-Blatt theory (11). His results showed that Lock's data agreed best with the London theory. However, Lock used equation 48 to find a value of λ_o, which is necessary in order to interpret his results. Since the BCS theory predicts a somewhat different dependence at temperatures close to critical, Lock's results may be slightly in error. Also, as Lock himself showed, the theoretical results are not very sensitive to the exact form of the penetration law.

The temperature dependence of $\lambda(T)$ is demonstrated by Figure 8 in which $[\lambda(0)/\lambda(T)]^2$ is plotted versus t. Equation 49 yields $1-t^4$ while the BCS theory falls somewhat above this for t between 0.8 and 1.0. Since Lock established λ_o by obtaining the best fit to such a curve, his results depend on the fit between the theory and the data in

*These data seem somewhat open to question. For the four indium films he mentions, for example, λ_o ranges from 450Å to 708Å with a mean of 624Å and a standard deviation of 72Å. Presumably his figures are based on more extensive data, although he does not mention any.

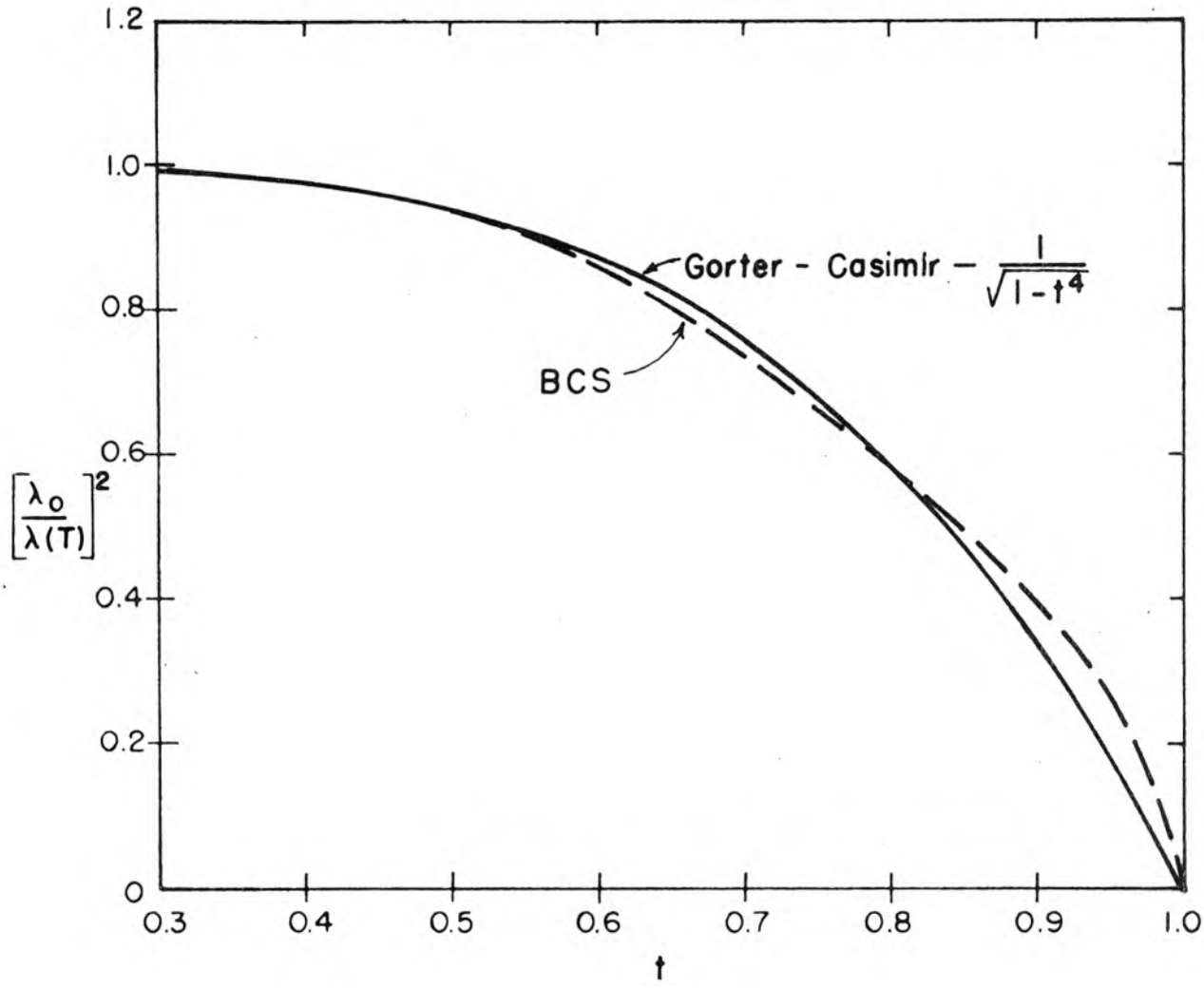

Figure 8. Temperature Dependence of Penetration Depth

the region where the deviation from λ_o is largest, i.e., just this same region near $t = 1$. We should note, however, that the deviation between the two theories is not large. Furthermore, as Bardeen himself notes (17), the experimental data fall between the curves predicted by his theory and that of the Gorter-Casimir model.

In our case we have the additional complication of the presence of a temperature dependent term due to the tantalum. However, T_{crit} for tantalum is $4.38^{\circ}K$ so that λ_{Ta} changes from λ_o at $T = 0$ to $.8\lambda_o$ at $3.41^{\circ}K$, the critical temperature for indium. Thus if we know λ_{oTa}, we can subtract out this factor accurately. Unfortunately λ_{Ta} apparently has not been measured. As shown in Chapter IV, we obtain a value of 580Å, but with considerable uncertainty. If we assume λ_{Ta} as known, then we may write, assuming London theory and the two-fluid model,

$$\frac{d}{K}\left(\frac{c}{v}\right)^2 - d - \lambda_{Ta} = \lambda_o y \coth\left(\frac{\tau}{\lambda_o y}\right) \qquad \text{(II.52)}$$

or if we use the non-local models, we write

$$\frac{d}{K}\left(\frac{c}{v}\right)^2 - d - \lambda_{Ta} = \lambda(T)\, G\left(\frac{\tau}{\lambda(T)}\right) \coth\left(\frac{\tau}{\lambda(T)}\right) \qquad \text{(II.53)}$$

where both $\lambda(T)$ and $G\left(\frac{\tau}{\lambda(T)}\right)$ are known, but are not expressible analytically. $G(\tau/\lambda)$ when multiplied by $\coth(\tau/\lambda)$ yields the L/ℓ function discussed in part 2 of this chapter.

In Chapter IV, we discuss and use the method used by Lock to extract T_{crit} and λ_o from the data, using equations 49 and 53. We shall use the Gorter-Casimir temperature dependence, since the experimental evidence seems to agree as well with this as with the BCS theory.

B. Losses

1. Transmission Line Analysis. In this part we consider our strip as an ordinary transmission line characterized by the usual parameters per unit length L, C, R and G in henries, farads, ohms and mhos per meter. We will apply transmission line theory to determine the Q of the line when it is nearly a half wavelength long. A general reference for this part is "Reference Data for Radio Engineers" (18) which summarizes the material presented in any standard text on transmission lines.

We consider a transmission line of characteristic impedance $Z_o = \sqrt{L/C}$. Z_o is of the order of milliohms. It is terminated in impedances Z_1 on each end (the 50 ohms of the signal source and load). It has a phase velocity $v_\phi = 1/\sqrt{LC}$. Since at low frequencies such as we consider, the electric field pentrates the superconductor very little, C is that measured at D.C. and calculated from the usual strip line formula $C = \epsilon W/d$ where ϵ is the dielectric constant, W is the width, and d the dielectric thickness. L , on the other hand, is not that calculated from the strip line, but is calculated from the theoretical or experimental phase velocity. That is, L varies to account for the properties of the superconductor. If we define v_K as the velocity on a strip line made of the same dielectric and perfect conductors, L_K as the inductance of such a line, Z_K as its impedance, and $\alpha = v_\phi/v_K$, then

$$L_o = L_K/\alpha^2 \qquad \text{(II.54a)}$$

and

$$Z_o = Z_K/\alpha \qquad \text{(II.54b)}$$

Thus the slower the phase velocity, the higher the characteristic impedance.

The transmission line also has a conductance per unit length G due to the dielectric, and a total series resistance per unit length R, which is the sum of the series resistance of the indium and the tantalum.

We will also use the customary attenuation constant α and phase constant β, defined by

$$\frac{E(z)}{E(0)} = e^{-\alpha z} e^{-j\beta z} \quad . \tag{II.55}$$

For small losses per unit length α is defined by

$$\alpha = \frac{R}{2Z_o} + \frac{GZ_o}{2} = \frac{R}{2}\sqrt{\frac{C}{L}} + \frac{G}{2}\sqrt{\frac{L}{C}} \tag{II.56}$$

β is given by

$$\beta = \omega/v_\phi = 2\pi/\text{WAVELENGTH} \quad .$$

We also use the parameter Q. It may be defined for a resonant circuit either as the ratio of stored energy to energy lost per radian, or in terms of the resonant frequency ω_o and the frequency difference between half power points $\Delta\omega$:

$$Q = \omega_o/\Delta\omega \quad . \tag{II.57}$$

In reference (18) it is shown that if there are several sources of loss, each of which acting alone yields a $Q = Q_i$, then the total Q for all acting is given (if the total Q is much greater than 1) by

$$\frac{1}{Q_{TOT}} = \sum \frac{1}{Q_i} \quad . \tag{II.58}$$

Reference (18) also gives the following expression for a resonant line n quarter wavelengths long with a load Z_1 at the high voltage end:

$$\frac{1}{Q} = \frac{\beta}{2\alpha} + \frac{4}{n\pi}\frac{Z_o}{Z_1} \quad . \tag{II.59}$$

For a resonant line n half wavelengths with high voltage points (nearly open circuit) at each end, loaded with Z_1 at each end, the same formula holds. We join the two low voltage ends, doubling both the stored energy and the losses. Since the Q is a ratio of stored energy to losses, it is unchanged. We may also eliminate β and α by the use of the definitions above, so

$$\frac{1}{Q} = \frac{v_\phi}{\omega}\left(\frac{R}{2Z_o} + \frac{GZ_o}{2}\right) + \frac{4}{n\pi}\frac{Z_o}{Z_1} \quad . \tag{II.60}$$

For a given length line, n will be directly proportional to ω. Hence, if R, G, Z_o and v_ϕ are independent of frequency, Q should rise linearly with frequency. Experimentally, however, R appears to increase with frequency. G, Z_1, Z_o and v_ϕ appear to be constant.

We now show that we can neglect the term containing Z_1. Since Z_1 = 50 ohms and Z_2 is approximately 1 milliohm or less, Q would be $\approx 40{,}000\,n$, if R and G were zero. Since observed Q's were less than 2000, this term must contribute less than 5% to $1/Q$, and for our accuracy may be ignored.

We also will consider that G is approximately zero, based on the following argument. Q's were highly temperature dependent, ranging from 13 at $3.338^{\circ}K$ (very near the critical temperature of indium, $3.410^{\circ}K$)

for one film to 1670 at $1.35^{\circ}K$ for another. Also the Q was rising steeply in the region near $1.35^{\circ}K$. Since we would not expect the G of the dielectric to be a rapidly varying function of temperature in this region, it should be essentially constant and very high. Hence the temperature dependent part of $1/Q$ must come from the superconductors. Even if we assign only the Q of 1670 to the dielectric, a Q of 1670 at the frequency and phase velocity of interest would require a G of about 1 mho/cm. Since G was found to be of the order of 10^{-9} mho/cm. at D.C., and since losses in reasonable dielectrics do not change drastically at 100 mc, it appears that 1 mho is unreasonably high.

Hence we conclude that the only important contribution to $1/Q$ comes from R , which is the sum of the series resistance of the indium and the tantalum. Since Q drops rapidly toward zero near the critical temperature of indium, it appears that the major part of the loss is due to the indium.

In order to decide whether we can reasonably assign all of the loss to the indium, we ask whether the reduced temperature t (defined as T/T_{crit}) for tantalum at $3.41^{\circ}K$ (the critical temperature for indium) is low enough so that losses are essentially constant. If at the same t for indium the Q is nearly constant, then we may assume, since losses appear to depend primarily on t , that the tantalum losses below $3.41^{\circ}K$ are constant.

The value of t we want is $3.41^{\circ}K/4.38^{\circ}K = .78$. The corresponding absolute temperature for indium is $.78 \times 3.41^{\circ}K$ or about $2.7^{\circ}K$. At this point Q is changing rapidly so it appears that we cannot neglect

the temperature varying losses in the tantalum. Of course, the magnitude of the tantalum losses may be much smaller than those of the indium, but we have no way of telling.

There appears to be no satisfactory way to separate the losses due to the indium and those due to the tantalum except perhaps near T_{crit} for indium. This is one of the reasons that the use of two different metals is unsatisfactory. We are forced to assume that all of the variation with temperature is due to the indium, but we realize that our results will not be very accurate.

If we do make this assumption, then we conclude that the surface resistance of the indium, as discussed in the next section, is linearly proportional to R and hence to $\omega/\alpha^2 Q$. This follows because the superconductor is a linear material for small fields and currents. This was checked experimentally by comparing resonant frequency and Q measured at different signal levels.

2. Physical Theory of Losses and Experiments. Most of the papers which have been written on this topic discuss loss mechanisms in terms of a surface resistance R_s defined by

$$R_s = \mathrm{Re}\left[\frac{E_{TAN}\ (\mathrm{Surface})}{\int_0^\infty J_{TAN}(x)\ dx}\right] \qquad (II.61)$$

where the x coordinate extends normally into the metal. For our purposes we need note only that R_s is proportional to the R of the previous section, and hence to $\omega/\alpha^2 Q$.

As many investigators have noted [for example, Sturge (19) and

Kaplan, Nethercot and Boorse (20] the surface resistance is extremely sensitive to surface condition. For this reason, comparison of data taken on different samples is seldom meaningful. Hence variations of R_s of one sample with frequency and temperature are of the most interest. Since no absolute value can be given, the proportion between R_s and $\omega/\alpha^2 Q$ is sufficient.

We have discussed in Section II-A the fact that loss effects in the London two-fluid model appear as a modification to ϵ . (See equation 16). However, Pippard (21) considered the general two-fluid, two-parameter theory, i.e., one in which two non-interacting currents are present, and in which each is related to the fields by a single parameter. In particular, the London theory assumes $\Lambda \dot{J}_s = E$ and $J_n = \sigma E$. He found from dimensional arguments that the dependence of surface resistance on frequency must be as ω^2 . This has been verified for tin from 220 to 1500 mc/sec. and for indium from 220 to 5000 mc/sec. by Sturge (19). He finds a slower increase above these frequencies.

In an experimental paper closely related to reference (21), Pippard found (22) that R_s may be expressed in general as

$$R(s) = B(\omega)\, \phi(t) \quad . \tag{II.62}$$

He found empirically that

$$\phi(t) = t^4(1 - t^2)/(1 - t^4)^2 \tag{II.63}$$

where the reduced temperature $t \equiv T/T_{crit}$. No theoretical basis for this has been found, although Kaplan et al (20) mention unpublished work on a two-fluid theory by Serber in which a $t^4/(1 - t^4)^2$ dependence is

found. Their data fit equation 63 more closely, however, so they used the latter.

A great deal of experimental work has been reported on surface impedance (usually described in the literature in terms of r, defined as R_S/R_N, where R_N is the normal resistance just above the transition temperature). In nearly all of the work equation 63 was found to be a satisfactory temperature dependence. For example, Sturge (19) found it adequate between $2^{\circ}K$ and the transition temperature at frequencies from 220 mc/sec. to 8000 mc/sec. for tin and indium. Kaplan et al (20) verified it for tin from 17 gc/sec. to 77 gc/sec.

A full theoretical analysis of the surface impedance for either the two fluid theory or the BCS theory is quite complicated, inasmuch as in the frequency range of interest the anomolous skin effect plays an important part. Physically, this is the region where the electron mean free path becomes long compared to the skin depth. It is therefore important at low temperatures and high frequencies. In view of the uncertainty of our data, and of the agreement of other workers with a frequency dependence of the form ω^2 and temperature dependence of the form of equation 62, we shall not attempt to use the more accurate but complicated theories. We shall discuss briefly how losses arise in the BCS theory, however, and some predictions that show that $B(\omega) \sim \omega^2$ and that equation 62 is a reasonable approximation to the temperature dependence.

The BCS theory visualizes the superelectrons as being bound in pairs. The two members of a pair have equal and opposite momentum and spin. A finite amount of energy $\mathcal{E}g$ is required to separate a pair.

At zero temperature this energy gap is found to be $\sim 3.5\ kT_{crit}$ where k is the Boltzmann constant. Because of this gap the pairs cannot interact with the lattice, and there is no resistance to current flow. However, if enough energy is supplied, as by a photon of frequency higher than $\mathcal{E}g/h$, some pairs separate into normal electrons. These normal electrons can interact with the lattice when set in motion by an electric field. At D.C. no field can exist in the superconductor but by equation 1b there can be an A.C. field which will accelerate the normal electrons, allowing loss of energy to the lattice, so that the metal will show some normal resistance. The net effect is that at zero temperature the metal will show no resistance at frequencies below $3.5\ kT_c/h$ which is about 250 gc/sec. (250×10^9 cps) for indium and will show an abrupt increase above this frequency, eventually reaching the normal value.

At finite temperature two effects occur. First, the energy gap decreases, reaching zero at the critical temperature. Second, some electrons are excited thermally over the energy gap, where they become normal electrons which can be acted on by an A.C. field. Since the electric field is proportional to frequency, the normal resistance must be dependent on both frequency and temperature. At any finite frequency and temperature, some normal resistance will be found. This will increase from zero slowly as the frequency is raised, then abruptly as the frequency reaches $\mathcal{E}g/h$. Since $\mathcal{E}g$ is a function of temperature, the exact frequency of the knee will depend on temperature. Biondi and Garfunkel (23) in an elegant measurement of energy absorption in aluminum have shown this effect quite clearly.

The theory of the surface impedance has been worked out by Mattis and Bardeen (24) under the assumption that $\delta/\ell \ll 1$ and $\lambda/\xi_o \ll 1$. The skin depth δ is defined by

$$\delta = \sqrt{\frac{2}{\omega\mu\sigma}} \quad ,$$

and ℓ is the electron mean free path. The first inequality defines the condition that we be in the extreme anomalous region; the second that the penetration depth be much less than the coherence distance.

The derivation has been carried out for the more general case by Miller (25). The most important results for our use are, the justification of the ω^2 dependence below about 10 gc/sec. and the justification of equation 63 for $\phi(t)$. He finds the latter valid within 10% for $0.4 < t < 0.8$. He points out that the lower bound on t is somewhat less than 0.4 for $h\nu < 0.1$. He sets a lower frequency bound of $0.01 \frac{kT_c}{h}$ (about 2.5 gc/sec. for indium) but it is not clear whether he means that he has not investigated $\phi(t)$ below this, or that he actually found a difference. In view of Sturge's work we shall assume that $\phi(t)$ does represent the temperature dependence over the frequency range of our experiment.

III. EXPERIMENTAL APPARATUS AND PROCEDURES

A. Preparation of Films

As discussed in Chapter I, and shown in cross section in Figure 1, the experimental transmission line was formed of a sandwich of tantalum, tantalum oxide, and indium. Since in thin film experiments the results are often influenced considerably by the exact method of preparation, we shall discuss this in some detail. For the same reason a standard preparation procedure was developed and followed for all films. In this way it was hoped to minimize unknown variations so that the results would be as meaningful as possible. It is this standard procedure which is described.

Actually, of course, the procedure evolved somewhat during the series of experiments described here, and in particular, we did not discover the effect of storage of the anodized tantalum in water for a time as short as a day, until two-thirds of the films had been tested. Further discussion is given in Chapter IV.

Certain procedures in the purification of tantalum and in the evaporation of indium which might also improve reproducibility or modify our results came to our attention too late to be incorporated in our experiments. These are discussed in Chapter V.

1. Electropolishing. The substrate was formed from a cold-rolled sheet of tantalum, 0.013" thick, of 99.9% purity obtained from Fansteel Metallurgical Company. It was cut to 1" by 3-1/4", then washed with trichloroethylene, acetone, reagent methanol and distilled water in that order. It was then electropolished in a bath of 90% 36N H_2SO_4 and 10% concentrated HF, following the method listed by

Tegart (26). The tantalum was the anode, and a half-inch rod of graphite was the cathode. We used a current of 4.5 to 5.0 amps at 11-12 volts. The current rises linearly as the voltage is increased from zero, levels out on a plateau, then rises sharply again. We found, as Tegart recommended, that the best polishing was obtained at the high end of the plateau. Too little current etches, while too much causes excessive gassing and formation of large pits. We found that much closer control of temperature than Tegart recommended was necessary for best results. We controlled to $40 \pm 2^{\circ}C$ by a water bath. The polishing solution was also stirred, both to maintain uniform temperature and to mix the solution which tended to be used up in the vicinity of the tantalum. Usually we polished for 30 minutes, which seemed to give the best finish.

A few films were made without electropolishing, but they were invariably shorted between the indium overlay and the tantalum. Apparently the electropolishing removed surface roughness which caused the shorting.

2. Anodization. After electropolishing the metal was washed with water and a soft tissue, then cleaned with acetone, methyl alcohol and distilled water. Our next step was anodization to form the insulating layer. To anodize, one applies a positive voltage to the metal and negative voltage to a counter electrode, in our case another piece of tantalum, in an oxygen-rich solution. This forms a layer of tantalum oxide whose thickness is accurately proportional to voltage, though perhaps with dependence of the form

$$d_{anodize} = d_o + KV \quad . \qquad \text{(III.1)}$$

This relationship was investigated by Vermilyea (27) who used a weighing method to obtain

$$d_{anodize} = 19 + 16.32V \qquad \text{(III.2)}$$

where thicknesses are in angstroms. Later Charlesby and Polling (28) used a spectrophotometer to observe the brilliant colors formed by the anodization. They obtained $K = 16.0$ Å/V , but stated only that d_o is less than 50Å .

As discussed in Chapter IV, we found from capacitance measurements that if we used $K = 16.0$ Å/V , d_o must be taken to be 138Å , somewhat at variance with the results above.

Charlesby and Polling's explanation of the formation of the colors is incorrect, since they assume the insulator to be perfect and the metal substrate to have zero resistance. As MacSwan (29) points out, under these conditions no colors would be formed, since all energy would be reflected. Using a Smith chart and the analogy between plane waves and a transmission line, he gives the correct explanation. Charlesby and Polling's experimental results are correct, however.

In order to be as close to their results as possible, we used Charlesby and Polling's method. That is, we used a saturated solution of ammonium borate at room temperature; we maintained a constant current of 2.5 ma/cm^2 until the desired voltage was reached, then constant voltage until the current dropped to 0.1 ma/cm^2.

The brilliant coloring of the Ta_2O_5 film and consequent ease of determination of thickness was one of the principal reasons for the

choice of tantalum as a substrate. It also had a conveniently high transition temperature (4.38°K), so that the variation of its penetration depth with temperature contributed relatively little to the change of phase velocity. At the time that the experiment was started, anodization appeared to be virtually the only way to get insulating films of sufficient uniformity and freedom from holes. New methods of forming thin insulating films, and the reasons why we would not use tantalum if we were starting the experiments now, are discussed in Chapter V.

After anodization the films were either used immediately or stored in a covered beaker of water so that no deposits from the drying of the water could be formed.

3. Evaporation of SiO and Indium. To prepare for the evaporation the following cleaning process was used.

a) Wash with Aerosol OT (a wetting agent) and distilled water.

b) Wash with reagent grade acetone and distilled water.

c) Immerse in a beaker of distilled water in an ultrasonic cleaner for at least five minutes.

d) Immerse in cleaning solution (chromic acid) in an ultrasonic cleaner for five minutes.

e) Rinse thoroughly, then again immerse in distilled water in an ultrasonic cleaner.

f) Allow the film to drain; observe while draining to see that the water flows off smoothly, indicating absence of dirt and grease.

All handling during and after the cleaning procedure was with tools cleaned with acetone, to avoid contamination by grease.

The apparatus used for evaporation is shown in Figure 9 and sketched in Figure 10. The basic system was a Vacuum Electronics Corporation 4-inch system with an oil diffusion pump, nitrogen and water baffles and high vacuum valve. This system could attain a vacuum of about 10^{-6} mm Hg. in a 14" bell jar. However, as is shown in Figure 10, nitrogen pot number 1 was attached to a cold plate of copper in the top of the jar. When liquid nitrogen was in this pot the cold plate acted as a very rapid pump for condensible vapors such as water, CO_2 and pump oil. Vacuum as measured by the nude Baird-Alpert ionization gauge on the top plate was 5×10^{-8} mm Hg. The charges (indium, SiO and silver) were held in the boat holder, so arranged that each boat was rotated to the same position during its heating. Tantalum boats were used, heated by a Variac and step down transformer as shown. Over the charge was a shutter which was kept in place during degassing, but swung aside during actual evaporation.

The substrate was fixed to the copper block on nitrogen pot number 2, with high vacuum grease between to insure good thermal contact. Measurement showed that the surface of the substrate was about $110^{\circ}K$ compared to $77^{\circ}K$ for the nitrogen in the pot.

The cooling of the substrate reduced the mobility of the indium atoms, thus reducing the clumping of the material into small isolated spots. We found that the thinnest continuous films we could make were of the order of 400Å.

Just below the substrate was a rotating disc which carried the several maska necessary to form the final film. A mechanical stop insured that each mask was located in the proper position to about .005".

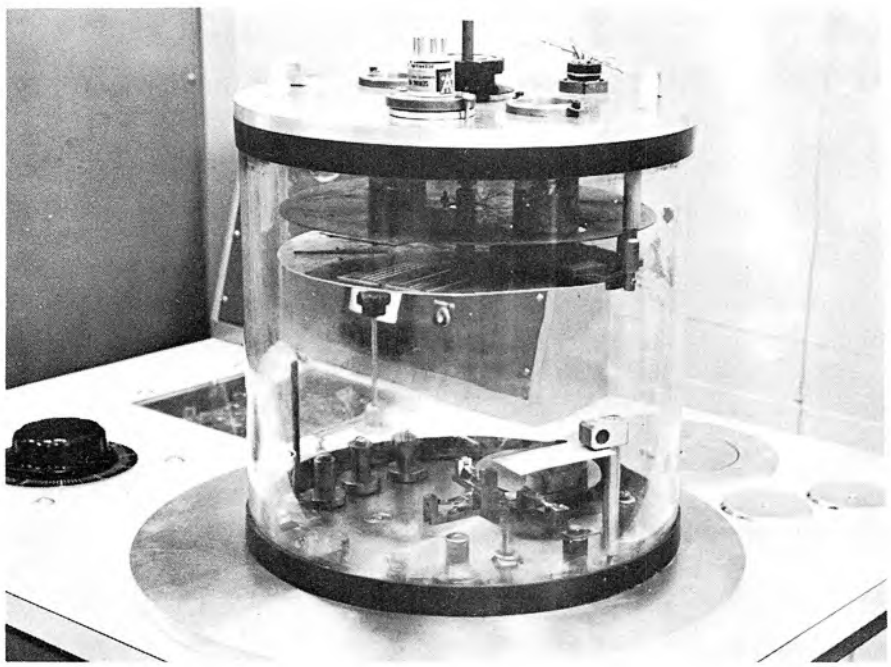

Figure 9a. Complete Evaporating Apparatus

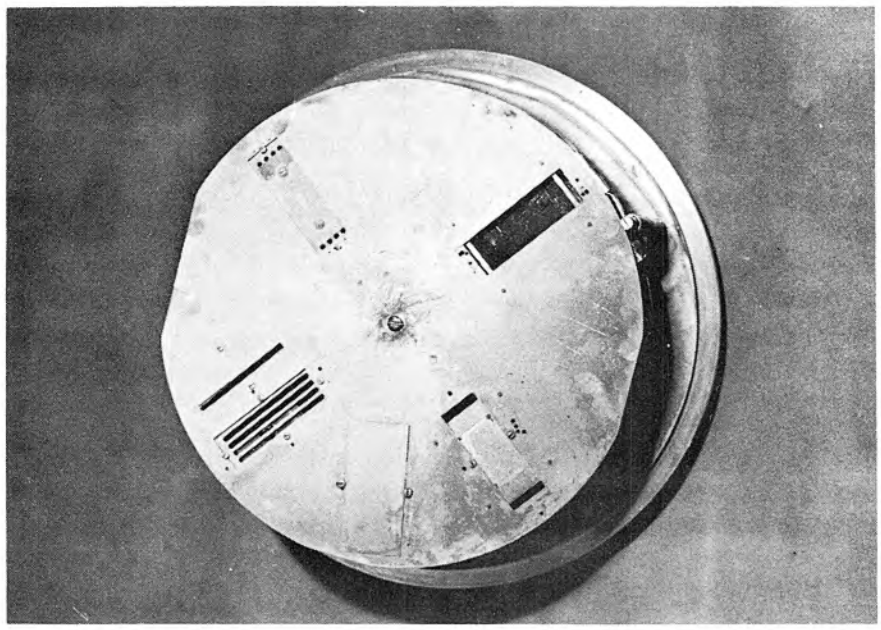

Figure 9b. Top Plate Assembly with Mask in Place.

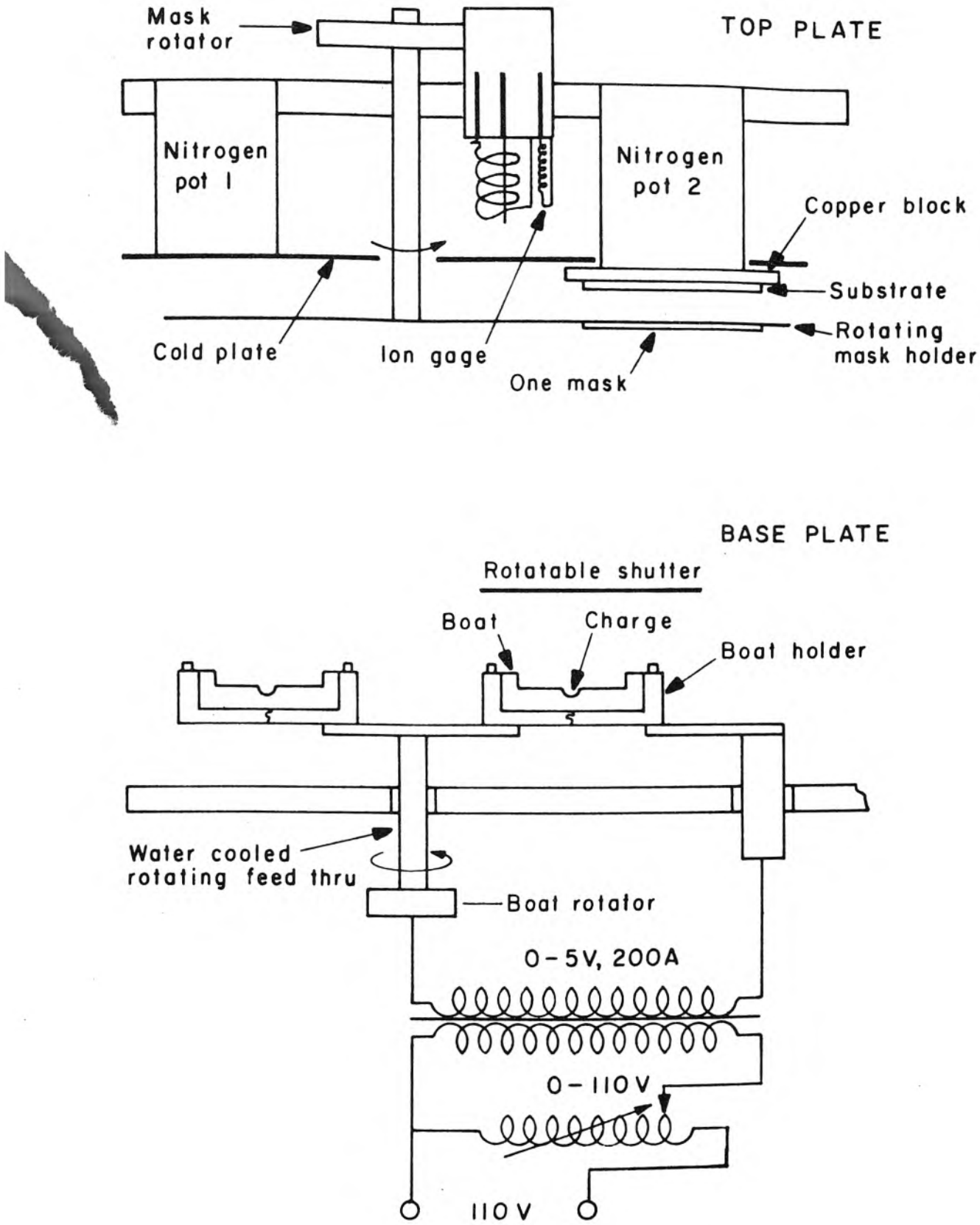

Figure 10. Vacuum Evaporation Apparatus

Omitted in the sketch for clarity is the holder for a glass slide whose resistance was used to monitor thickness during evaporation and as a calibrator for accurate measurement of thickness. This holder was a copper block attached to the cold plate by aluminum stand offs. It was parallel to and about 1.3" (center to center) from the tantalum as shown in Figure 11. The temperature of the surface of the glass was within 10° of that of the tantalum substrate.

The glass calibrator was cleaned in the same way as the tantalum and was also backed with high vacuum grease. Electrical leads 2" apart were formed on the glass with indium solder. A mask was so arranged that a strip of indium 3" long by 1/8" wide was evaporated over the leads. An ohmmeter monitored the resistance of the film continuously during evaporation, allowing us to obtain the desired thickness within $\pm$ 20% .

The sequence of events during evaporation was as follows: The tantalum boats were outgassed by heating in vacuum to white heat. The proper charges of SiO (select grade, manufactured by Kemet Company), indium (spectroscopic grade, guaranteed 99.99% pure, obtained from Johnson, Matthey and Company), and pure silver, were then placed in the boats and heated in vacuum below evaporation temperature for several minutes, then raised well above evaporation temperature long enough to evaporate perhaps one quarter of the charge. This removed most of the absorbed gases.

The top plate with cleaned substrates was then placed on the system and the system pumped down over night with liquid nitrogen in the baffle between the diffusion pump and the bell jar. Vacuum was then

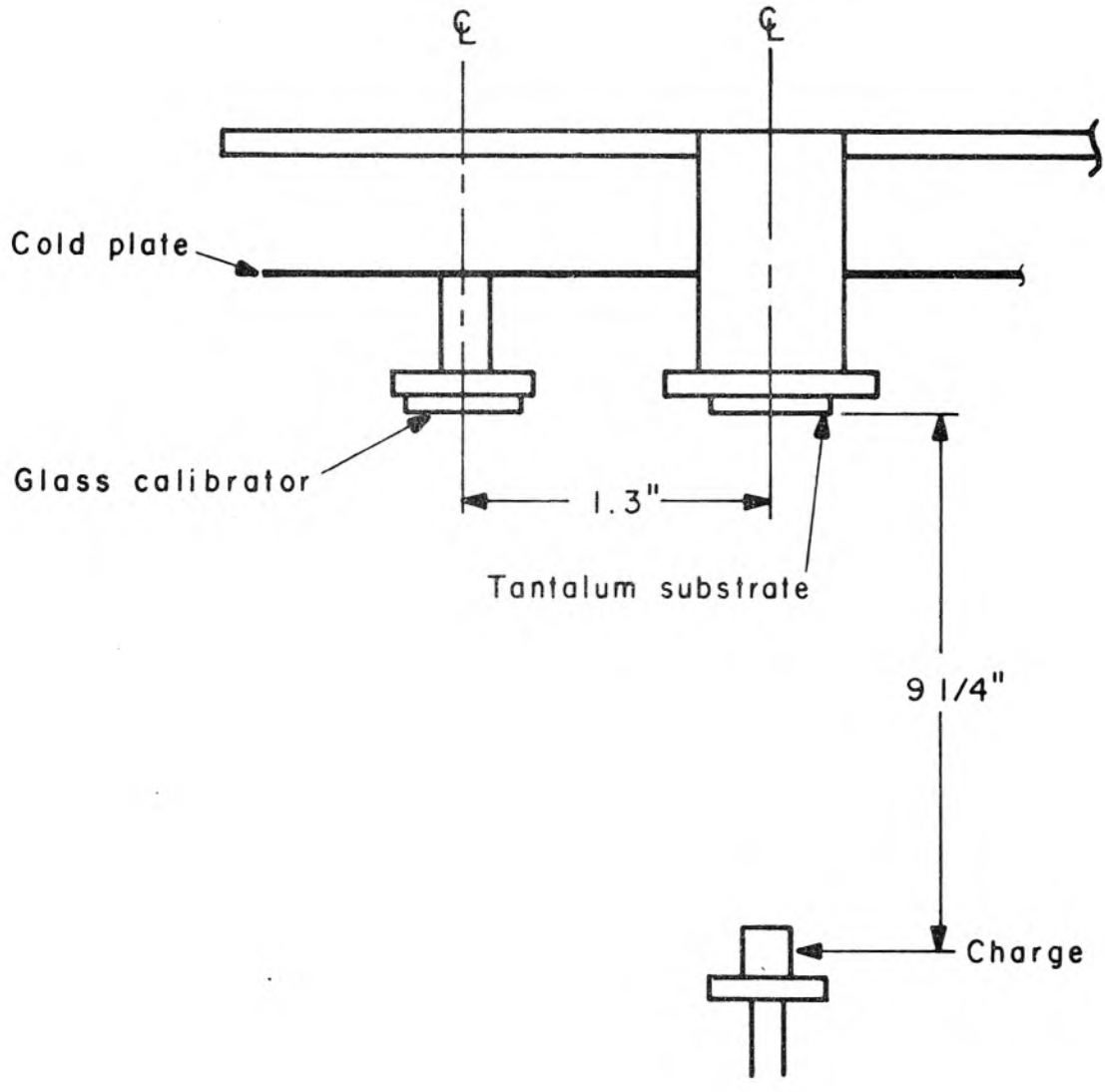

Figure 11. Evaporation Geometry

1 or 2×10^{-6} mm Hg. Liquid nitrogen was then put in pot number 1, bringing the vacuum to 5×10^{-8} mm Hg. Then SiO was evaporated to 3000 to 5000Å on the ends to form protective pads for subsequent soldering. Vacuum was usually less than 10^{-5} during this evaporation. Figure 12 shows the location of these pads. Their inside edges also serve to define the length of the resonant strip.

Liquid N_2 was then placed in pot number 2, reducing the temperature of the tantalum surface to 110°K. The indium was then evaporated in four parallel strips as shown in Figure 12. Each was 70 mm long by 3.18 mm wide (these are mask dimensions--actual dimensions are increased by parallax and finite source size and distance). Vacuum during the evaporation was usually less than 5×10^{-7} mm Hg with a properly outgassed source. For thin films, thick indium dots were also evaporated over the ends to provide enough material for soldering.

The substrate was then warmed to room temperature over a period of an hour to avoid peeling due to thermal stresses. At room temperature an overlay of SiO 3000 to 4000Å thick was put on all except the ends in order to prevent oxidation of the indium. The cold plate and calibrator were then warmed to room temperature and the two substrates removed. The completed test strip was immediately placed in a vacuum dessicator while the thickness of the calibrator was determined as described below.

4. Preparation of Test Strip for Experiment and Auxiliary Measurements. After thickness measurements of the calibrator, which took about two hours, the test strip was prepared for measurement. It was fastened in the test fixture shown in Figure 13. The copper grounding

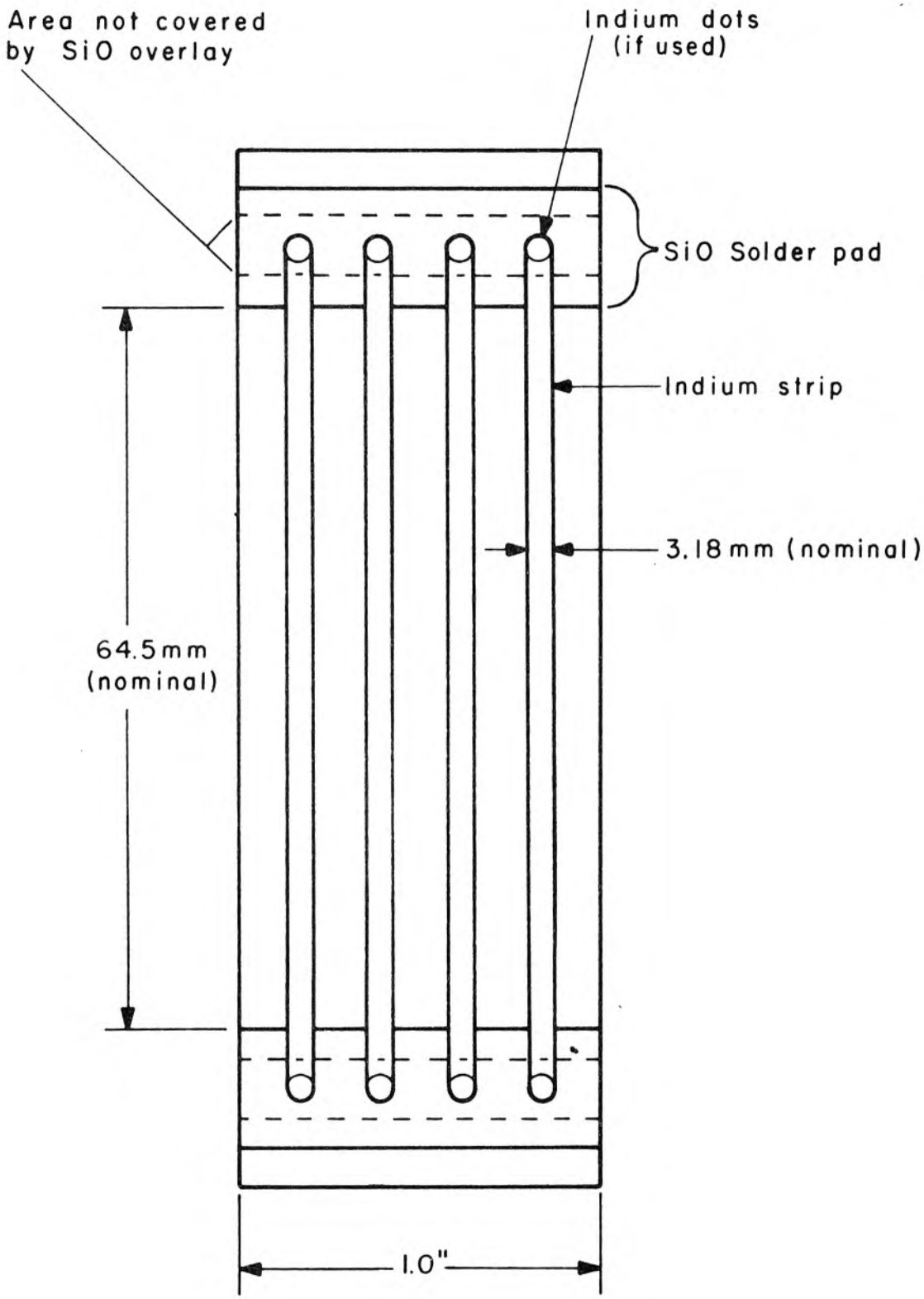

Figure 12. Completed Test Strip with Four Evaporated Transmission Lines

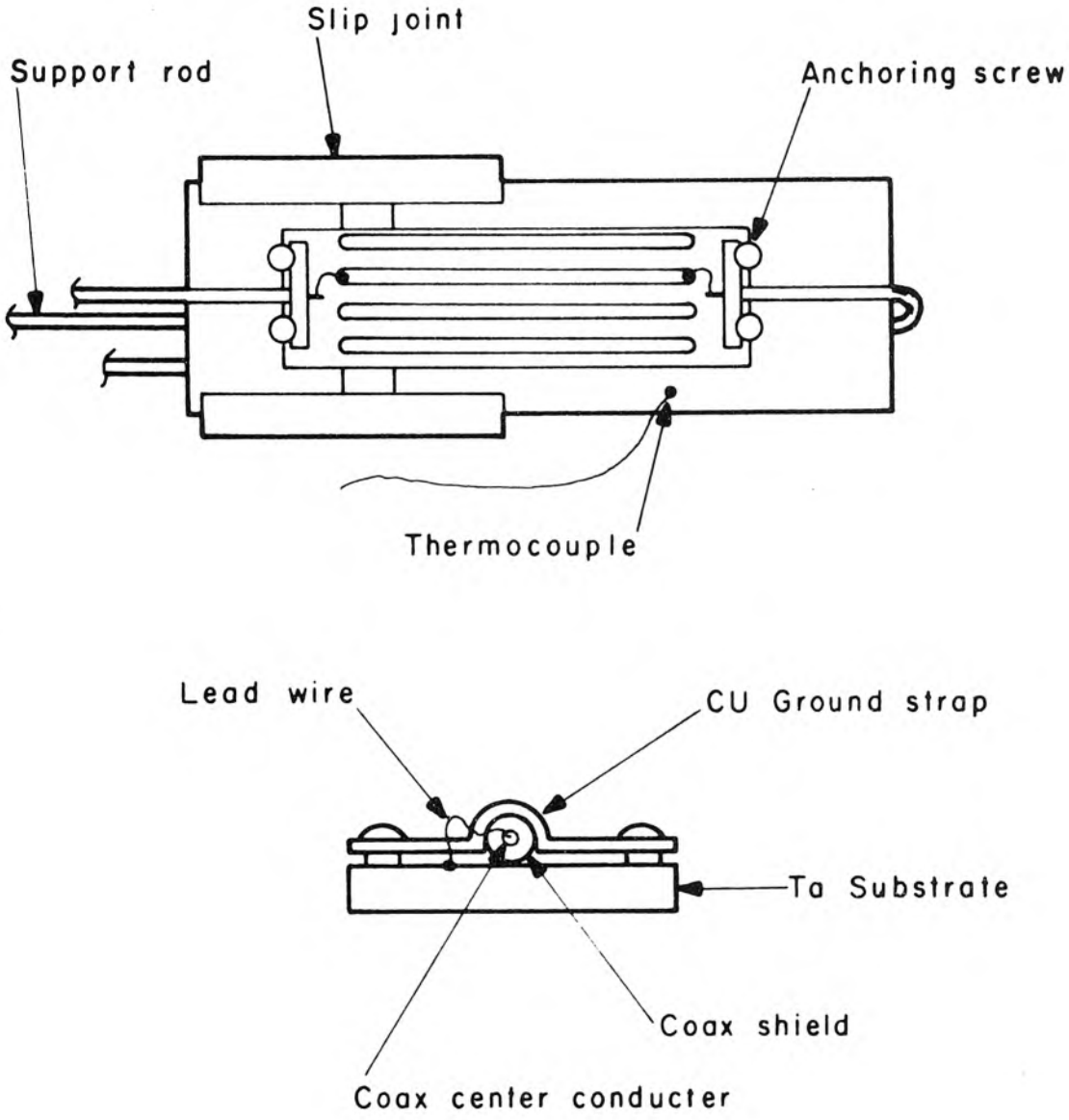

Figure 13. Test Fixture with Test Strip in Place

straps were soldered to the coaxial shield, then clamped to the scraped tantalum substrate by brass screws. The slip joint shown was necessary to allow for relative expansion of the tantalum and the bakelite fixture.

A fine wire (about No. 40) was soldered to the center conductor of the coaxial cable, carefully bent into an S shape to relieve thermal stresses, then indium soldered to the ends of an indium strip--one of the center ones if possible, but in one or two cases these were shorted.

This latter solder joint proved to be one of the major experimental difficulties, for it frequently broke when cooling to nitrogen temperature or from nitrogen to helium temperature, causing much loss of time. Apparently the rapid heat loss to the tantalum prevented high enough temperature to get a good solder joint, but if a hotter iron was used, the indium film was ruined and the indium solder badly oxidized. A partial solution was the use of a hot iron and a weak solution of rosin in alcohol as a flux, but it finally proved necessary to lower temperature from nitrogen ($77^{\circ}K$) to helium ($4.2^{\circ}K$) temperature over a period of a half hour by introducing small amounts of the helium blow-off from the storage dewar. The resistance of the indium strip was monitored as a measure of temperature [a standing wave meter was used to measure voltage drop for a constant 1000 CPS current, thus providing probably the first (and last) measurement of temperature in decibels. The resistance at $4.2^{\circ}K$ was from 5 to 7.2 db below that at $77^{\circ}K$].

After the test strip was placed in the fixture, the capacitance between the indium and tantalum, the dissipation factor, and the end to end resistance of the film were measured. The film was then placed in the test dewar, the dewar evacuated, and the system cooled to liquid

nitrogen temperature. C, D and R measurements were repeated, as they were at 4.2°K, and again in several cases at temperatures as low as 1.35°K. No measurable difference in C was seen in the latter two cases even though this might be expected when the indium became superconducting. These measurements were repeated at room temperature after the test.

Also at this time the width and length of the indium were measured by a microscope with a vernier mechanical stage. Accuracy was .05 mm. The part of the strip on the SiO solder pad was then cut from the rest and its capacitance measured.

5. Measurement of the Thickness of the Indium. We have described in the preceding section the measurement of all the important physical parameters except the resonant frequency and the thickness of the indium. The latter was measured using Tolansky's method of multiple beam interferometry (30). In essence the method is as shown in Figure 14. A half silvered mirror is placed in contact with the film to be measured, which has been overlaid with a fully reflecting coating of silver, and illuminated with monochromatic light. When viewed from the mirror side, narrow interference fringes are seen. For details one should see Tolansky's book.

In our case we could not use the test specimen directly since the tantalum was not flat enough. Instead the calibrator mentioned above, which was on a glass microscope slide, was used. The slide was flat enough over small areas to be entirely satisfactory. Also, in order to increase accuracy, a narrow channel was made in the indium by cutting through to the glass with a screwdriver blade. This was found to give far more reproducible results than measuring across the relatively broad

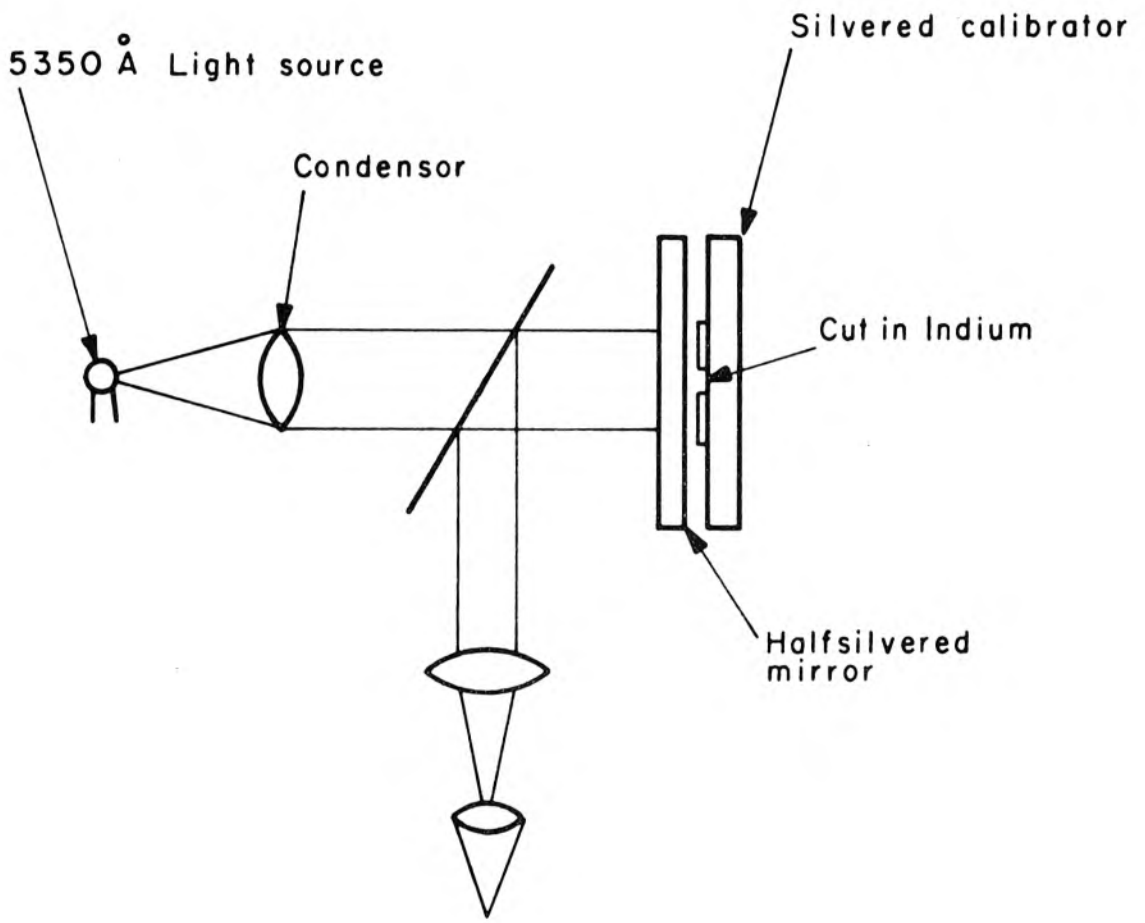

Figure 14. Multiple Beam Interferometer

edge formed by the mask. Figure 15 shows a photograph of typical interference fringes. This film is 1.64 fringes (4520Å) thick. Measurements were made on the photographs using the microscope and mechanical stage mentioned above. Typical reproducibility in readings on ten fringes was about 20Å in the thin films (5%) up to 50Å in the thick ones (1/2 to 1%). The thickness of the calibrator was increased by 3% to account for the greater distance from and tilt with respect to the source, as shown in Figure 11.

B. Cryostat and Auxiliary Apparatus

The apparatus for producing the low temperatures was entirely conventional. A glass double dewar was used with a nitrogen heat shield enclosing the helium dewar. Thermocouple leads entered through a soldered-in glass header, while the RF signals entered through BNC pressurized coaxial connectors. The helium dewar had a one-inch pumping tube attached, which connected by rubber pipe to a pressure regulator, which was simply a scaled-up version of an ordinary diaphragm regulator as described by Sommers (31). Another pipe led from the regulator to a pump, either a Welch 1397 of 6 liters/sec capacity, or a Kinney KD-110 of 50 liters/sec capacity. With the latter a temperature of 1.35°K could be reached.

A mercury and an oil manometer were connected to the system to measure helium vapor pressure and hence temperature.

C. Pulse and R.F.

1. Pulse Apparatus and Tests. In order to locate the RF resonances, we found it very helpful to use pulse techniques. The apparatus is shown in Figure 16. A Spencer Kennedy Laboratories mercury

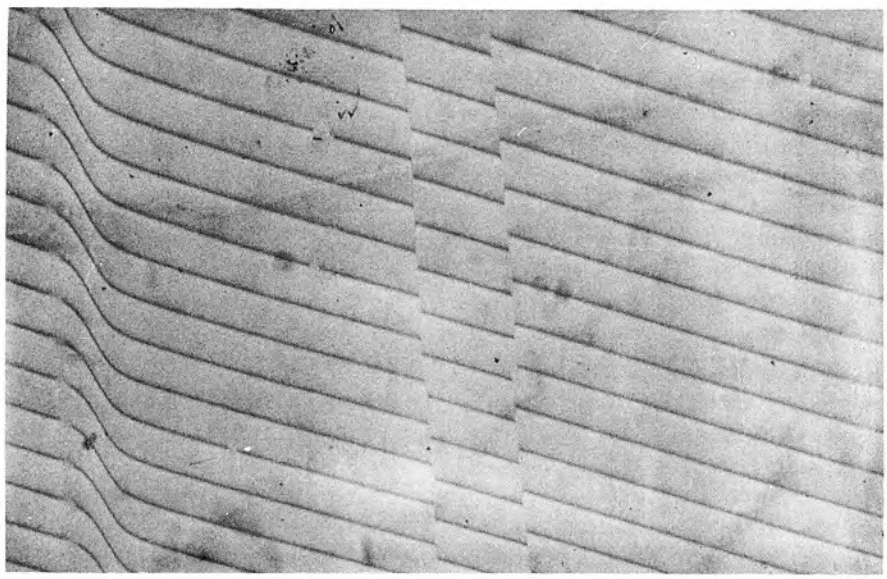

Figure 15. Multiple Beam Interference Pattern. Film about 1.64 Fringes (4520Å) Thick.

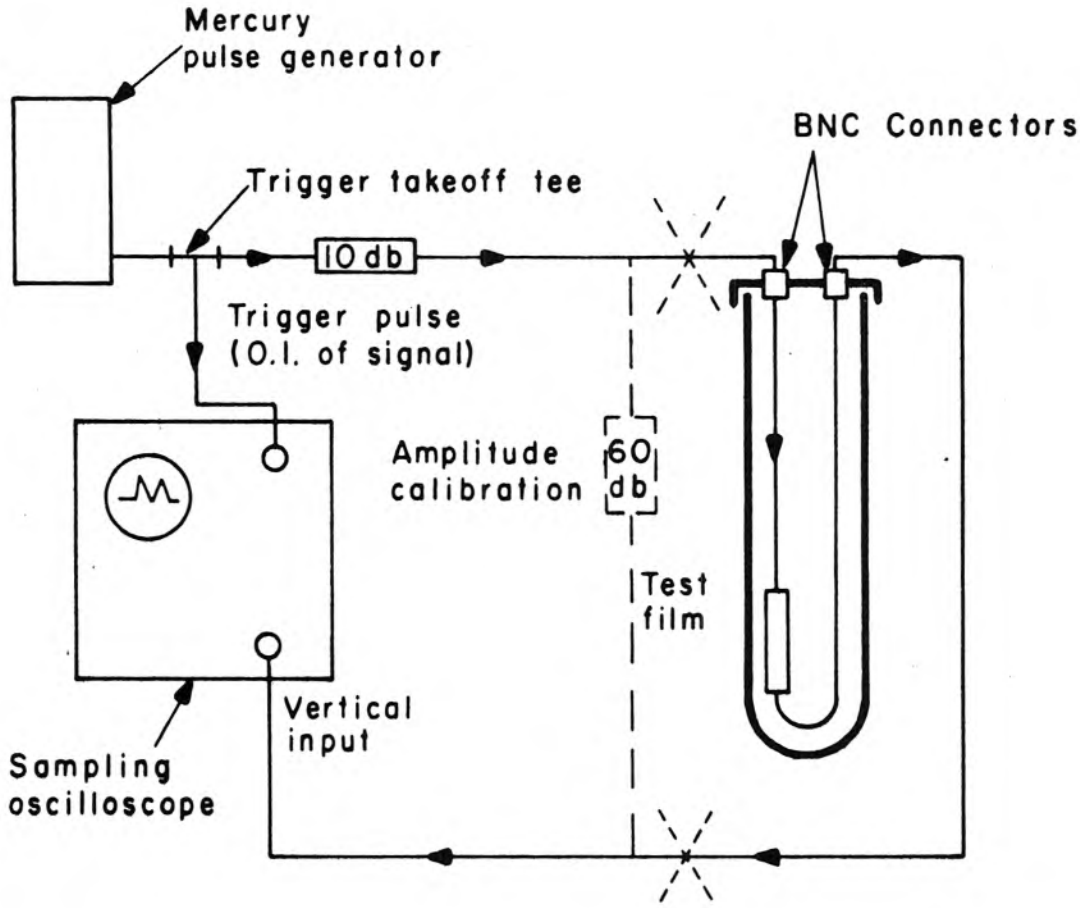

Figure 16. Pulse Test Apparatus

switch delay line pulse generator emitted a pulse about 2 nanoseconds long. This pulse was transmitted through the strip, then detected by a Lumatron sampling oscilloscope with a rise time of 0.4 nanoseconds. Both these instruments and the interconnecting coaxial cables were of 50 ohm characteristic impedance, while the test strip had a Z_o of the order of 0.001 ohm, so that the pulse was reduced to about 15 mv at the junction between the input line and the strip. Further, when it reached either end it was reflected almost completely. Thus the pulse was trapped on the line until it decayed to zero. Typical input and response pulses are shown in Chapter IV.

On the sampling scope a series of pulses spaced two transit times apart was observed. Since the line was resonant in the lowest mode when it was one-half wavelength long, the reciprocal of the observed pulse spacing gave the resonant frequency. Once one resonance was located, that at a slightly different temperature was easy to find, so the apparatus was not necessary. As a matter of interest, however, a number of photographs of pulses were made, usually at the highest and lowest test temperatures.

We could also measure the decrement and hence the expected Q of the resonant peak. In a few cases this was calculated and agreed very well with the Q measured by RF techniques.

Amplitude calibration was done by replacing the test strip by a 60 db attenuator. Comparison of the input pulse with the transmitted pulse could then be made photographically.

2. R. F. Apparatus and Tests. The RF apparatus is shown in Figure 17. A Hewlett Packard (HP)608A signal generator supplied the

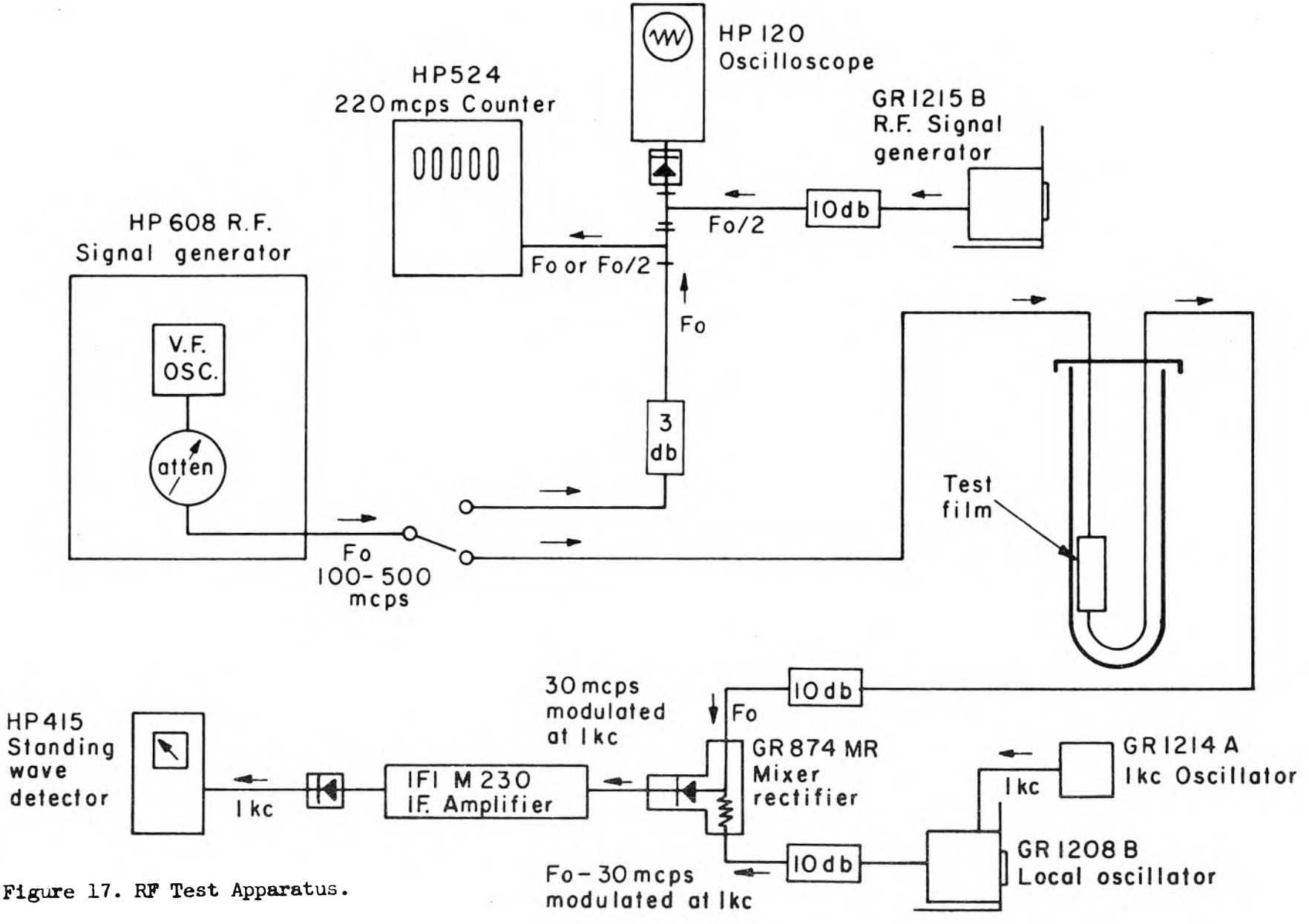

Figure 17. RF Test Apparatus.

test signal. This instrument delivered +7 dbm (0.5 volts into a 50 ohm load) at frequencies from 10 mc/sec to 500 mc/sec. It has a precision attenuator with a range from +7 dbm to -125 dbm with an accuracy of $\pm$ 0.5 db. Since the output varied considerably as frequency was changed, we added a feedback loop which monitored the output, amplified it, and then changed the bias on the output tube. With this loop in operation the output was constant within 0.1 db over the entire range.

The signal generator output passed through the test strip, then was detected on a superheterodyne receiver consisting of a General Radio (GR) 1208-B local oscillator modulated at 1000 cps, a GR874-MR mixer rectifier, an Instruments for Industry M-230 30 mc/sec IF amplifier, a HP 420B crystal detector, and finally a HP415 standing wave meter. This is a sensitive voltmeter (10^{-7}V) tuned to 1000 cps and calibrated to read decibels directly, correcting for the crystal square law characteristic. The system shown could just detect a signal of -75 dbm. The limiting factor was noise rather than gain.

Since outputs of higher than 0 dbm proved impractical, we could test only films which had less than 75 db loss. In fact our films always had less than 62 db loss. Whenever possible the source was set to -10 dbm (70 mv) in order to avoid effects of change of power, although several checks were made which showed no measurable effect.

For frequency calibration we used a Hewlett Packard 524 10 mc counter with a 525 converter head useful up to 220 mc. The counter accuracy was not necessary for resonant frequency measurements, but proved very helpful in obtaining Q measurements by finding the half

power points. Above 220 mcps the HP608 signal was heterodyned with a harmonic of a GR 1215B oscillator. An oscilloscope was used to detect frequency coincidence. The GR 1215B fundamental frequency was then measured with the counter.

Several attenuators were used to isolate the components. These reduced sensitivity, but were found necessary to prevent rapid variations in power output of the GR 1208B as frequency was changed. The sensitivity of the system shown was constant within ± 2 db over the range of 100 to 500 mcps.

All interconnecting cables were 50 ohm coaxial cables, either RG-55U or RG-58U , except in the dewar itself, where Microdot Inc. subminiature 50 ohm coaxial cable was used to minimize heat leaks into the dewar.

RF readings were made first at the highest temperature at which pulses were visible on the oscilloscope, then at successively lower temperatures. This avoided the thermal lag problems present when the temperature increased. In a few cases it proved easier to work up toward the critical temperature from a known point, since in this region the film insertion loss was greatest and Q lowest, increasing the difficulty of finding the peak. We could follow the resonant peak as the temperature slowly increased, hence we could tell that thermal equilibrium had been reached when the resonant frequency ceased moving.

To obtain readings at a given temperature, we first set the HP608 test oscillator to the expected resonant frequency with an output (in most cases) of -10 dbm. The GR 1208B local oscillator was tuned 30 mc/sec away so that the I-F amplifier output would be a maximum. We often had to search over 10 or 20 mc for the peak, a rather tedious procedure

since the test and local oscillators had to be tuned separately. The search was particularly difficult if the width of the peak was about the same as the width of the I-F amplifier bandpass, about 2 mc, since we had difficulty telling whether a given peak was due to the test strip characteristic or the I-F amplifier. Some sort of coupling between the two oscillators would have been very convenient, but as we gained skill in finding the peaks, we felt that it was not necessary to take time to do this. When the peak was found by maximizing the output signal with both the test and local oscillators, we set the gain of the I-F amplifier so that the HP415 standing wave meter read -40 db. (In this region the crystal output was very close to square law as checked using the HP608 attenuator). We then bypassed the test strip, increased the precision attenuator setting to bring the meter reading to the same point, and recorded the attenuation. (Attenuation in the coaxial leads within the dewar was 1.7 db over the frequency range of interest.) Thus the only factors involved were the short term amplitude stability of the system, the short term temperature stability (since we had to remain at the resonant peak) and the accuracy of the attenuator calibration. We checked stability by reconnecting the test strip, returning the attenuator to -10 dbm and checking that the meter reading was still -40 db. We then switched the test oscillator to the counter (or above 220 mc, to the zero beating circuit) and recorded frequency.

To determine Q we offset the test oscillator frequency (and shifted the local oscillator to match) until the reading of the meter fell 3 db, i.e., to half power. We recorded the frequency of the two half power points. Here we depended upon the accuracy of the meter,

which was checked, and the amplitude stability of the system both with respect to time and to frequency change, but these were found to be quite good. In fact the principal problem was the temperature stability of the helium bath, particularly near the critical temperature where resonant frequency changed very rapidly with temperature. A swept oscillator with visual display of the peak would have been more accurate, but suitable apparatus was not at hand, nor was it felt worth the time to build it.

For some of the early films we measured the effect of magnetic field on velocity. To generate the field we placed a solenoid outside the helium dewar in the nitrogen contained in the outer dewar. Since the solenoid was coaxial with the dewar, the generated field was nearly parallel to the film. The solenoid was about 6 inches long (about twice as long as the film) so that the field was uniform to about 3% over the film. However, our test fixture was supported only by a thin rod from the dewar cap; this was not perfectly straight, so that the fixture was not quite vertical. Hence several degrees of misalignment existed between the film and the field. As several investigators have noted [see, for example, (32)], if the thin superconducting film is not quite parallel to the field, very large demagnetization fields are generated perpendicular to the film. Since we did not have time to rebuild the fixture, we made a few preliminary measurements to explore the effect. These are discussed in Chapter IV.

IV. EXPERIMENTAL RESULTS AND DISCUSSION

A. Phase Velocity

It is convenient to divide this discussion into two parts: 1) zero temperature dependence of c/v on thickness parameters τ and d, and, 2) dependence ov c/v on temperature for fixed thickness. The first is possible because our data can be extrapolated easily to zero temperature.

1. Zero temperature results. We first discuss the extrapolation to zero temperature. As shown in Figure 18, $(c/v)^2$ varies rapidly near the critical temperature, but becomes extremely flat at the lowest temperatures, which range from $1.9^{\circ}K$ for early experiments to $1.4^{\circ}K$ later. Since the dependence of λ on temperature is very close to the form

$$\lambda = \lambda_o / \sqrt{1 - (T/T_{crit})^4} \qquad \text{(IV-1)}$$

the total variation in λ_{Ta} from $1.9^{\circ}K$ to $0^{\circ}K$ is 2%, while that of λ_{In} is 5% . The dependence of $(c/v)^2$ on the λ's is given by

$$(c/v)^2 = (K/d)(d + \lambda_{Ta} + \lambda_{In} \coth \frac{\tau}{\lambda_{In}}) \qquad \text{(IV-2)}$$

for the London local theory, but the results of the non-local theories do not differ much.

In the worst case, where τ/λ_{In} is small enough so that

$$(c/v)^2 \cong \frac{K}{d} (\frac{\lambda_{In}^2}{\tau}) \qquad \text{(IV-3)}$$

we have

$$\frac{\delta(c/v)^2}{(c/v)^2} = 2 \frac{\delta\lambda_{In}}{\lambda_{In}} \quad . \qquad \text{(IV-4)}$$

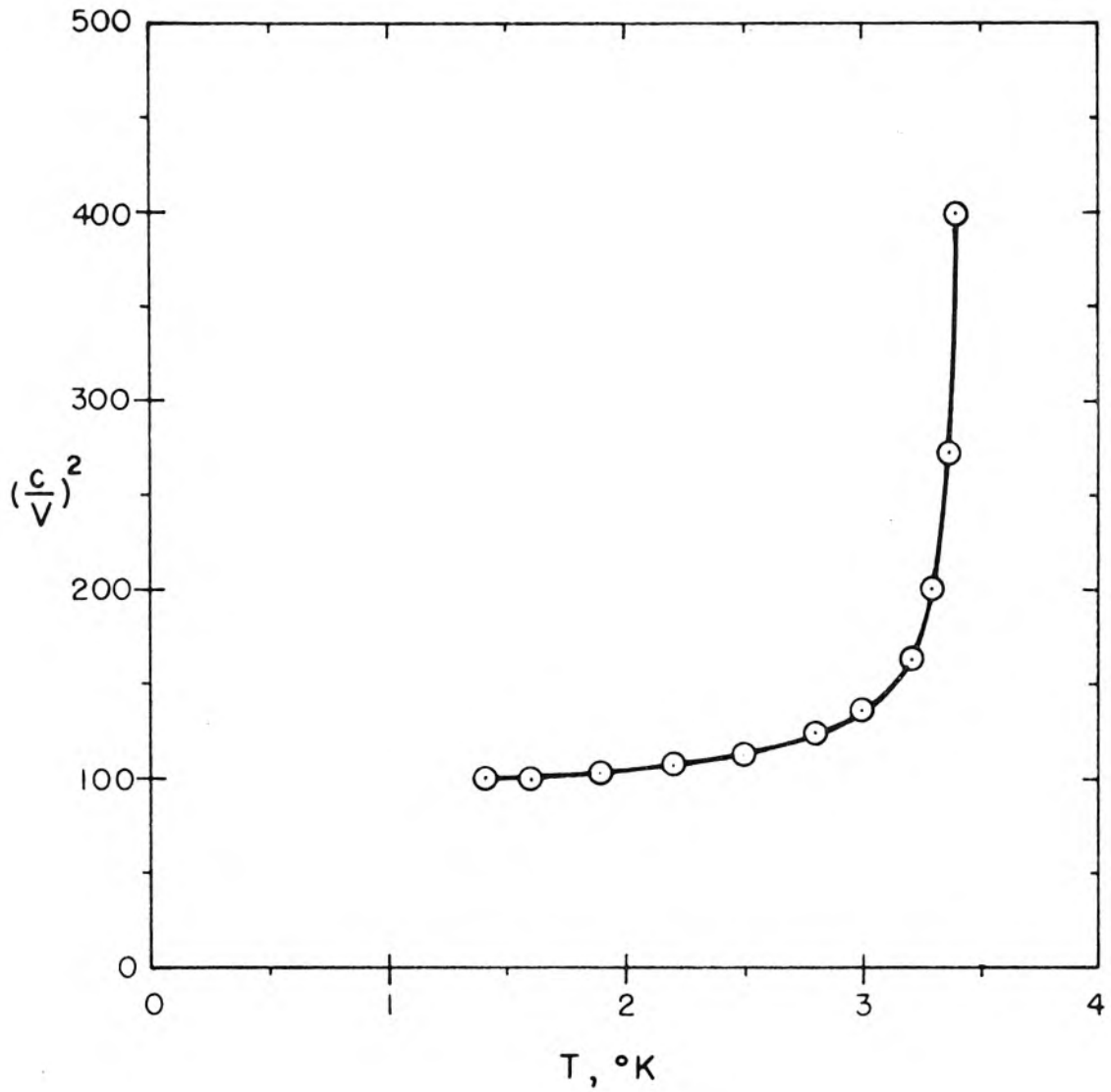

Figure 18. Experimental Dependence of Velocity Function $(c/v)^2$ on Temperature. Film 28.

A 5% change in λ_{In} leads to a 10% change in $(c/v)^2$. In fact, for the thinnest films we examined, $d \approx 300\text{Å}$ and $\tau = 400\text{Å}$, the factor multiplying $\delta\lambda_{In}/\lambda_{In}$ was close to 1 so we would expect only about 5% change in $(c/v)^2$.

To extrapolate we considered a dependence of the form

$$(c/v)^2 = \frac{K}{d}\left(d + \frac{\lambda_{Ta}}{\sqrt{1-(\frac{T}{4.38})^4}} + \frac{\lambda_{In}}{\sqrt{1-(\frac{T}{T_{crit}})^4}}\right) . \qquad \text{(IV-5)}$$

By an iterative procedure λ_{Ta}, λ_{In} and T_{crit} were chosen to fit the curve to the experimental data at three points: at the lowest measured temperature, at 2.8°K, and at the highest temperature, usually so close to the critical temperature that $(c/v)^2$ was two to four times its low temperature value. The value of this function at $T = 0$ was then taken as $(c/v)_o^2$. As might be expected, if λ_{Ta} was fixed at some arbitrary value, and λ_{In} and T_{crit} were used to fit the data at the lowest and highest temperatures, then the result was very insensitive to the choice of λ_{Ta}. Changes of λ_{Ta} from 0 to 1000Å would change $(c/v)_o^2$ by less than a percent.

The values of $(c/v)^2$ for all films are shown in Figure 19 plotted versus τ. The film identification number is shown beside each point. Theoretical curves for $\lambda_{Ta} = 580\text{Å}$ and $\lambda_{In} = 640\text{Å}$ are also shown. The solid curves are for a London material, while the dotted are for a BCS material with $\Delta k = \frac{0.186}{\lambda_{In}}$, the value used by Schrieffer (10). The penetration depths were chosen by a method described below, to be a best fit to all the data for a London material. Shown in Figure 20 is the same data but with theoretical curves drawn

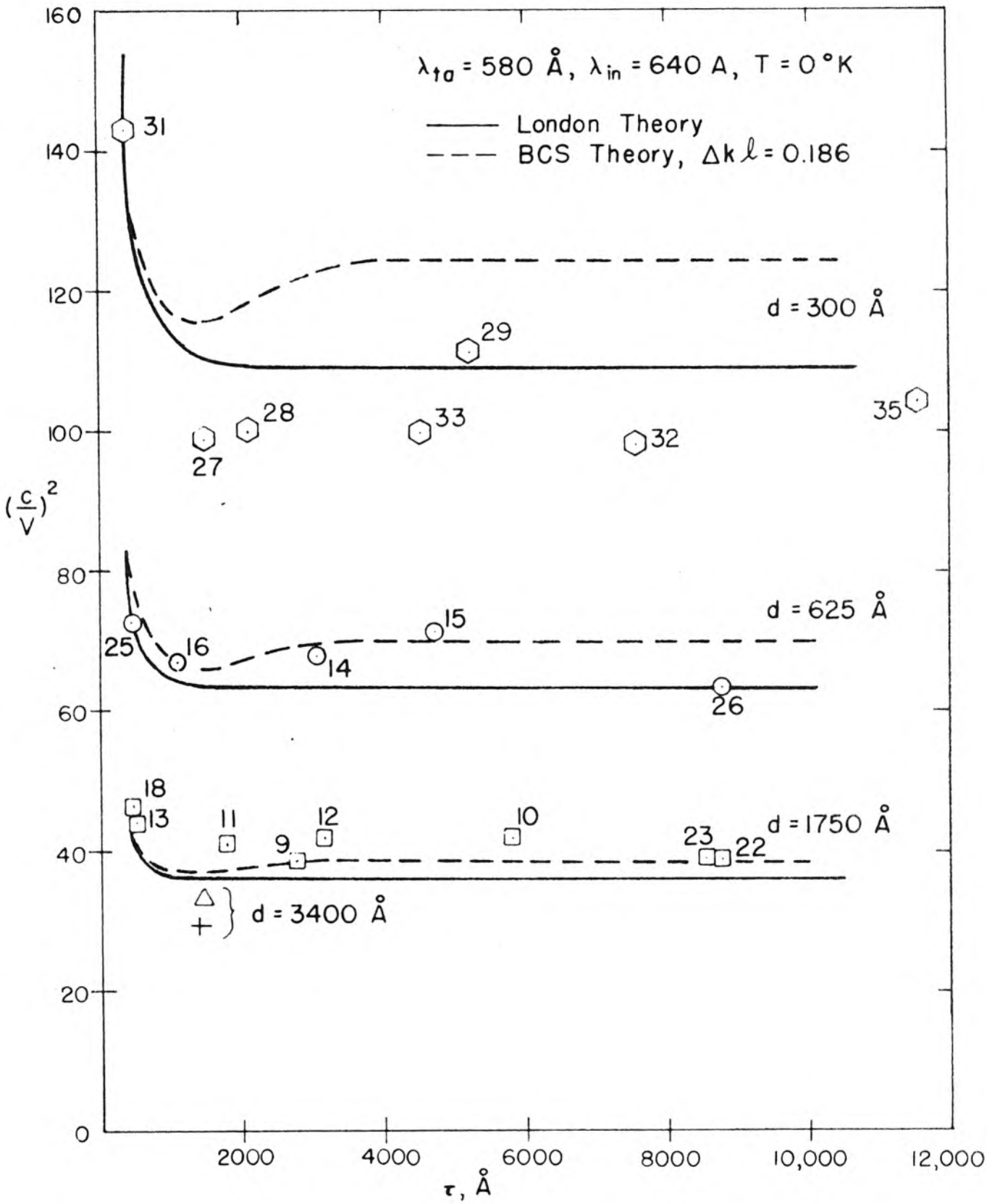

Figure 19. Comparison of Experimental and Theoretical Values of $(c/v)^2$ versus τ. λ_{In} and λ_{Ta} Averaged for All Values of d.

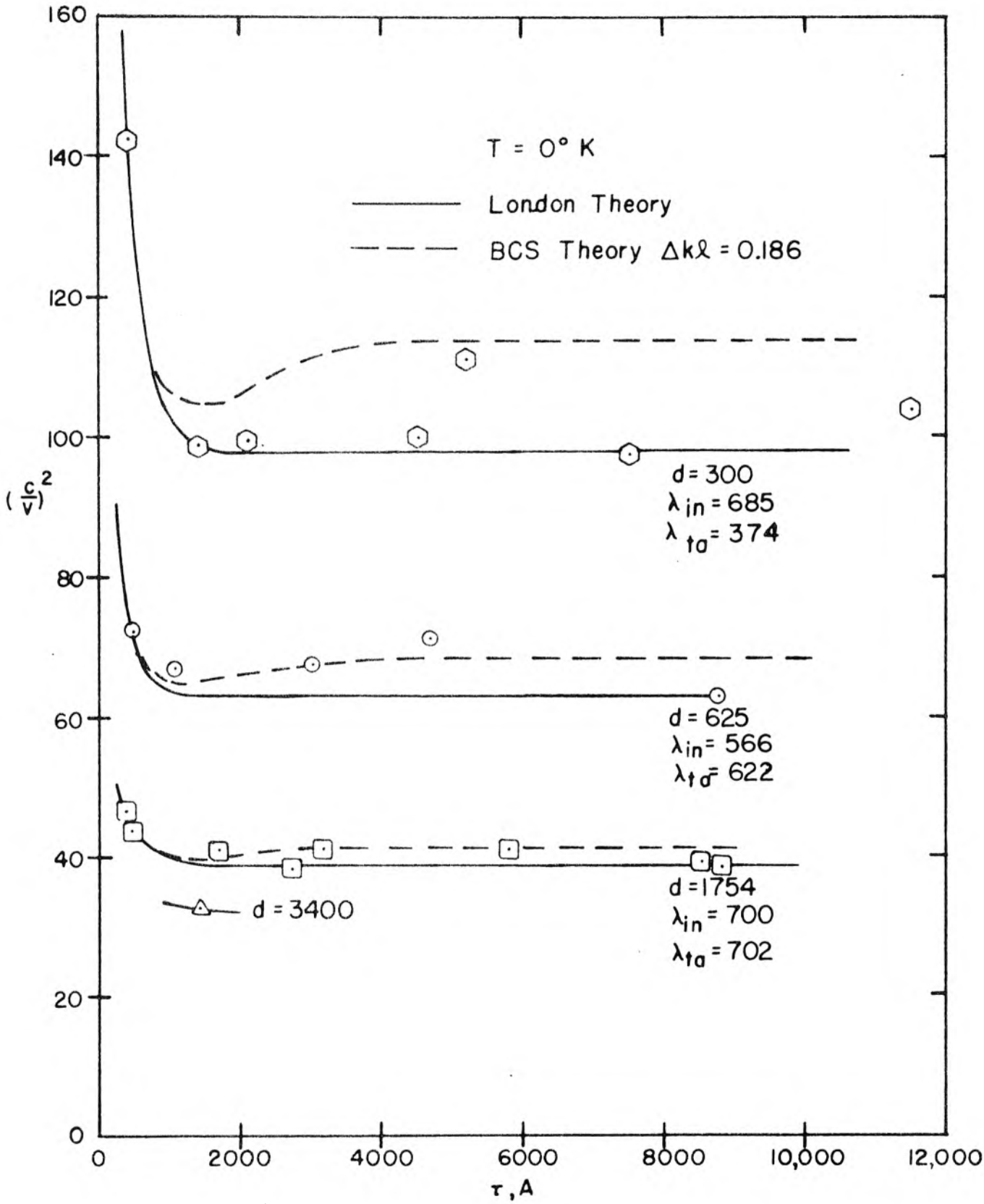

Figure 20. $(c/v)^2$ versus τ . λ_{In} and λ_{Ta} Best Values for Each Value of d

with λ_{Ta} and λ_{In} chosen for best fit for each value of d.

Three data points are particularly subject to question. These are for films 15, 27 and 29. Films 27 and 29 showed a very high and nearly constant dissipation factor of about 0.5 when measured as a capacitor at 1000 cps. This contrasted sharply with the normal film, such as No. 28, whose dissipation factor was 0.113 at room temperature but dropped to .007 at liquid nitrogen and less than .001 at liquid helium temperature. In the normal cases the dissipation was clearly due to the series resistance of the indium film, which drops in much the same ratio. Since the series resistance of films 27 and 29 showed normal behavior with temperature, we conclude that the dielectric was the source of the loss. A recheck of the preparation of 27 and 29 showed that they (and 15) were anodized, then placed in water for storage for several days before deposition of the indium strip. Apparently this affected the dielectric seriously.

The measurements of c/v showed no particular difference either in terms of temperature dependence or of the Q of the resonant peaks. However, at such a low characteristic impedance a shunt conductance of 0.2 mho/cm such as these films showed would be completely unimportant. Probably the dielectric constant of the material was affected, however, leading to the anomalous values shown for c/v.

It should be mentioned that film 15 did not show the high dissipation factor. However, the dielectric layer is more than twice as thick so that even if a 300Å surface layer showed a high conductance, the remaining 300Å would act as a good insulator, but the total dielectric

would still show an effective dielectric constant different from films prepared in the normal manner. We note that film 15 shows about half the deviation from the majority of the data that 29 does, which agrees with the hypothesis that the effect is due to the modification of the surface of the tantalum oxide by a reaction with the water. Perhaps a hydrated tantalum oxide has been formed, but we do not pretend to have investigated whether this is even theoretically possible. We simply note that very little weight should be given to these three points. After the effect was noted, film 33 was made as similar to 29 as possible but with evaporation immediately after anodization. The excellent fit of 33 with the general trend of the data shows that film 29 must be held very suspect.

The first observation to be made from our data is that $(c/v)^2$ follows the expected general trend of nearly constant value as τ is decreased, until a sharp rise commences at about $2\lambda_{In}$. Below this point the value of $(c/v)^2$ should follow a $1/\tau$ dependence. Our data is somewhat sketchy in this region but a large increase is clearly shown. The thinnest continuous film that we could make was of the order of 400Å due to the clumping of the incoming indium atoms. This well known effect results from the kinetic energy which the incoming atoms have, enabling them to bounce on the surface until they reach preferred positions on the substrate surface (33). Because the effect is reduced by low temperature of the substrate, we held ours at liquid nitrogen temperature. Liquid helium temperature would be better but much more difficult and expensive. (But not impossible; Glover and Tinkam (9) formed indium films thought to be 20Å thick by evaporation in the experimental dewar at helium temperatures). In this region the films are about 1/7

fringe thick, making accurate measurements by interferometer difficult.

The next important point to observe is that our data agree quite well with the London local theory. The minimum expected according to the non-local BCS theory (and also the Pippard theory which is so close to BCS that we have not shown a separate curve) is simply not there. If one could believe that points 27, 29 and 15 were valid, perhaps a case could be made for the non-local theory, but our reliable data clearly indicate no such effect. This is in good agreement with Lock's results which agree much better with the London theory than the BCS or Pippard theory, at least for a range large enough to be significantly different from the London case. (See Figures 5 and 6 for dependence of L_{In} on the range. Note that as ξ decreases and Δk increases the value tends to the London value.)

The London theory is equivalent to the non-local theories with range zero. The BCS and Pippard theories predict a range or coherence distance for pure metals of about 10^{-4}cm, equivalent to $\Delta k \ell \approx 0.2$ or $\xi/\ell \approx 5$. This has been verified by numerous experiments discussed by Bardeen and Schrieffer in a recent review paper (34).

Hence we conclude either that the non-local theories do not apply to our experiments (which seems unlikely) or that our materials differ from those of other investigators in some way which affects the range. The most obvious difference is in the purity of the deposited film. As Pippard (6) points out, a small amount of impurity (of the order of 3% indium in tin in his experiment) will double the penetration depth. In fact this unexpected effect led him to propose the original non-local theory. He postulates a coherence distance of the

order of 10^{-4} cm. He then supposes that the impurities act to reduce this distance according to the formula

$$\frac{1}{\xi} = \frac{1}{\xi_o} + \frac{1}{\alpha \ell} \qquad \text{(IV-6)}$$

where ℓ is the mean free path of a superelectron in the metal and α is an experimentally determined factor near 1 . If ℓ is infinite, $\xi \to \xi_o$, but if ℓ is reduced either by impurities which act as scattering centers or by a smallest dimension of the sample which is of the order of ξ_o , then ξ is reduced. That our conditions of evaporation do not yield a pure film is verified by Caswell (35), who found that a vacuum of the order of 10^{-9} mm Hg is necessary if the superconducting properties of thin tin films are to be those of the bulk metal. Our vacuum was at best 10^{-7} mm Hg during evaporation and typically 5×10^{-7}. We do not have a system at present which can reach the necessary vacuum, so we cannot examine the effect of a better vacuum.

A second way in which our films differ from the bulk material is that there may be large strains in the material. It is well known (45) that vacuum deposited materials are highly strained. Furthermore, Lock (16) showed that the strain affects the critical magnetic field and critical temperature of thin films. However, he also found that the penetration depth and critical field were not much affected by the strain. It is not unreasonable to expect that any strain effect would vary with thickness. We do anneal our films by bringing them to room temperature before measurements are made. We see a definite effect on the nitrogen temperature resistance, which is lower when the film is at

nitrogen temperature just before addition of helium. Perhaps annealing at a temperature nearer the melting point of indium would improve the strain relief.

We cannot completely rule out the effect of the tantalum substrate on $(c/v)^2$, but it seems that it should add random scatter to the data rather than cancel a definite trend.

Another possibility is that the surface roughness of the indium affects the value of $(c/v)^2$. Electron micrographs (46) show that films which are just thick enough to be continuous are quite irregular due to the clumping effect mentioned earlier, but that as the films become thicker they tend to smooth out. Since this smoothing occurs just about 400Å, and since this is the region in which we expect the minimum, it is possible--though unlikely--that the effect of surface roughness just cancels that of the non-local theories. This question could be answered by making depositions of thinner films at lower temperatures and by electron micrographs of the surfaces. The dependence of the $(c/v)^2$ on d, the thickness of the anodized layer, is shown in Figure 21. Since we may write

$$\left(\frac{c}{v}\right)^2 = K\left(1 + \frac{\lambda_{Ta} + L_{In}(\tau,\lambda_{In})}{d}\right) \qquad \text{(IV-7)}$$

it is natural to plot $(c/v)^2$ versus $1/d$, which should result in a straight line of intercept K on the ordinate, and with slope $K\left(\lambda_{Ta} + L_{In}(\tau,\lambda_{In})\right)$. L_{In} is an expression which is constant for fixed d, but depends on τ/λ_{In}. For a London material, i.e., one in which the range is zero, $L_{In} = \lambda_{In} \coth \frac{\tau}{\lambda_{In}}$. The resulting curves are shown for $\tau = 402$, 1500, and 8800Å. Also shown are the theoretical lines for $K = 21.5$, $\lambda_{Ta} = 580$Å, $\lambda_{In} = 640$Å.

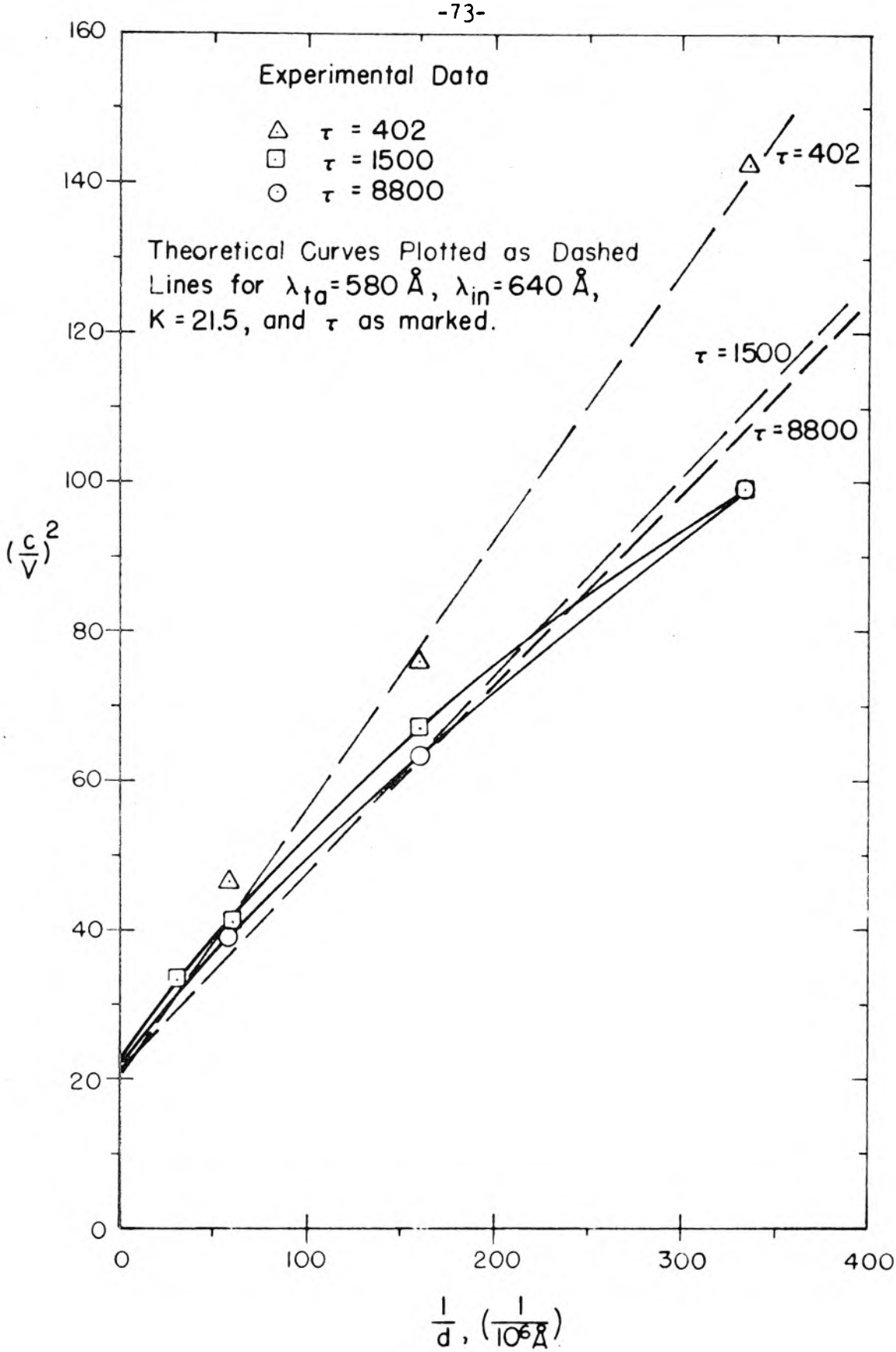

Figure 21. Comparison of Experimental and Theoretical Values of $(c/v)^2$ versus $1/d$.

The data fits the experimental curves extremely well for $\tau = 402\text{Å}$, but shows distinct curvature for the larger τ's. However, the theoretical line is close to a best linear fit to the data.

All curves tend to an intercept quite close to the value of 21.5 which agrees well with value of K obtained as discussed below. In order to extend the data to smaller 1/d, one film was made with a value of $d = 3400\text{Å}$ and with $\tau = 1500\text{Å}$. This is film 34 on Figure 19.

The value of K is obtained from measurements of capacitance at 1000 cps by conventional bridge techniques. Since C varies with temperature, the values used were those found at 4.2°K. Since

$$C = \frac{K}{d} \cdot A \qquad \text{(IV-8)}$$

and since A, the area, is known by measurements on the film, K/d can be calculated. We assume that

$$d = d_o + 16\text{Å/volt}\ V_{anod} \qquad \text{(IV-9)}$$

(see equation III-1). d_o is an unknown to be determined from our data. Combining equations 8 and 9, we have

$$\frac{A}{C} = \frac{d_o + 16(\text{Å/v})V_{anod}}{K} \quad . \qquad \text{(IV-10)}$$

Thus if we plot A/C versus V_{anod} we should obtain a straight line whose intercept on the ordinate is d_o/K and whose slope is 16/K. We used a least-squares fit of our data for all films to obtain a slope of .744 with a standard deviation of .012 and an intercept of 6.41 with

a deviation of .98 . These yield $K = 21.5 \pm .3$ and $d_o = 138\text{Å} \pm 21$. Using this least-squares data we also obtain best values for d and K/d for the various anodizing voltages. These are summarized in Table IV-I.

V_{anod}, V	d_{anod}, Å	K/d, /Å
10.05	300	13.89
30.5	625	29.11
101	1755	81.55
204	3400	158.2

Table IV-I. d_{anod} and K/d for various anodizing voltages.

We also wish to deduce from the values of $(c/v)_o^2$ the values of λ_{Ta} and λ_{In} at $T = 0$. To do this we must assume a functional form for the dependence of L_{In} on τ . Since our data seems to agree with the London theory best, we shall use it. We have then

$$\frac{d}{K}\left(\frac{c}{v}\right)^2 - d = \lambda_{Ta} + \lambda_{In} \coth \frac{\tau}{\lambda_{In}} \quad . \qquad \text{(IV-11)}$$

Thus a plot of $\frac{d}{K}\left(\frac{c}{v}\right)^2 - d$ versus $\coth \frac{\tau}{\lambda_{In}}$ should yield a straight line of slope λ_{In} whose value for large τ/λ_{In} , i.e., $\coth \tau/\lambda_{In} = 1$, is $\lambda_{Ta} + \lambda_{In}$. Since we do not know λ_{In} , to enter in $\coth \tau/\lambda_{In}$ we must assume a value, plot the line, then measure the slope. The value of the slope is used as a new value of λ in the $\coth \tau/\lambda_{In}$ expression. After a few cycles the process converges on λ_{In} . The data points,

first line, and final line are shown in Figure 22 for $d = 300\text{Å}$. Results are summarized below:

d, Å	λ_{In}, Å	λ_{Ta}, Å
300	685	374
625	566	682
1755	700	702

Table II

The average λ_{In} is 650Å, remarkably close to Lock's value of 640Å. Average λ_{Ta} is 580Å. We can say that λ_{In} is 650 ± 75Å, while $\lambda_{Ta} = 580 \pm 175$. Apparently the iterative procedure forces the λ_{In} to be consistent while the λ_{Ta} is forced to absorb the deviation of $(c/v)^2$ from expected linear dependence on $1/d$.

The points for $\tau = \lambda_{In}$, where coth τ/λ_{In} becomes large are most important in determining slope. More data in this region would make the result more accurate.

2. Temperature Dependence of $(c/v)^2$. We have shown in Figure 18 a typical plot of $(c/v)^2$ versus temperature. We wish to fit the experimental curve to an equation of the form

$$\frac{d}{K}\left(\frac{c}{v}\right)^2 - d - \frac{\lambda_{Ta}}{\sqrt{1-\left(\frac{T}{4.38}\right)^4}} = \lambda_{In}(T)\, G\left(\frac{\tau}{\lambda_{In}(T)}\right) \coth\left(\frac{\tau}{\lambda_{In}(T)}\right) . \qquad \text{(IV-12)}$$

The factor $G(\tau/\lambda)$ is simply a computational convenience. If $G(\tau/\lambda) = 1$ the right hand side of equation 12 (which we call L_{In}) is that derived

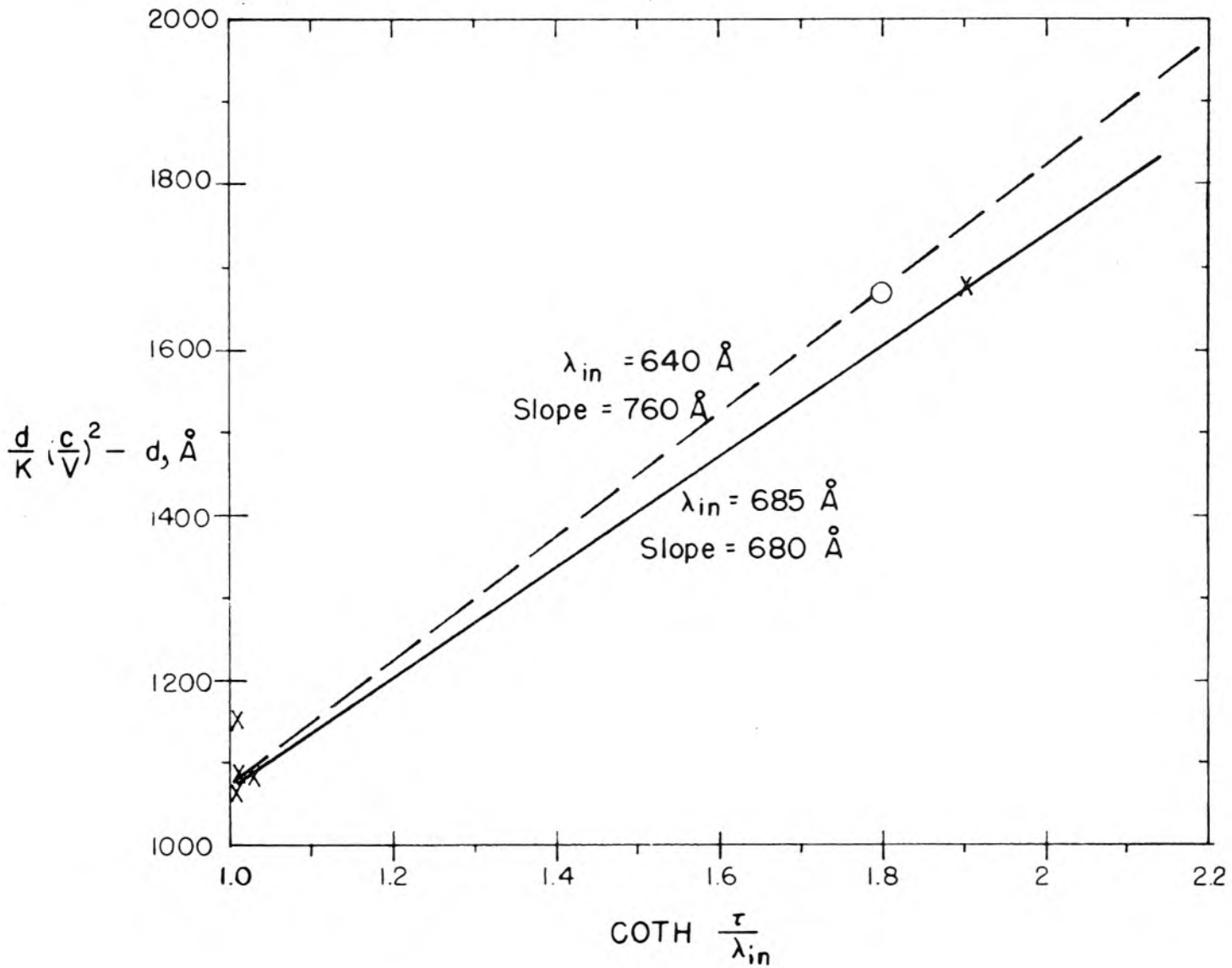

Figure 22. Graphical Calculation of $\lambda_{In}(0)$ from Data Extrapolated to Zero Temperature. Film 10.

from the London theory. By suitable choice of $G(\tau/\lambda)$ we can approximate L_{In} for any value of $\Delta k\ell$ of the BCS theory. In particular, for $\Delta k\lambda = 0.186$, we found that if we chose

$$G(\tau/\lambda) = 1.1574 + 0.1715 \tanh [0.525(X - 2.90)] , \qquad \text{(IV-13)}$$

then $G(\tau/\lambda) \coth(\tau/\lambda)$ fit the exact value of L_{In}/λ for the BCS theory given by equation II-42 within 2%. Since the exact expression is a slowly convergent infinite series, it is convenient to use $L_{BCS}/\lambda = G(\frac{\tau}{\lambda}) \coth (\frac{\tau}{\lambda})$ for machine computation.

We will assume that

$$\lambda_{In}(T) = \frac{\lambda_{In_o}}{\sqrt{1 - (T/T_{crit})^4}} = \lambda_{In_o} y \ . \qquad \text{(IV-14)}$$

That is, we assume the Gorter-Casimir two-fluid model rather than the BCS model. As discussed in Chapter II, the difference is small, and the experimental evidence seems to fall between the two.

The basic data we wish to obtain are the values of the penetration depth, λ_{In_o} and the critical temperature of the indium films, T_{crit}. We would like to obtain λ_{Ta} also, but as we shall show, the technique we use is extremely insensitive to λ_{Ta}. This is fortunate, however, since λ_{Ta} is not known except by the methods of part 1 and it would be quite difficult to extract λ_{Ta} as well as λ_{In_o} and T_{crit} from the temperature data.

We follow a method devised by Lock (16) to obtain T_{crit} and λ_{In_o}. In brief, we first plot $1/\lambda^2(T)$ versus T^4 to obtain T_{crit}.

Using this value we then plot L_{In} versus x to obtain λ_{In_o}. These are defined by

$$L_{In} = \frac{d}{K}\left(\frac{c}{v}\right)^2 - d - \frac{\lambda_{Ta}}{\sqrt{1-(T/4.38)^4}} \qquad \text{(IV-15)}$$

and

$$x = y\, G\left(\frac{\tau}{\lambda_o y}\right) \coth\left(\frac{\tau}{\lambda_o y}\right) \quad . \qquad \text{(IV-16)}$$

(For convenience we write $\lambda_o = \lambda_{In_o}$ for the remainder of this section.)

To obtain T_{crit} we note that equation 14 may be rewritten

$$\frac{\lambda_{In_o}^2}{\lambda_{In}^2(T)} = 1 - \left(\frac{T}{T_{crit}}\right)^4 \quad . \qquad \text{(IV-17)}$$

Thus a plot of $1/\lambda_{In}^2$ versus T^4 should intercept the T^4 axis at T_{crit}^4. While the actual data does not yield the theoretical straight line, an accurate curve may be drawn through the data to obtain the intercept. Figure 23 shows the curve for film 10. For machine computation we fit a quadratic through the three points nearest the T^4 axis.

To obtain λ for the above plot we solved the following equation for each $[(c/v)^2, T]$ data pair.

$$\lambda(T) = \frac{L_{In}}{G\left(\frac{\tau}{\lambda(T)}\right) \coth\left(\frac{\tau}{\lambda(T)}\right)} \quad . \qquad \text{(IV-18)}$$

Equation 18 results from calculating L_{In} from equation 15, then substituting in equation 12. To solve equation 18 we assumed $\lambda(T) = 640\text{Å}$ on the right side, calculated $\lambda(T)$, then used the new value of $\lambda(T)$ on

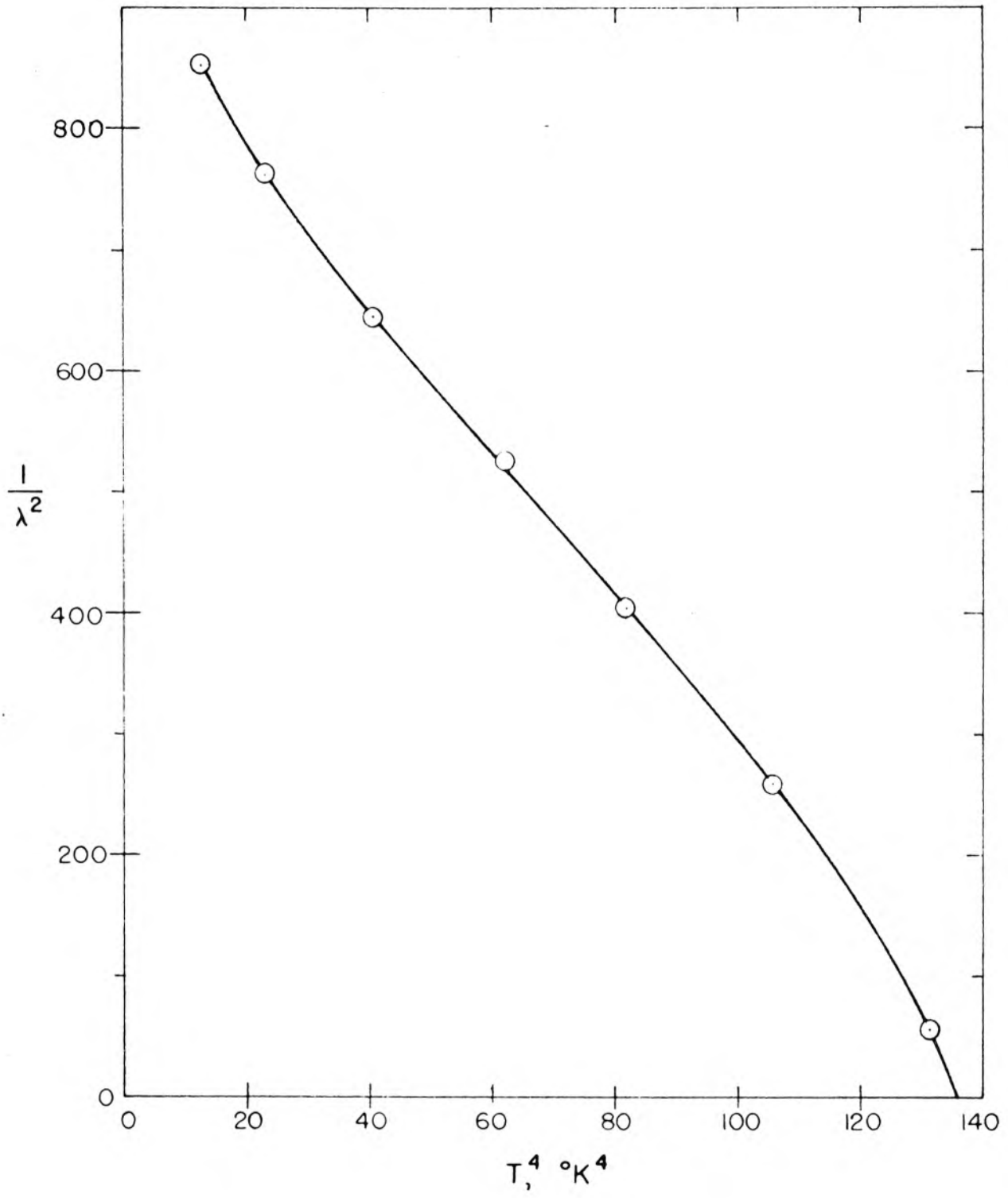

Figure 23. Determination of T_{crit} for Film 10

the right. Since G and coth were slowly varying functions in the range of interest, the process converged to the solution in three or four iterations.

Having obtained T_{crit} we now found λ_o by the following method. Note that equations 12, 14 and 16 may be combined to obtain

$$L_{In} = \lambda_o x \quad . \tag{IV-19}$$

Hence the slope of a plot of L_{In} versus x should be λ_o. Since x depends on λ_o, we must again use an iterative procedure.

The actual computation was done using a digital computer. A least-squares fit was made to the data of L_{In} versus x with the constraint that the curve go through the point $0,0$. The resulting plot and least-squares fit is shown in Figure 24. Since the value of λ_{Ta} is uncertain, the data was computed for λ_{Ta} ranging from 400 to 1000. We also computed σ_{LSQ}, the standard deviation of the least-squares fit for each film. The average value of λ_o and the average σ_{LSQ} for all films is shown in the tables below. Also given is the σ_{λ_o} which is the standard deviation of the values of λ for all films. σ_{LSQ} measures the accuracy of fit to equation 19, while σ_{λ_o} gives the spread of λ_o for the different films.

Table IV gives the data assuming a London material (one with $\Delta k\, \lambda_{In} = \infty$), while Table V assumes a BCS material with $\Delta k\, \lambda_{In} = 0.186$, i.e., a range of 5.38 times the penetration depth, or about 3500Å.

The value of λ_o shows a steady decrease as λ_{Ta} is increased. The total range from 730 to 679Å for λ_{Ta} ranging from 400 to 700Å (the range found in part 1) is well within the smallest σ_{λ_o} value, 115.

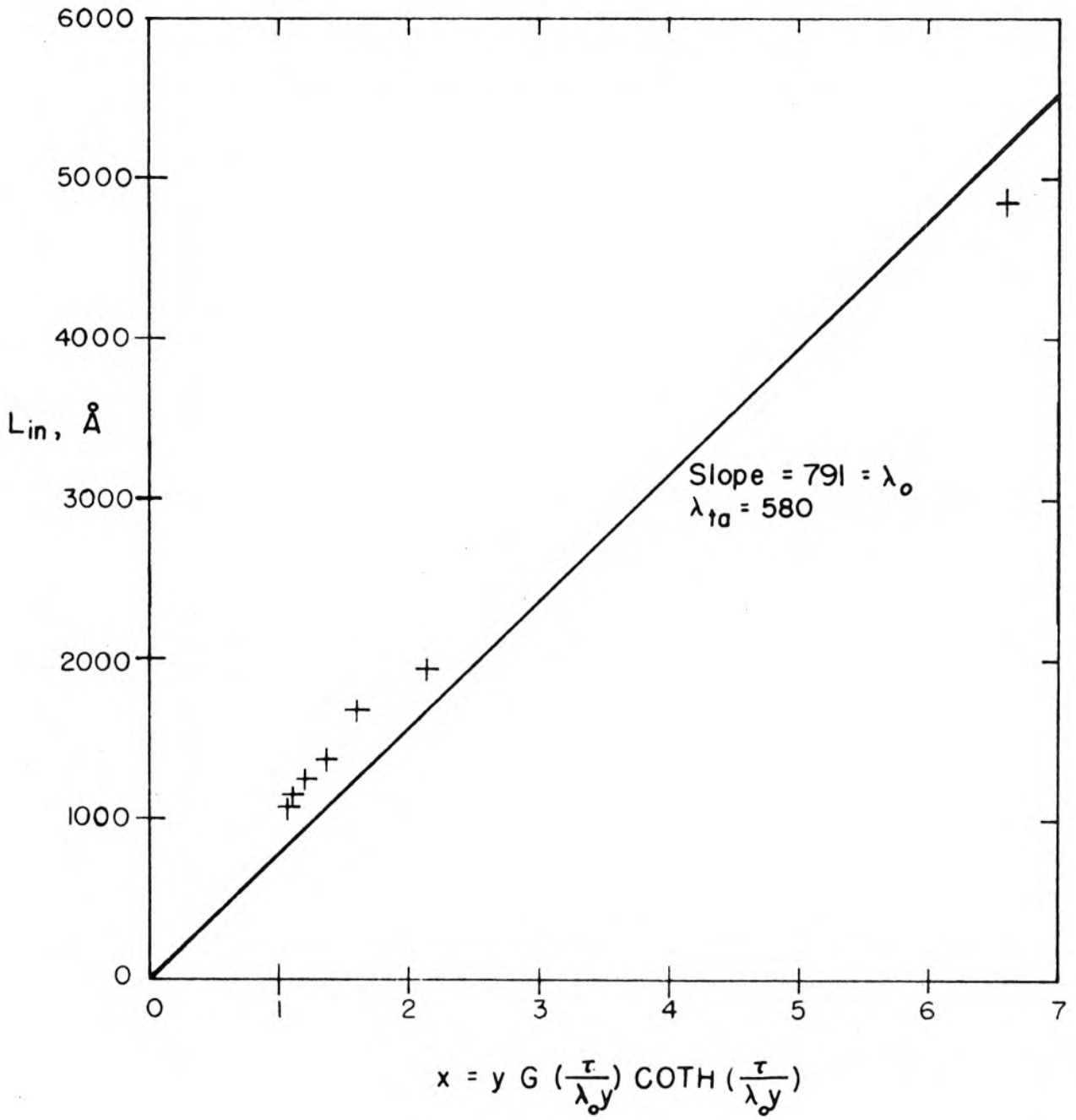

Figure 24. Graphical Calculation of $\lambda_{In}(0)$ from Dependence of $(c/v)^2$ on Temperature. Film 10.

λ_{Ta}, Å	$\bar{\lambda}_o$, Å	$\bar{\sigma}_{LSQ}$, Å	σ_{λ_o}, Å
400	730	27	143
500	717	22	128
580	704	18.6	120
600	700	18	118
700	679	16.3	115
800	655	16.1	115
900	629	17.6	120
1000	601	20.4	127

(Average λ_{Ta})

Table IV. λ_o from Temperature Data, London Theory

The value of λ_o for the average λ_{Ta} (580Å) is 704 ± 120Å . This agrees fairly well with the zero temperature value obtained in Part 1, of 650 ± 70Å .

We have included three values outside the range of λ_{Ta} , at 800, 900 and 1000Å to show that both σ_{LSQ} and σ_{λ_o} show a broad minimum in the vicinity of λ_{Ta} = 700 to 800Å. This tends to show, although not very strongly, that λ_{Ta} should be larger than 580Å.

λ_{Ta}, Å	$\bar{\lambda}_o$, Å	$\bar{\sigma}_{LSQ}$, Å	σ_{λ_o}, Å
400	685	19.1	128
580	648	13.6	132
800	595	16.0	147

Table V. λ_o from Temperature Data, BCS Theory
$\Delta k\ \lambda_o = 0.186$

Again we note a decrease in λ_o as λ_{Ta} is increased. All values lie about 50Å below those for the London theory. The minimum $\bar{\sigma}_{LSQ}$ is

somewhat smaller, but the σ_{λ_o} is slightly larger, so we cannot make a very strong case for either theory.

In Table VI we present a summary of the results for each film, on the assumption that $\lambda_{Ta} = 580\text{Å}$, the value deduced in Part 1. For the BCS theory we assumed $\Delta k\lambda_{In_o} = 0.186$. The values from the London theory are fairly close to those from the BCS for τ small, but deviate increasingly as τ increases. This agrees with the fact that the L_{LOND} and L_{BCS} approach each other for small τ/λ. Since λ increases with temperature, the agreement is best for high temperatures. Thus the difference between the two at larger τ's is due primarily to the low temperature behavior of the metal.

The values of λ_o for the London case fall in the range 500Å to 791Å except for films 12 and 23.2. Film 23.2 was a second run of film 23, and data was taken at only a few points so that we can probably disregard it. In particular, no data near the critical temperature (which is most important in determining λ_o) was taken. The data of 23.1 shows a critical temperature of $3.349^{\circ}K$ which is probably much more accurate than the value of 3.407 obtained from 23.2. Film 12, however, was a perfectly normal film. We have checked over our experimental data carefully, but have failed to find any reason for its wide deviation, 340Å, from the average λ_o. Since the standard deviation of λ_o over all films is 120Å, we cannot discard the point entirely, but we do regard it with some suspicion.

The critical temperatures derived using the two theories agree within 1 or 2 millidegrees in most cases. For a few of the thickest films it is somewhat larger; the maximum being 17 millidegrees for

			LONDON		BCS $\Delta k\lambda_o = 0.186$		LONDON	BCS $\Delta k\lambda_o = 0.186$
FILM	D, Å	τ, Å	λ_o, Å	σ_{LSQ}, Å	λ_o Å	σ_{LSQ}, Å	T_{crit} °K	T_{crit}, °K
31	300	402	773	9.6	771	9.8	3.510	3.510
27	"	1497	567	4.2	563	6.7	3.430	3.431
28	"	2110	500	12.7	495	9.5	3.413	3.414
33	"	4520	652	11.2	583	25.0	3.422	3.420
29	"	5210	532	33.6	554	7.6	3.409	3.415
32	"	7560	606	8.1	461	7.2	3.411	3.405
30	"	11500	651	5.6	469	5.5	3.408	3.402
25	625	455	688	7.8	685	7.9	3.483	3.483
16	"	1080	670	10.6	667	8.6	3.449	3.449
14	"	3025	784	8.3	761	10.3	3.440	3.440
15	"	4720	772	17.5	761	6.3	3.439	3.440
26	"	8785	753	10.6	545	5.5	3.432	3.415
18	1755	413	775	3.5	773	3.8	3.505	3.505
13	"	496	745	1.4	743	1.4	3.499	3.499
11	"	1740	688	52.2	706	41.3	3.427	3.432
9	"	2375	644	28.3	638	12.5	3.411	3.415
12	"	3140	1042	34.2	1022	36.1	3.470	3.469
10	"	5800	791	42.8	714	13.3	3.410	3.402
23.1	"	8548	601	40.4	517	23.5	3.349	3.347
23.2	"	8548	883	5.0	653	3.1	3.407	3.390
22	"	8844	716	25.4	522	20.7	3.415	3.404
34	3400	1456	650	36.8	649	33.6	3.439	3.439
AVG			704	18.6	648	13.6		

Table VI. Values of λ_{In_o} and T_{crit} Deduced from Temperature Variation of $(c/v)^2$, assuming $\lambda_{Ta} = 580$Å.

film 26. This again was a film for which data was not taken very close to the critical temperature.

In order to illustrate the qualitative features of the dependence of phase velocity on temperature, we have plotted v/c versus T for two extreme cases; in Figure 25, film 31, the thinnest film (402Å) on the thinnest dielectric (300Å) and hence propagating at the slowest phase velocity; and film 34, the thickest dielectric (3400Å) with an intermediate thickness film (1497Å). v/c rather than $(c/v)^2$ is plotted because the differences show more clearly.

We may write

$$v/c = 1/\sqrt{\frac{K}{d}\,(d + L_{Ta} + L_{In})} \qquad . \qquad \text{(IV-20)}$$

A large value of d tends to dominate the increase in L_{In} as we increase the temperature, until L_{In} becomes large; hence we expect the curve to be much flatter and with a sharper knee. We observe that this is indeed the case; 34 shows a very sharp knee while 31 drops off quite gradually. Another interesting point is that critical temperature of the thinner film is considerably higher, as may be seen by extrapolating the curves to zero velocity (a process we have carried out more exactly in our plots of $1/\lambda^2$ versus T^4, discussed earlier.)

We also show the effect of varying τ with d constant in Figure 26. We see that the velocity is very slow for thin films, but very nearly the same for the two thicker films. The rapid approach of the τ dependent term $\lambda_{In} \coth \tau/\lambda_{In}$ to λ_{In} as τ/λ_{In} becomes large is evident here. We also see that the knee becomes sharper as τ increases.

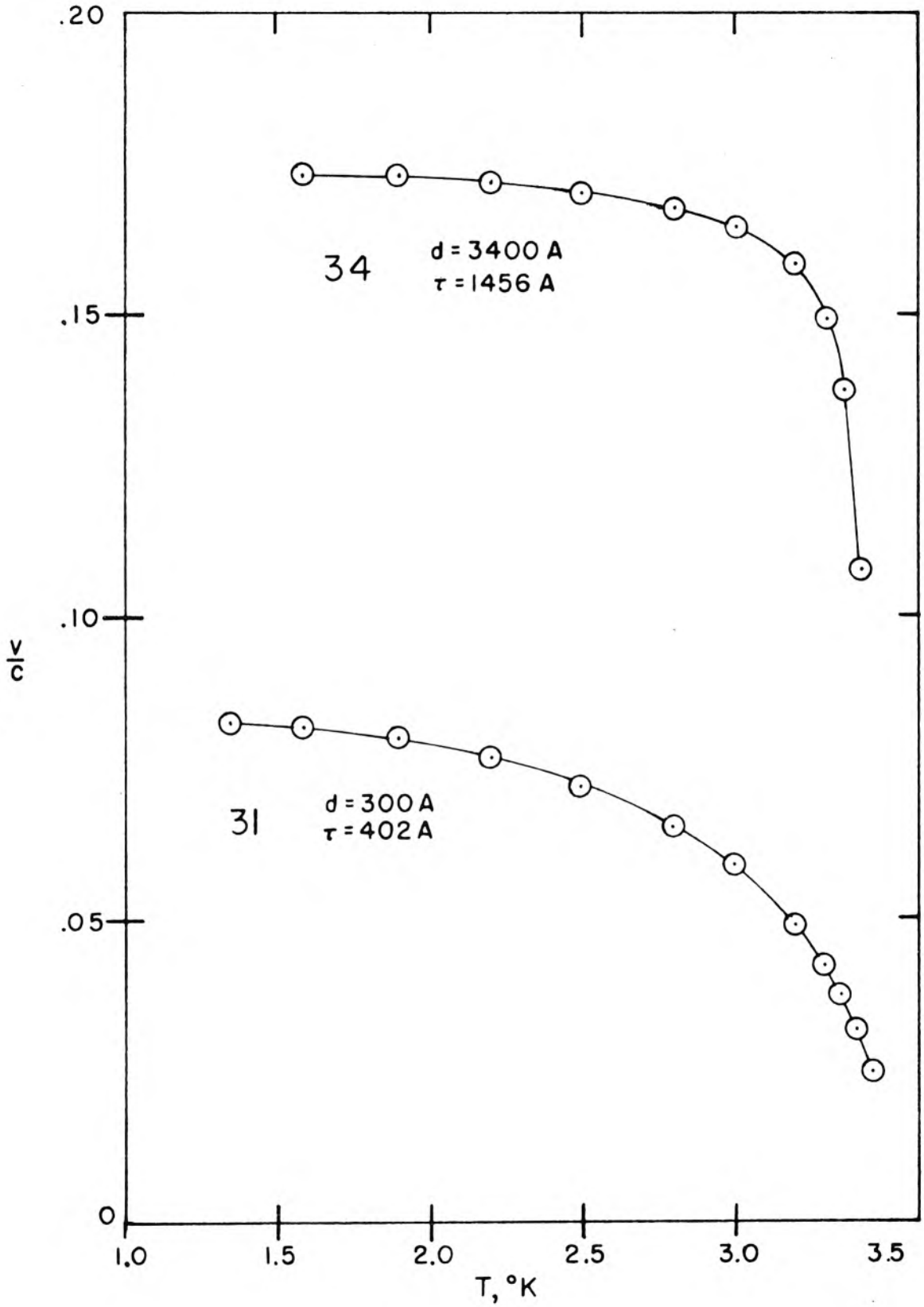

Figure 25. Phase Velocity versus T for the Fastest and Slowest Films

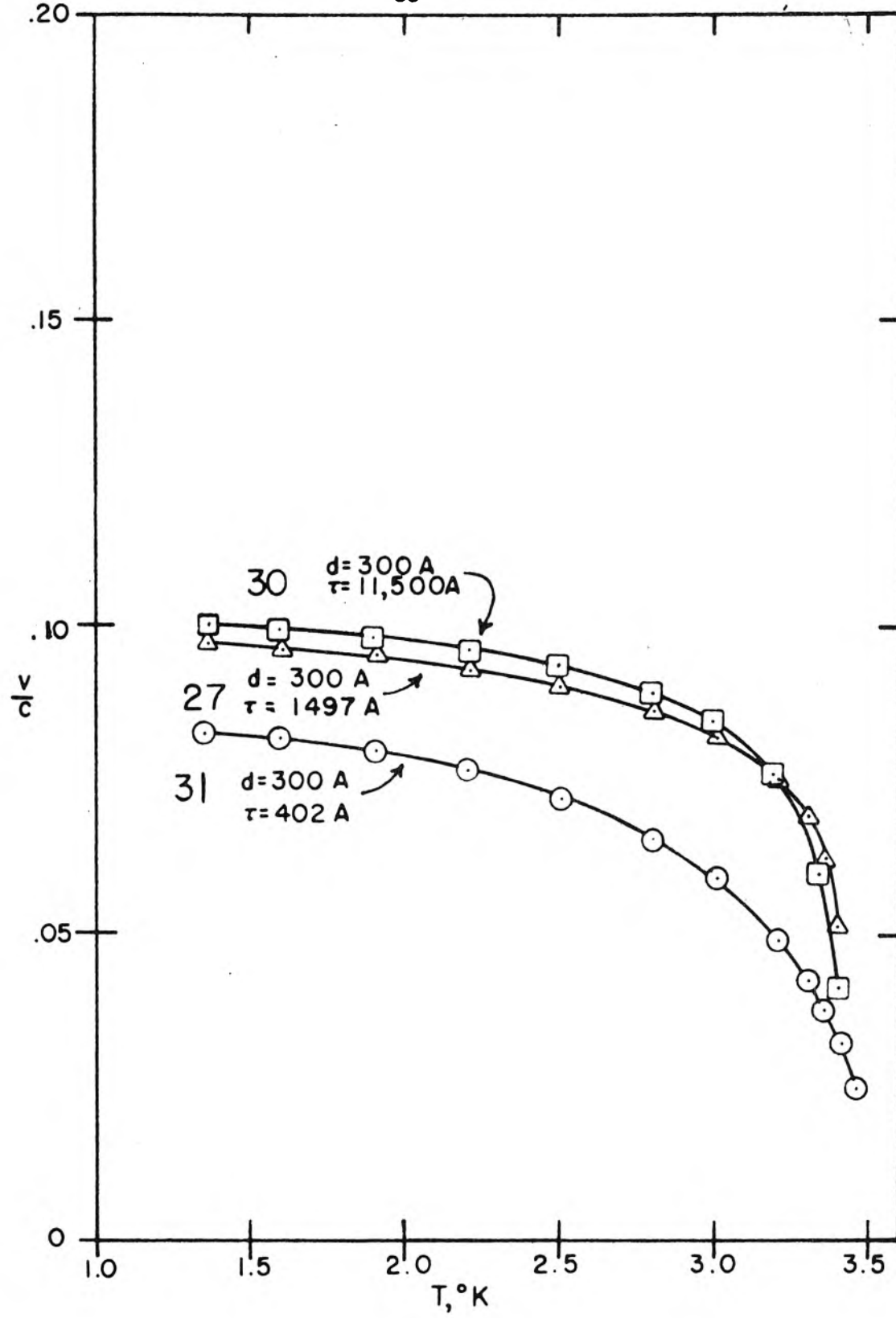

Figure 26. Phase Velocity versus Temperature with Constant Dielectric Thickness and Various Values of Indium Thickness

To illustrate the dependence of v/c on d, we have graphed v/c for films with τ's as close together as possible in Figure 27. Fortunately, v/c is a slowly varying function of τ in the region of interest so the difference in τ's is unimportant. We see the strong dependence on d which was evident in Figure 19. We also see the increase in the sharpness of the knee.

B. Losses

We measure losses in the test strip by measuring the Q of the resonant peak. There are four sources of losses: the loads at the ends, the dielectric layer, the tantalum substrate and the indium film. The first two should be nearly independent of temperature over the range of the test; the third will vary appreciably; while the fourth will be strongly dependent, since the Q tends to zero at the critical temperature of the indium. As discussed in Chapter II, the comparison of data taken from different films does not give meaningful results. In order to check this, we graphed the Q of several different films in Figure 28.

Film 10 shows a low, nearly constant Q which was typical of several early films, i.e., 10, 11, 14 and 15. None of the later films showed this behavior. It is probable that this change is due to some improvement in technique. Vacuum during evaporation decreased from about $5 \cdot 10^{-6}$ mm Hg for the early films to about $5 \cdot 10^{-7}$ mm for the later ones. However, films 9, 12, and 13 showed normal behavior so this is not the entire answer. The work by Caswell (35) mentioned earlier in this chapter showed that if the partial pressure of O_2 was kept below

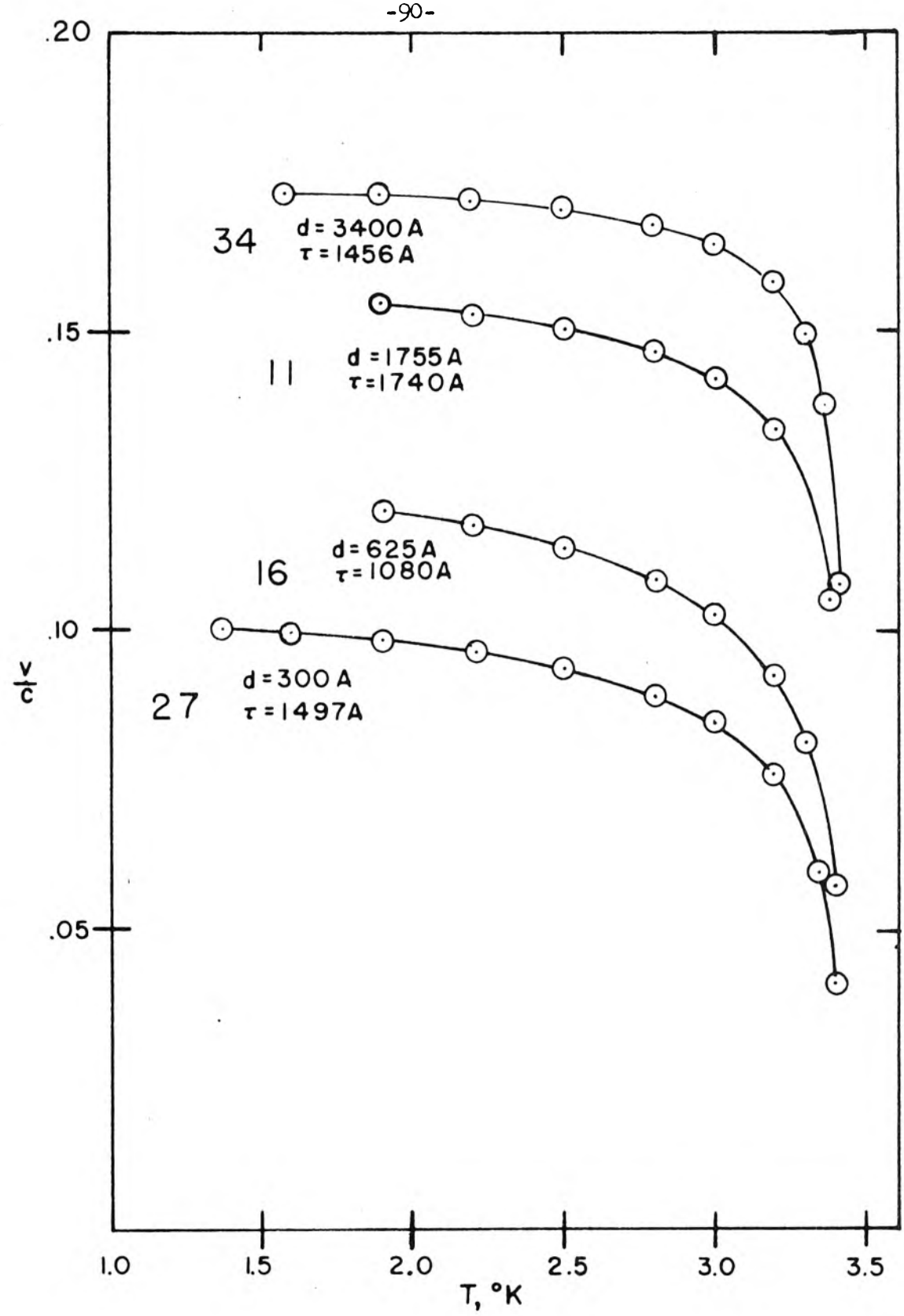

Figure 27. v/c versus T, τ Approximately Constant, d Varied.

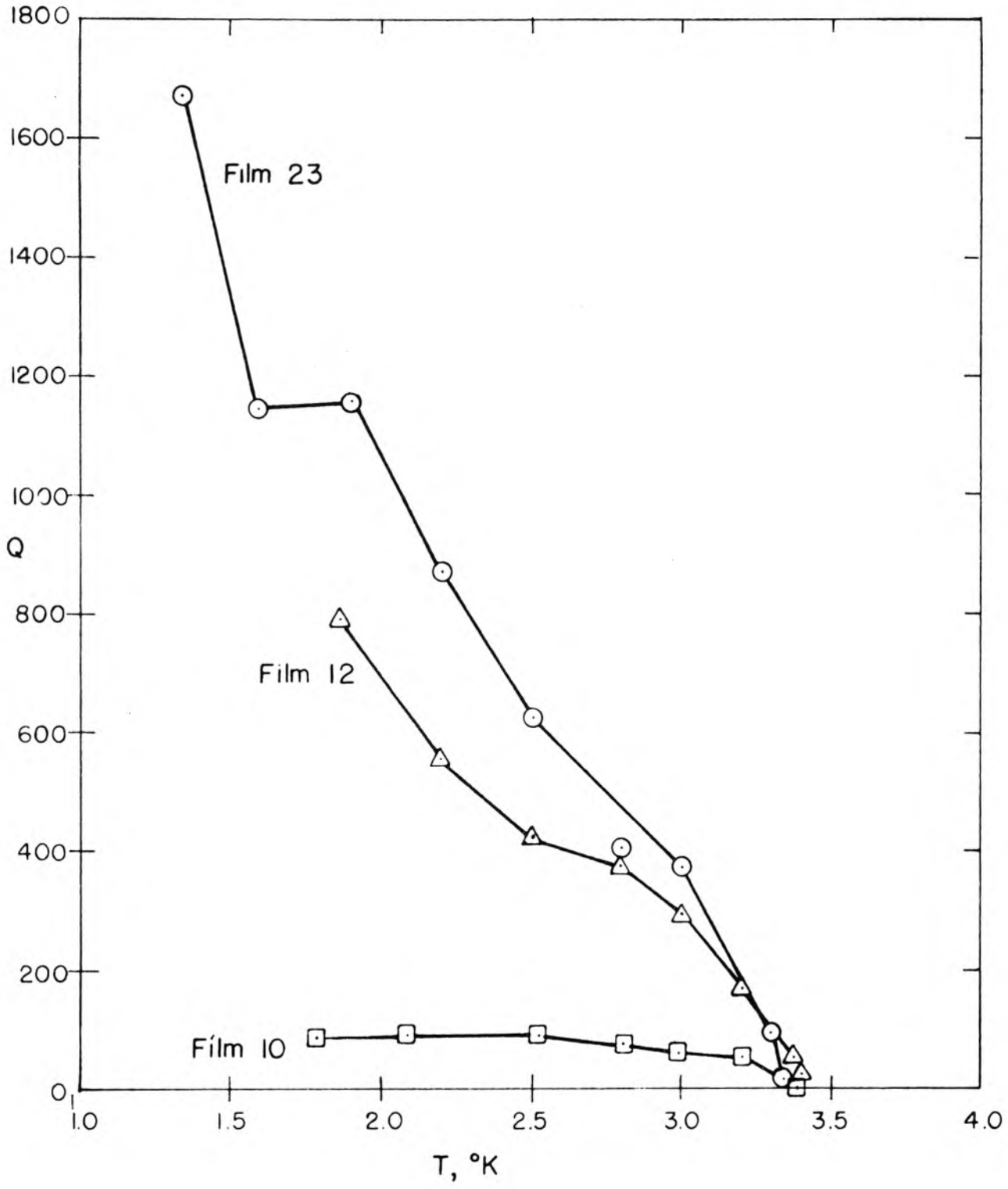

Figure 28. Dependence of Resonance Q on Temperature

$5 \cdot 10^{-8}$ mm Hg and that of H_2O and CO_2 was below $4 \cdot 10^{-7}$ mm, the films were nearly as good as those made in a vacuum of total pressure $< 10^{-9}$ mm regardless of other gases present. It is possible that our later technique of outgassing the indium charge may have helped. In any case, it appears that the low Q is dependent on the exact method of preparation rather than being an intrinsic property of the indium.

We have also tabulated the data in Table VII. Each group has constant d and is in order of increasing τ. We have given Q at two temperatures; the first at $1.9^{\circ}K$, and the second at $.985\ T_c$. The latter was chosen rather than a fixed temperature because theory indicates that the losses are functions of the reduced temperature. As we have discussed in Chapter II, the losses at the higher temperature should be due almost entirely to the indium, whereas those at $1.9^{\circ}K$ may be influenced by the tantalum substrate also. In neither case is there any definite trend to the data, either as a function of τ for fixed d or as a function of d for fixed τ. This agrees with experience of other observers.

In view of the lack of any definite trend we have not graphed the data, nor do we feel that it is worth attempting to fit it to the general expression for the London two-fluid theory with losses due to the normal current and the dielectric, which has been derived recently by Swihart (36).

There are two possible sources of variation which we should point out. The first is the vacuum. It seems likely that improvement to 10^{-9} mm Hg would lead to much more consistent results. The second source of variation is the tantalum substrate. Budnick has shown that careful purification of tantalum causes a great improvement in the

Q Data

FILM	d	τ	$Q_{1.9}$	$Q_{.985T_c}$
31	300	402	550	51
27	"	1497	183	30
28	"	2110	406	70
33	"	4520	153	40
29	"	5210	340	79
32	"	7560	309	49
30	"	11500	208	60
25	625	455	481	58
16	"	1080	96	21
14	"	3025	35	16.5
15	"	4200	28	16.5
26	"	8785	165	46
18	1755	413	265	31
13	"	496	520	37
11	"	1140	52.5	16.5
9	"	2375	-	19
12	"	3140	770	45
10	"	5800	87	16
23.1	"	8548	1160	94
23.2	"	8548	1040	-
22	"	8844	960	63
34	3400	1456	998	38

Table VII. Q at Two Temperatures for All Films

superconducting properties (37). The sharpness of the temperature and magnetic field transitions is greatly increased, while the trapped flux is reduced. The latter would be especially important in our case, since small areas of normal metal caused by the trapped flux would lead to high losses, but would not affect the phase velocity much. Since trapped flux is roughly proportional to the flux present during transition, we cancelled earth's field to less than 1% with a Helmholtz pair of coils. It is possible that this cancellation was not correct in some cases, but one would expect this to occur at random rather than just for the early films.

Examination of the data for a single film gives much more consistent results. The discussion given in Section II-B-2 showed that a suitable though semi-empirical expression for the surface resistance of a superconductor in the frequency and temperature region of interest is

$$R_s \propto \omega^2 \phi(t) \qquad \text{(IV-21)}$$

where

$$\phi(t) \equiv t^4(1-t^2)/(1-t^4)^2 \quad . \qquad \text{(IV-22)}$$

Equation 22 is valid within 10% for $0.4 \leq t \leq 0.8$ according to Miller (25), who compared it with the results of the BCS theory. We also showed in Chapter II that the surface resistance is related to the measured Q and the slowing factor α, defined as v/v_k, by

$$R_s \propto \omega/\alpha^2 Q \quad . \qquad \text{(IV-23)}$$

We make the assumption in this discussion that all of the loss may be assigned to the indium. This is certainly not true (see Section

II-B-2), but we have no clear way to separate the two. This assumption is satisfactory for frequency dependence, but will cause errors in the temperature dependence.

We first examine the frequency dependence. For fixed temperature α and $\phi(t)$ are constant. Combination of equations 21 and 23 gives

$$R_s \propto \frac{\omega}{Q} \propto \omega^2 \qquad (t \text{ fixed}) \qquad \text{(IV-24)}$$

Thus if we graph ω/Q versus ω on log log paper we should find a slope of 2. As shown in Figure 29, this very nearly is the case, for the actual slope is 1.85.

Unfortunately, data over a wide frequency range were taken for only one film. Since we can measure Q only at resonances which are integral multiples of the fundamental frequency, we must cover a wide frequency range in a technically difficult region. Film 31 had the lowest fundamental frequency, 98 mc, of all our films, so we were able to measure up to the fifth harmonic with our signal generator. For several other films data were taken at the second harmonic.

Table VIII summarizes the results for all films on which measurements at harmonics were made. We show f/Q and also fQ. The latter should be constant with frequency if $R_s \propto \omega^2$ for fixed temperature, as may be seen from equation 24. This is seen to be roughly true. Comparison of Figure 29 with the data for film 31 in the table shows that rather wide variations in fQ do not seriously affect the fit of the log log plot. The points of largest deviation in fQ seem to occur for high temperatures, 3.0 or 3.2°K, as in films 9, 25, 29 and 30. For 31, 32 and 33 agreement is fairly good at 3.2°K.

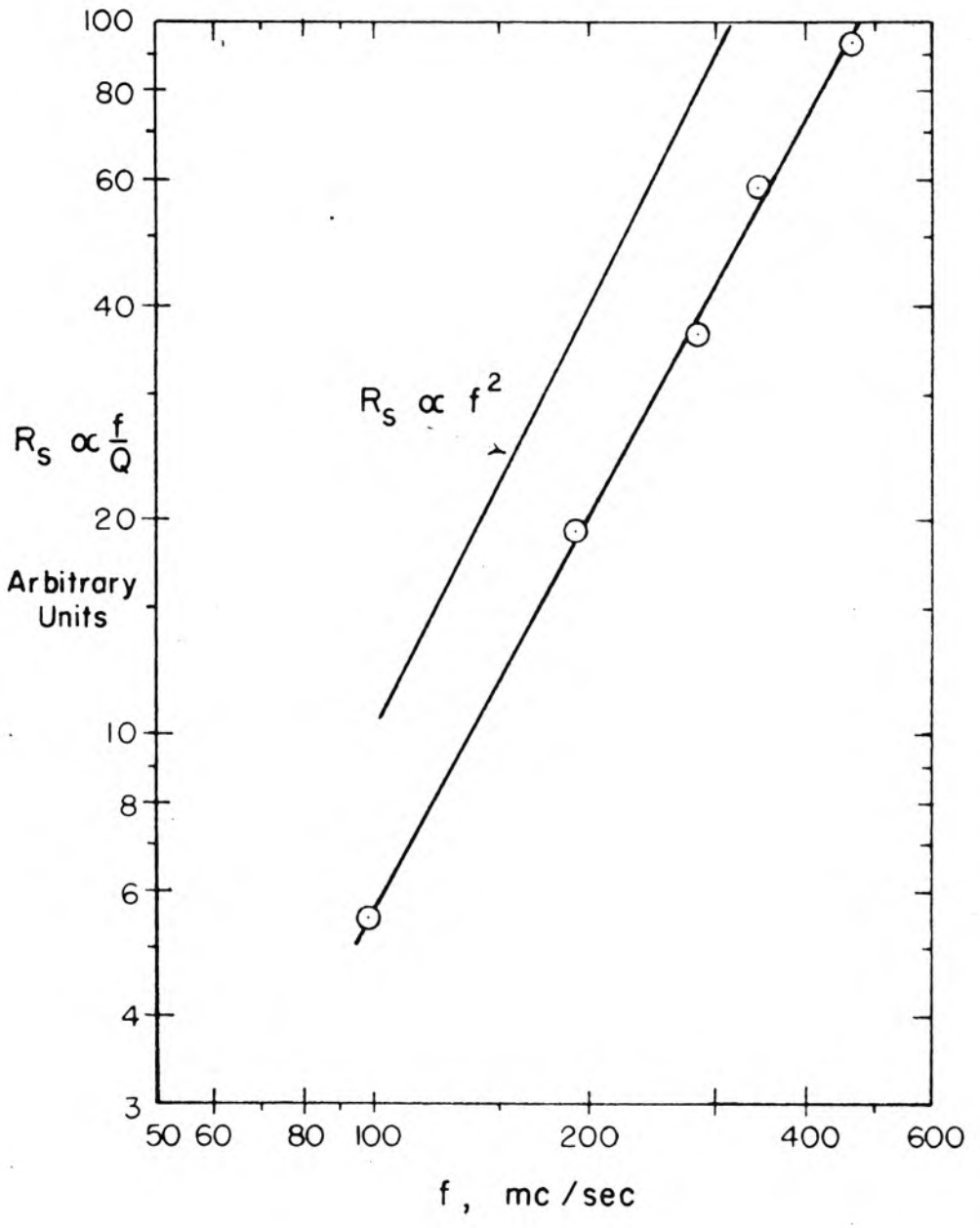

Figure 29. Surface Resistance as a Function of Frequency on Log-Log Scale

Table VIII. Effect of Frequency on Phase Velocity and Q

Film	T, ^{o}K	f_o, mc/sec	v/c	Q	f_o/Q	$f_oQ/10^4$
9	3.003	346	.1492	108	3.21	3.73
		694	.1500	167	4.15	1.16
13	1.549	350.92	.1500	-		
		696.0	.1487	-		
16	1.832	281	.1196	-		
		560	.1192	-		
		839.5	.1191	-		
25	3.198	175.17	.0758	108	1.62	1.89
		353.45	.0764	105	3.36	3.70
	2.999	205.30	.0887	148	1.38	3.04
		415.94	.0901	76	5.48	3.10
	2.796	223.72	.0965	203	1.10	4.54
		451.81	.0977	104	4.34	4.70
	2.504	241.31	.1041	299	.807	7.21
		487.38	.1054	107	4.55	5.21
28	3.202	180.82	.0778	116		
		366.03	-	-		
29	3.200	171.95	.0736	149	1.15	2.56
		340.34	.0731	106	3.22	3.60
30	3.202	174.72	.0755	102	1.71	1.79
		345.2	.0746	80	4.31	2.76
31	3.297	98.07	.0424	176	.556	1.72
		191.00	.0413	99	1.93	1.89
		282.30	.0407	103	3.65	2.90
		344.75	.0405	59	5.82	2.05
		466.84	.0404	49	9.4	2.31
32	3.202	180.53	.0784	123	1.465	2.22
		356.36	.0773	69	5.16	2.45
33	3.202	180.33	.0780	81	2.23	1.45
		356.54	.0771	42	8.5	1.50
	1.361	230.50	.0997	237	.976	5.45
		455.10	.0984	105	.434	4.77

We have also shown in Table VIII the quantity v/c, which is proportional to α. This quantity should be, and in general is, nearly independent of frequency. The variations present were probably due to small discontinuities in the properties of the structure, such as changes in thickness of dielectric or film. In most cases where v depended on frequency, pulse tests showed small reflections indicating discontinuities.

In order to examine the effect of temperature, we must correct our data for the change in ω and α as the temperature was lowered. For measurements at a given harmonic (the fundamental in all cases described here) α was proportional to ω. We assumed that R_s was proportional to ω^2. Our frequency range was less than an octave in all cases; the difference between 2^2 and $2^{1.85}$ (as found in Figure 29) was only 10% which was satisfactory for our data.

Combining equations 21 and 23 with $\alpha \propto \omega$ gave

$$\frac{1}{\omega^3 Q} \propto \phi(t) \quad . \tag{IV-25}$$

In Figure 30 we plotted $\frac{1}{\omega^3 Q}$ versus $\phi(t)$ for a number of films. For the best of these, e.g., films 31 and 18, the result was quite linear for $\phi < 0.424$, which corresponded to $t < 0.8$, the upper limit set by Miller (25). Others, such as 26, showed a definite curvature for small ϕ. In all cases it was necessary to assume a dependence of the form

$$\frac{1}{\omega^3 Q} \sim \phi(t) + C \tag{IV-26}$$

This was also found necessary by Kaplan, Nethercot and Boorse (20)

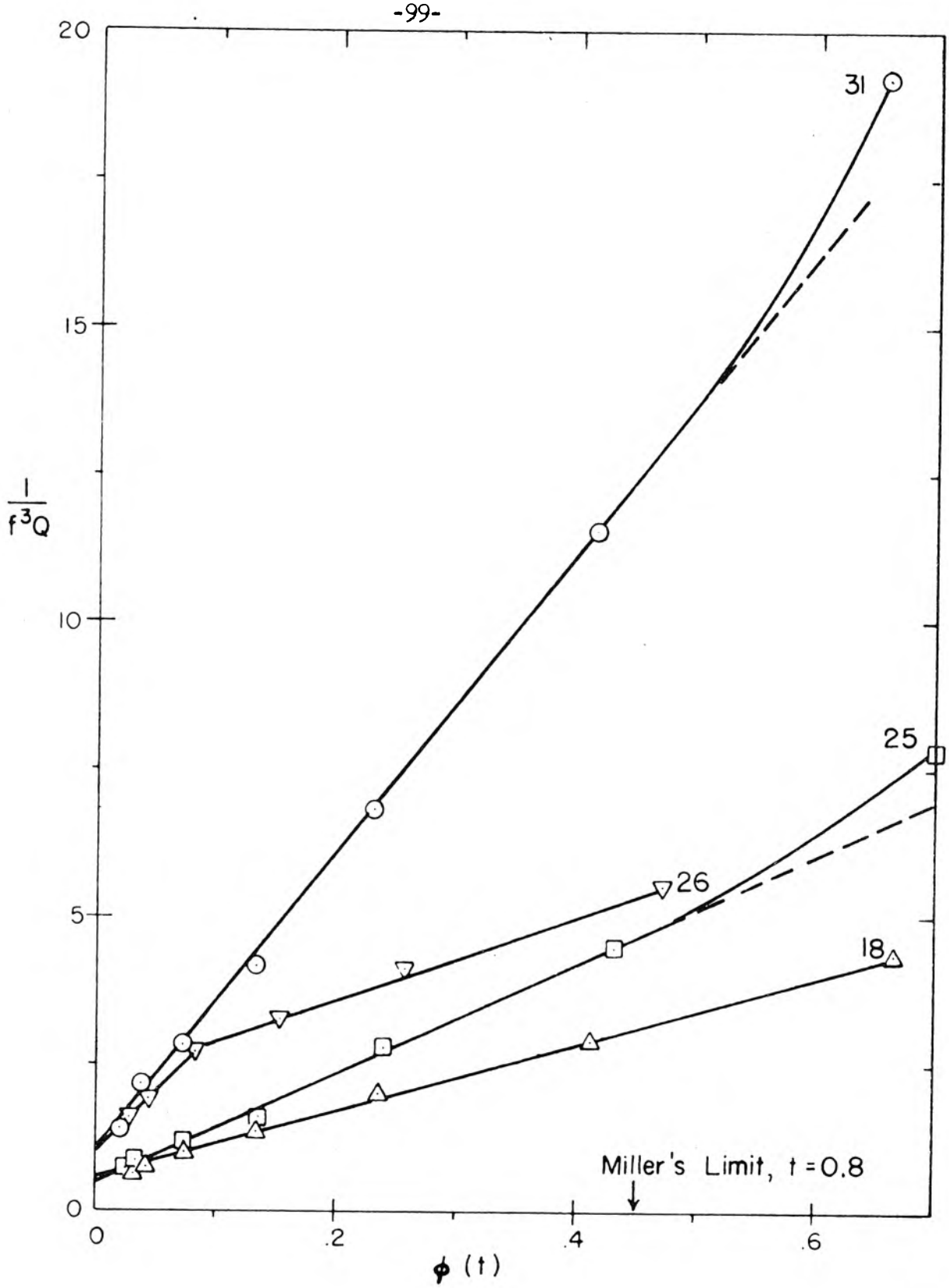

Figure 30. Dependence of R_s/ω^2 on $\phi(t)$

and Biondi and Garfunkel (23). Presumably the energy losses at zero temperature are those we have ignored; the effect of the 50 ohm termination, the losses in the dielectric, and possibly some energy losses out the sides of the strip, although these should be very small. In any case, we cannot definitely conclude from our experiment that the superconductor itself exhibits loss at zero temperature.

Since our graphical results showed a fairly good fit to a straight line for most of the films for $t < 0.84$, $\left(\phi(t) < 0.6\right)$, we performed a least-squares fit over this range for all films. The results are given in Table IX. The slope, fractional expected error in slope, intercept and fractional error in intercept are given, as well as the standard error of estimate, which is a measure of the total scatter of the data from the line of best fit.

The films noted as being poor previously, 10, 11, 14 and 15, show up again as very poor fits. Film 23.2 is based on only three points, hence the good results here are not too meaningful. Several films show poor fit because of one bad point; these are 9, 11, 12 and 14. Probably this is due to some error. Several show distinct curvature, clearly failing to obey the expected dependence. These are 10, 26, 30 and 33. The rest fit quite well, with the three films with smallest τ , namely, 18, 25 and 31, showing excellent fit.

In general our results show that there is fair agreement with a temperature dependence of the form of equation 22. In view of the many sources of error, this is the best we can hope for.

It might also be pointed out that a dependence of the form

$$g(t) = e^{-\mathcal{E}_g(T)/kT}$$

n	d	τ	SLOPE	$\frac{\sigma_{SLOPE}}{SLOPE}$	INTERCEPT $\left(\frac{1}{\omega^3 Q}\right)_{t=0}$	$\frac{\sigma_{INTER.}}{INTER.}$	STANDARD ERROR OF ESTIMATE
31.0	299	402	25.45	.017	1.05	.085	.149
27.0	299	1497	17.88	.031	3.15	.041	.220
28.0	299	2110	8.15	.048	1.31	.072	.158
33.0	299	4520	18.80	.084	3.84	.097	.627
29.0	299	5210	9.42	.076	2.47	.071	.295
32.0	299	7560	10.45	.052	1.77	.074	.220
30.0	299	11500	15.52	.098	3.10	.118	.617
25.0	626	455	8.93	.041	.42	.182	.128
16.0	626	1080	10.65	.027	3.94	.020	.084
14.0	626	3025	20.69	.190	13.02	.073	1.362
15.0	626	4720	20.72	.256	17.26	.086	1.595
26.0	626	8785	8.59	.094	1.73	.108	.308
18.0	1754	413	5.83	.043	.57	.089	.082
13.0	1754	496	1.87	.038	.28	.063	.024
11.0	1754	1740	3.31	.427	3.52	.114	.433
9.0	1754	2375	.94	.684	.94	.233	.152
12.0	1754	3140	.95	.205	.24	.219	.056
10.0	1754	5800	2.11	.274	2.18	.079	.189
23.1	1754	8548	.86	.048	.11	.100	.018
23.2	1754	8548	1.03	.015	.11	.022	.002
22.0	1754	8844	.81	.082	.13	.131	.024
34.0	3402	1456	.59	.051	.10	.064	.011

Table IX. Least-Squares Fit of $1/\omega^3 Q$ versus $\phi(t)$

could reasonably be expected from the energy gap model if we do not take the anomalous skin effect into consideration. This is reasonably close (within 20%) to the value of $\phi(t)$ over the temperature range of interest, so that the data would probably agree about as well with $g(t)$ as with $\phi(t)$. Since our data is rather inaccurate, and since $g(t)$ is not the correct temperature dependence, we have not attempted to see if this would give a better fit.

C. Dependence of T_{crit} on Film Thickness

If we plot the critical temperatures of the indium films against their thickness, we see a systematic increase as the film is made thinner, as in Figure 31. This same effect was found recently by Toxen (12). He discussed the theory at some length. He considered the temperature change to be due to stresses in the film caused by relative contraction of the substrate and the film on cooling. He found that the indium must flow plastically. He was able to compute the amount of stress in the film, and from the work of Jennings and Swenson (38) was able to relate this to the change in critical temperature.

For indium on a vitreous quartz substrate, he found that

$$T_{crit} = T_{crit}(\infty) + \frac{52}{\tau} - \frac{750}{\tau^2} \qquad \text{(IV-27)}$$

where τ is in angstroms. He found that $T_{crit}(\infty) = 3.408 \pm .003^{\circ}K$. This function was plotted in Figure 31 as a solid line. The agreement with our data was quite good, although rather scattered and not as good as Toxen's. He found agreement in most cases within 2 millidegrees. His substrate was vitreous silica rather than tantalum, so it seems

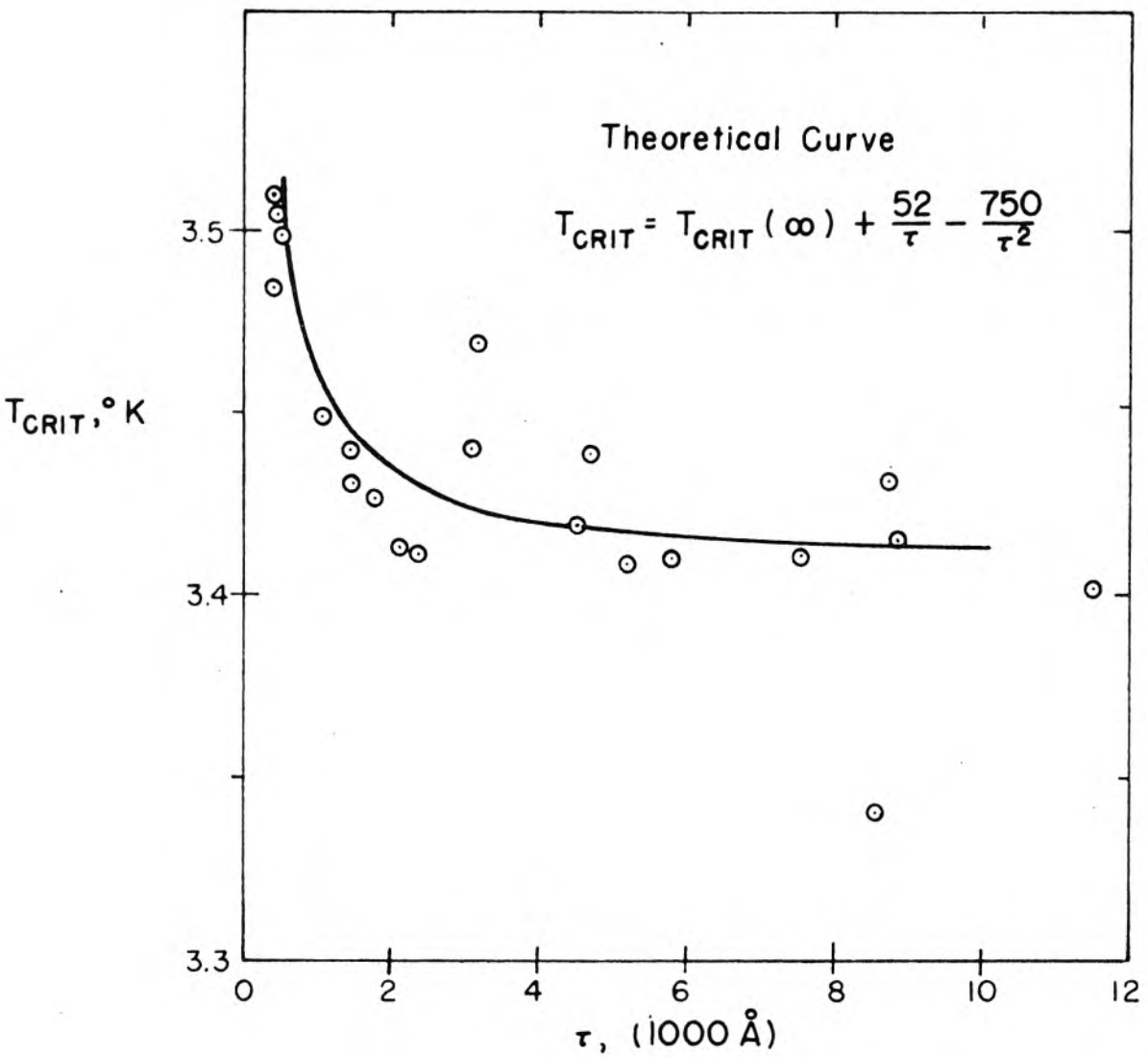

Figure 31. Critical Temperature of Indium Films as a Function of Film Thickness.

surprising that the fit should be so good. However, if we examine the contraction of the materials from room temperature to $4.2^{\circ}K$, we find that for indium $\Delta \ell/\ell = -7.3 \times 10^{-3}$, while for silica it is $+0.1 \times 10^{-3}$. We have no data for tantalum at low temperature, but the room temperature coefficient is about 1/7 that of indium, so presumably the total contraction of the tantalum is also small. Hence the dominant effect in both cases is the contraction of the indium. Also, since plastic flow occurs in each case, the yield stress of the indium will be the determining factor.

D. Effect of Static Magnetic Fields

A few measurements were made of the effect of static magnetic fields on the phase velocity and Q. A rather large effect was noted as compared with little or no effect observed by several other workers, for example, Pippard (39) who found less than 3% change for a static field near the critical value.

Our measurements were made with considerable misalignment between the film and the magnetic field, as discussed in Chapter III. As a result, parts of the tantalum substrate and the indium film may have been in the intermediate state, so our results are not very meaningful.

Results for a film 14 are shown in Figure 32. A decrease of 20% in v/c was observed. Q also decreased, but in more random fashion. The highest reading was as close to the critical field as possible. This was determined by the fact that no signal could be observed above this point. For other films the critical field ranged from 150 to 575 gauss. This was probably very dependent on the exact substrate--film misalignment.

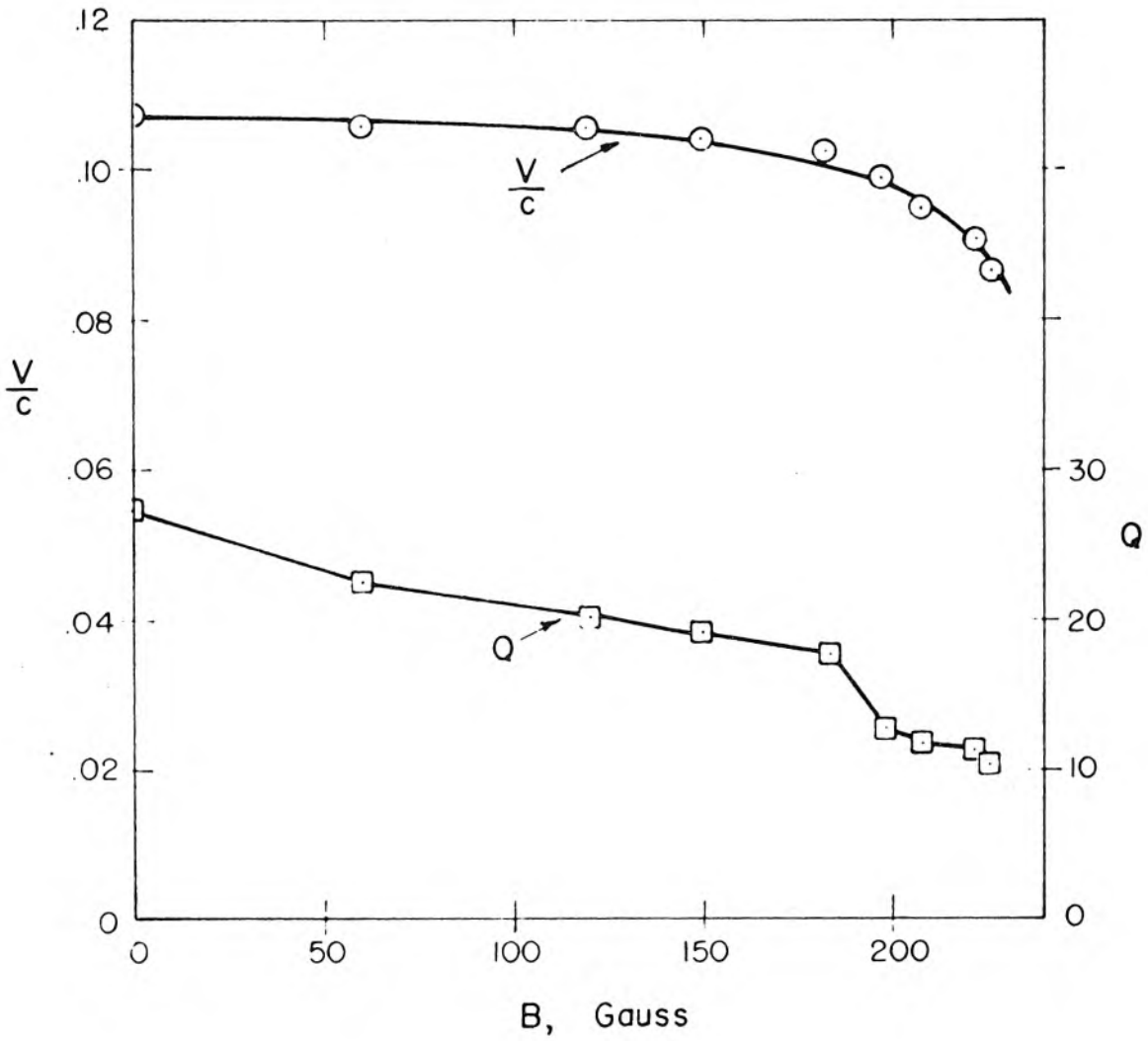

Figure 32. Dependence of Phase Velocity and Q on Static Magnetic Field.

E. Pulse Response

In order to locate the resonance, we first measured the pulse response of the film. Since both ends were approximately open circuited, the reflection coefficient at each end was approximately +1 , so the pulse was trapped on the line. At the output we observed a pulse every two transit times. Since the line is one-half wavelength long, the fundamental frequency was the reciprocal of the pulse spacing.

Figure 33 shows typical wave forms. The input pulse shown in (a) was the shortest possible from the mercury-switch delay-line generator, about 2 nanoseconds (2×10^{-9} sec.). Figure 33(a) shows the pulse after attenuation by 60 db.

Figure 33(b) is the response at 3.380°K. Peaks are about 3.7 n sec apart corresponding to 265 mc/sec. Measured resonant frequency was 275 mc/sec. The amplitude of the first pulse is 1/2000 that of the input pulse. For a line of impedance Z_1 feeding a line of impedance Z_o , the signal should be attenuated by the factor $2Z_o/(Z_1+Z_o)$. For this line whose spacing is 1750Å, and whose width is $\sim .35$ cm, the perfect conductor impedance Z_{ok} would be ~ 5 milliohms. As given by equation II-54b, Z_o for the superconducting line must be divided by α which is about 1/2. Using these numbers the expected attenuation is 1/2500; fairly close to that observed.

The pulses also show a decrease in amplitude. This may be converted to an equivalent Q which agrees quite well with that found from resonant measurements.

Figure 33(c) shows the response at 1.586°K . α is larger, so response should be smaller, as observed. Pulse spacing is now 2.75 n sec

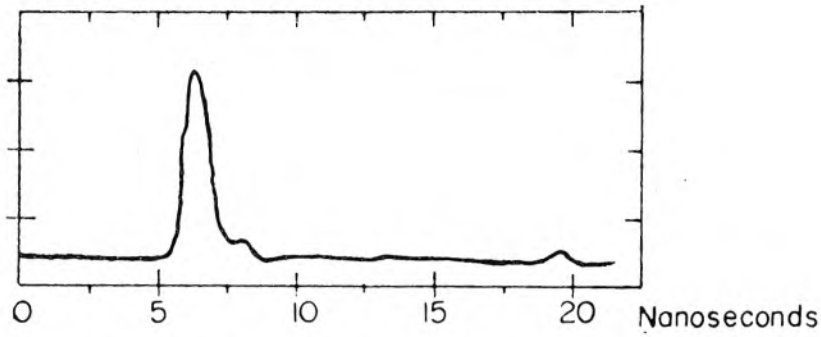

(a) INPUT PULSE - 60 db

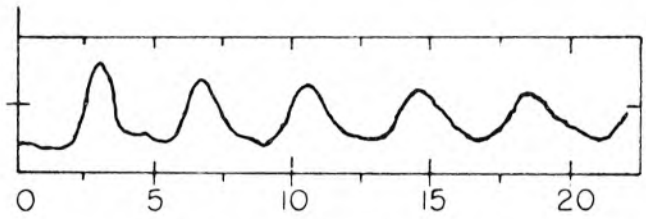

(b) RESPONSE AT T = 3.380° K

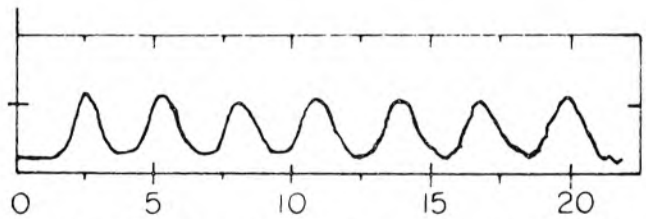

(c) RESPONSE AT T = 1.586° K

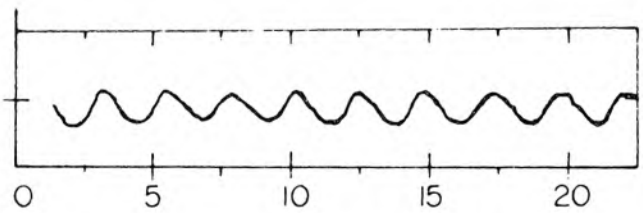

(d) RESPONSE AT T = 1.586° K AFTER 1 μSEC

Figure 33. Input Pulse and Pulse Response of Film 22.

showing the result of the decrease in λ .

Figure 33(d) shows the same response after 1 μ-sec, i.e., after about 350 cycles. Amplitude is down by a factor of about 1/2, while pulse shape is preserved well. The degeneration of pulse shape is caused by the relatively larger attenuation of the higher harmonics of the pulse. Clearly a superconducting transmission line would be satisfactory for storage of data pulses in a digital computer. Various switching techniques could also be used by causing magnetic fields to force certain parts of a pulse path into the normal state.

In some cases fairly large spurious pulses were observed in between the usual pulses (those of Figure 33b are normal, caused by the shape of the input pulse.) Presumably these were caused by reflections from discontinuities. When they were observed, the second harmonic was quite far from a multiple of the fundamental, as would be expected.

Measurements by Young, Swihart, Tansal and Meyers (2) were done entirely by this pulse technique. The principal disadvantage was the limited accuracy, probably not better than 5% for phase velocity measurements. Resonance methods, on the other hand, are accurate to better than 1% and probably to 0.5%.

F. Summary and Conclusions

We have derived a theoretical expression for the dependence of the phase velocity in a transmission line formed of two different superconducting materials; one conductor is of finite thickness; the other is assumed infinitely thick but our derivation may be readily modified for

finite thickness. We have specialized our equations to two important cases: first to the London phenomenological, two-fluid, two-parameter theory (3), which assumes a local or point relation between vector potential and supercurrent; and second to the Bardeen-Cooper-Schrieffer theory (5), based on a quantum mechanical microscopic model. The latter yields a dependence of current on the integral of the vector potential over volume of radius approximately 10^{-4} cm, the coherence distance. (The BCS theory gives a quantum mechanical justification of a phenomenological non-local theory proposed by Pippard (6); we have not discussed the latter separately.) For zero range, i.e., $\Delta k = \infty$, the BCS theory reduces to the London theory.

We find that the theoretical dependence of the quantity $(c/v)^2$ on the finite film thickness τ differs significantly in the two cases. For the London theory $(c/v)^2$ decreases monotonically to a fixed value as τ increases. For the BCS theory, $(c/v)^2$ decreases to a minimum, then rises to a fixed value somewhat above that for the London theory.

Our experimental results, which are based on a structure using tantalum for the thick superconductor and vacuum evaporated indium for the thin one, show no minimum. In general they seem to fit the expected curves derived from the London theory quite well. We conclude that our material has a very short coherence length compared to a penetration depth (a coherence length of zero corresponds to the London theory). This may be the result of impurities in the thin film resulting from the vacuum evaporation process used to form the thin film.'

For τ large, the experimental value of $(c/v)^2$ approaches a constant. This is in direct contradiction to the predictions of another non-local theory--that of Schafroth and Blatt (11).

Extrapolation of the data to zero temperature gives values for the penetration depths $\lambda_{In}(0)$ and $\lambda_{Ta}(0)$ at zero temperature. $\lambda_{In}(0)$ is found to be 640 ± 75Å, quite close to Lock's value of 640Å (16), and also Toxen's values for thick films, 625 to 725Å (12).

The value for $\lambda_{Ta}(0)$ is found to be 580 ± 175Å. Apparently no other investigators have measured λ_{Ta}.

The penetration depth λ, which enters into the expression for $(c/v)^2$, is temperature dependent. The London theory and the BCS theory predict slightly different dependence, but experimental results of other investigators do not show clearly which is correct. We have used the London dependence, since it is somewhat simpler.

The phase velocity tends to zero at the critical temperature T_{crit} of indium; therefore suitable extrapolation of our phase velocity data yields T_{crit}.

Once T_{crit} is found we may use either the London or BCS thickness dependence to find a value of $\lambda_{In}(0) + \lambda_{Ta}(0)$. It has been found that the value of $\lambda_{In}(0)$ is relatively insensitive to the choice of a value of $\lambda_{Ta}(0)$. Hence we assumed the latter and calculated the former. For the London dependence the average values of $\lambda_{In}(0)$ over all films ranged from 730 ± 140Å for λ_{Ta} = 400Å, to 680 ± 115Å for λ_{Ta} = 700Å. Values derived using the BCS theory were about 50Å lower, with about the same spread. For the BCS theory we used a value of $\Delta k\lambda_{In} = 0.186$, corresponding to a coherence length of about 3500Å.

Accuracy of fit to the data was about the same for the two theories. Hence we cannot use these results to decide which is a more valid description of the superconductor.

The critical temperature of indium, T_{crit}, was found to depend on film thickness τ, in good agreement with a theoretical expression derived by Toxen (12).

Dependence of losses on frequency follows quite well the theoretical increase as ω^2.

Losses from the 50 ohm load at each end, and from the dielectric are shown to be negligible. Losses from the tantalum and indium cannot be separated. We show that losses due to the tantalum are varying appreciably in the temperature range of interest, but we cannot show whether they are small enough to be neglected. Nevertheless, we find that if we assign all of the losses to the indium, a moderately good fit to an empirical temperature dependence proposed by Pippard (22) is found.

Preliminary measurements of the dependence of $(c/v)^2$ on static magnetic field show a much larger dependence than would be expected from the results of Pippard (39), and others. This may be the result of the existence of regions in the superconductor which are in the intermediate state.

V. IMPROVEMENTS AND EXTENSIONS

A number of improvements in technique have been mentioned in the previous chapters. In this chapter we review these in more detail.

A. Vacuum

The change most likely to improve the results is better vacuum. This may increase the coherence length of the evaporated superconductor and may also lead to less scatter in $(c/v)^2$ and Q data. Improvement in technique (primarily in oil diffusion pumps with reduced oil backstreaming and liquid nitrogen cooled traps which prevent creep of oil along warm surfaces into the working vacuum) has made possible demountable systems with vacuum better than 10^{-8} mm Hg. during evaporation. Other possible techniques include the use of gettering type pumps which have nearly constant pumping speed at least to 10^{-10} mm Hg. A recent improvement has increased the pumping speed for noble gases.

As discussed earlier, Caswell has shown that selective pumping for oxygen, water vapor and carbon dioxide produces films at an over-all vacuum of 10^{-6} which are identical in superconducting characteristics to those in a normal vacuum of 10^{-9} mm (35). Selective pumping is done by the use of getters for oxygen and a cold plate for water and CO_2. We use a liquid N_2 cooled plate pump now, but have no special mechanism to pump oxygen.

Another possible improvement is pumping with a finger containing liquid He_2. If this were done we might at the same time hold the substrate near liquid He_2 temperature to reduce clumping and hence obtain thinner films and more uniform thickness. In fact, we might do the

entire evaporation in the experimental dewar, as did Glover and Tinkam (9). This would eliminate exposure of the film to atmosphere as well. It does pose some problems in accurate thickness measurements, however. Glover and Tinkam used resistance but our experience on reproducibility has been poor. One method that has become widely used recently is measurement of the change in resonant frequency of a crystal which has been exposed to the evaporation. The frequency shift is linearly proportional to mass deposited to good accuracy, even though repeated evaporations are made without removing the previous deposit. The method is not absolute, but calibration against measurement by interferograms would be easy.

B. Elimination or Improvement of Tantalum

A second major improvement would be the elimination of the tantalum and tantalum oxide. This would remove the uncertainties in superconducting properties of tantalum, which is well known to be a rather poorly behaved superconductor unless it is extremely pure. Even if we purified the tantalum we would still not know λ_{Ta} or the losses which we might expect from the normal current.

At the time our experiments were started, the use of anodized tantalum seemed to be the only way to prepare thin, uniform, pin-hole free dielectrics of known thickness. Since that time two new techniques have been developed for making thin dielectric films. The first is simply an improved method of evaporating SiO. By evaporating the SiO in a hollow chimney structure, rapid deposition can be made even though the hot SiO is shuttered from the film. Since the high velocity particles from the SiO appear to cause the pin holes observed in thin

films, this method yields much thinner pin-hole free films.

A second method, developed by Christy (40), uses an electron beam to polymerize silicone pump oil vapor into a dielectric layer. Pin-hole free films as thin as 200Å have been prepared this way in our laboratories.

By using the dynamic thickness measuring method described above and one of the two methods of forming dielectric films, we could construct a transmission line using indium of the same thickness for both strips. This should reduce the uncertainties involved in calculating λ_{In} and in measuring the losses in superconducting indium.

Once the properties of indium are accurately known, it would be interesting to return to the tantalum-Ta_2O_5-indium structure in order to measure the properties of tantalum. To date there appears to be no measurement of λ_{Ta}, probably because until recently it has been a difficult material to work with, showing poor superconducting properties. Recently, however, Seraphim, Budnick and Ittner (41) have developed a method of purification which yields tantalum of excellent and reproducible properties. This has been reported by Budnick (37). To purify the tantalum it is heated to about 2700 to 2900°K in a vacuum of 1 or 2×10^{-8} mm Hg. This is followed by introduction of oxygen at pressures in the range of 1 to 4×10^{-5} mm for several hours to remove carbon. Residual resistivity was 10^{-9} ohm.cm, about 100 times better than previous results and was of the order of that reported for zone refined copper and silver. Temperature and magnetic field transitions were extremely sharp and reproducible. Such a process should be carried out on tantalum before further measurements of penetration

depth and surface resistance are made. Another interesting possibility is the use of evaporated tantalum films. Marchand and Venema (42) produced films with the critical temperature and field of bulk metal by evaporation from a hot tantalum filament in a vacuum of 10^{-11} mm Hg. This was obtained by using a sealed glass system pumped by liquid nitrogen trapped mercury diffusion pumps.

Another improvement of interest would be the reduction of the dielectric thickness. Since d and λ_{In} are added in the expression for $(c/v)^2$, reduction of d would show the nature of the dependence of λ_{In} on temperature and film thickness more clearly. Also, if the dielectric layer were thin enough, tunneling between the two superconductors would take place. This should yield negative resistance, so that by proper biasing a microwave oscillator could be built. In fact, in their report of the initial work on superconducting tunneling, Giaever and Megerle report that such oscillations interfered with their measurements (43), but they do not discuss such details as amplitude or frequency.

The principal difficulty in preparing films on very thin dielectrics is obtaining a pin-hole free dielectric. For this reason some sort of oxidation such as the tantalum anodization used for this experiment is probably necessary.

C. Effect of Magnetic Field

We have shown preliminary results of the measurement of the effect of magnetic field on phase velocity. By construction of apparatus which would permit precise alignment of the magnetic field parallel with the film, we should be able to get an accurate measurement of the dependence of λ on magnetic field, a topic of theoretical

interest. The principal experimental problem is to insure that the entire film is in the same magnetic field, a condition which is not met if the film is not exactly parallel to the field.

APPENDIX A

Derivation of the Velocity Function $(c/v)^2$

1. London Theory. A similar derivation is given by Swihart (14) but we repeat it here both for completeness and because $(c/v)^2$ for the non-local theories is derived by a modification of the same method.

We use the following definitions and conventions

c = free space phase velocity = $1/\sqrt{u_o \epsilon_o}$

v = phase velocity of wave on superconducting line

σ = equivalent normal conductivity of superconductor

ϵ_o = permittivity of free space

μ_o = permeability of free space

K = relative dielectric constant of dielectric

Λ = London parameter = $m_s/\rho_s e_s$

λ = London penetration depth = $\sqrt{\Lambda/\mu_o}$

β = propagation constant = ω/v

k = wave number = $\omega \mu_o \epsilon_o K$

γ = $\sqrt{\beta^2 - k^2}$

k_o and γ_o are for free space

k_{SF} and γ_{SF} refer to the superconducting indium film

λ_{IN} refers to the superconducting indium film, and is about 600Å

k_D and γ_D refer to the dielectric between the film and the substrate of relative permittivity K

k_{SS} and γ_{SS} refer to the superconducting tantalum substrate

λ_{Ta} refers to the superconducting substrate and is about 500Å

η = normalized surface impedance = $E_{TAN} / c\mu_o H_{TAN}$

We first give the solution of Maxwell's equations for a dielectric; then we show that if we choose a suitably defined dielectric constant we can obtain similar solutions for the superconductor.

We assume a wave propagating in the z direction (see Figure 34) so that all field functions vary as $e^{j(\omega t - \beta z)}$. We neglect attenuation. The structure extends to infinity in the x and z directions (a very good assumption, since width/thickness is of the order of 10^4). It is of thickness τ in the y direction.

From the curl equations one may derive the following relations* (44)

$$H_x = -\frac{1}{\gamma^2}\left[j\omega\epsilon \frac{\partial E_z}{\partial y} - j\beta \frac{\partial H_z}{\partial x} \right] \tag{A-1a}$$

$$H_y = \frac{1}{\gamma^2}\left[j\omega\epsilon \frac{\partial E_z}{\partial x} + j\beta \frac{\partial H_z}{\partial y} \right] \tag{A-1b}$$

$$E_x = \frac{1}{\gamma^2}\left[j\beta \frac{\partial E_z}{\partial x} + j\omega\mu \frac{\partial H_z}{\partial y} \right] \tag{A-1c}$$

$$E_y = -\frac{1}{\gamma^2}\left[-j\beta \frac{\partial E_z}{\partial y} + j\omega\mu \frac{\partial H_z}{\partial x} \right] \tag{A-1d}$$

We have here the customary division into E modes and H modes. If we assume E mode solutions ($H = 0$) and no x dependence, the relations become

$$H_y = E_x = 0 \tag{A-2a}$$

$$H_x = -\frac{j\omega\epsilon}{\gamma^2} \frac{\partial E_z}{\partial y} \tag{A-2b}$$

*Ramo and Whinnery's γ is our $j\beta$. Also, their $\gamma^2 + k^2$ is our $-\gamma^2$.

$$E_y = \frac{j\beta}{\gamma^2} \frac{\partial E_z}{\partial y} \tag{A-2c}$$

Hence we need solve only for E_z ; H_x and E_y are derived from it.

In a dielectric of permittivity $\epsilon = \epsilon_o K$, permeability μ_o with no free charges or currents, we have (44)

$$\nabla^2 E_z = - \omega^2 \mu_o \epsilon_o K E_z \tag{A-3}$$
$$= - k_o^2 E_z$$

Upon applying the assumptions of independence of x and dependence on z of the form $e^{-j\beta z}$, we have

$$\frac{\partial^2 E_z}{\partial x^2} - \beta^2 E_z = - k_D^2 E_z$$

or

$$\frac{\partial^2 E_z}{\partial x^2} = \gamma_D^2 E_z \tag{A-4}$$

Since we wish slow wave solutions, i.e., $(v/c) = \frac{\omega\sqrt{\mu_o \epsilon_o K}}{\beta} = k_D/\beta < 1$, we see that γ_D is real, hence the solution is of the form

$$E_z = A \sinh \gamma_D y + B \cosh \gamma_D y \tag{A-5}$$

or the equivalent exponential form.

In the superconductor we have the field equation (see equation II-16)

$$\nabla^2 \bar{E} = - \omega^2 \mu_o \epsilon_o \left(1 - j \frac{\sigma}{\omega \epsilon_o} - \frac{1}{\omega^2 \Lambda \epsilon_o}\right) \bar{E} \tag{A-6}$$

Hence if we replace $\epsilon_o K$ by

$$\epsilon_s = \epsilon_o\left(1 - \frac{j}{\omega_o} - \frac{1}{\omega^2 \Lambda \epsilon_o}\right) \tag{A-7}$$

we can use the above derivation, providing we also replace k_D and γ_D by the appropriate k_s and γ_s for the superconductor. In the low frequency approximation we neglect the first two terms so

$$\epsilon_s \cong - \frac{1}{\omega^2 \Lambda} \cong - \frac{1}{\lambda^2 \mu_o \omega^2} \tag{A-8a}$$

$$k_s = - \omega^2 \mu_o \epsilon_s \cong - \frac{1}{\lambda^2} \tag{A-8b}$$

and

$$\gamma_s^2 = \beta^2 - k_s^2 \approx - k_s^2 = + \omega^2 \mu_o \epsilon_s = \frac{1}{\lambda^2} \tag{A-8c}$$

In the last equation we have used the fact that $\beta \ll k_s$. We show this as follows:

$$\beta = \frac{\omega}{v} = \frac{2\pi f}{v} = \frac{2\pi}{\text{wavelength}} \quad .$$

Since the wavelength is of the order of centimeters and since $k_s \cong \frac{1}{\lambda} \approx \frac{1}{5 \times 10^{-6} \text{cm}}$, then $k_s >> \beta$, so we neglect the β^2 in the expression for γ_s^2 . Our result then is

$$\frac{\partial^2 E_z}{\partial y^2} = \gamma_s^2 E_z \tag{A-9}$$

and the solution is

$$E_z = C \sinh \gamma_s y + D \cosh \gamma_s y \quad . \tag{A-10}$$

We now must match the boundary conditions at the three interfaces. These are usually stated as requiring that E_{TAN} and H_{TAN} be continuous, but all that is really required is that the dimensionless

surface impedance $\eta = E_{TAN}/\mu_o c\, B_{TAN}$ be continuous. This is somewhat more convenient since we can choose our coordinate zero at different stages of the solution, then transform the impedances to a common point and match.

Assuming an E mode solution, the surface impedance in a dielectric is

$$\eta = \frac{E_z}{c\mu_o H_x} = + \frac{j\gamma_D^2 E_z}{c\omega\mu_o\epsilon_o K \frac{\partial E_z}{\partial y}} = \frac{j\gamma_D^2 E_z}{ck_D \frac{\partial E_z}{\partial y}} \quad . \tag{A-11}$$

In the superconductor we may substitute the values from equation A-8 into equation 2b. The surface impedance becomes

$$\eta = - j \frac{(\omega/c)\, E_z}{\partial E_z / \partial y} \quad . \tag{A-12}$$

We are now prepared to match surface impedances. We will first consider $y = 0$ at the upper film edge (see Figure 34), match impedances across this interface, then transform the film impedance to the lower edge.

In the region above the film (which we take to be free space), $E_z = Ae^{-\gamma_o y}$, since we must take only the solution which is not infinite at $y = \infty$. We have

$$\eta = - \gamma_o / (\omega/c) \quad . \tag{A-13}$$

In the superconductor both exponentials are permissible, hence

$$E_z = B(\sinh \gamma_{SF} y + C \cosh \gamma_{SF} y) \tag{A-14}$$

and

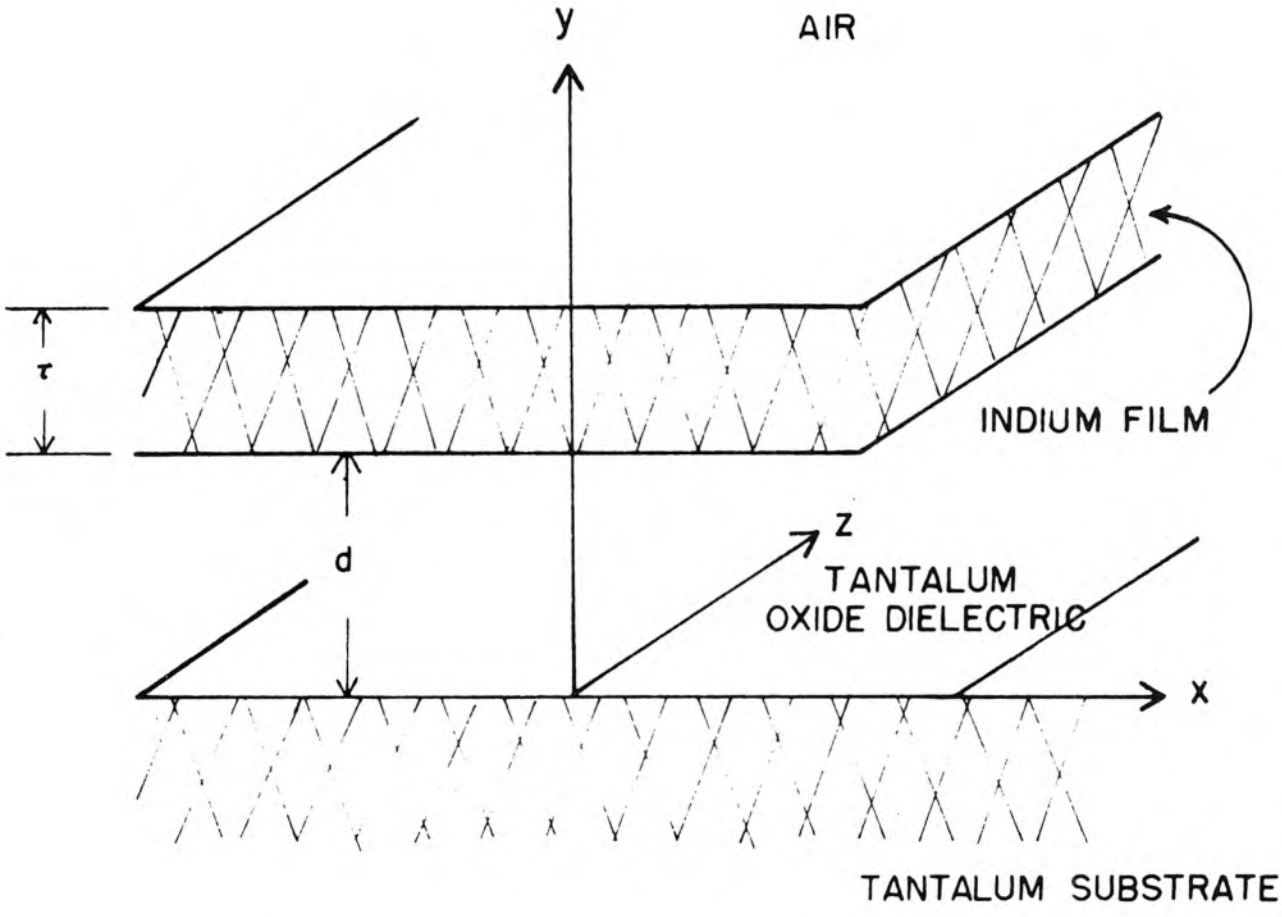

Figure 34. Superconducting Transmission Line

$$\eta = - j \frac{(\omega/c)}{\gamma_{SF}} \frac{(\tanh \gamma_{SF} y + C)}{(1 + C \tanh \gamma_{SF} y)} \tag{A-15}$$

Equating A-13 and A-15 at $y = 0$, we find that $C = \gamma_o \gamma_{SF} / (\omega/c)^2$. Inserting in A-15 we have

$$\eta = - j \frac{(\omega/c)}{\gamma_{SF}} \frac{\frac{\gamma_o \gamma_{SF}}{(\omega/c)^2} + \tanh \gamma_{SF} y}{(1 + \frac{\gamma_o \gamma_{SF}}{(\omega/c)^2} \tanh \gamma_{SF} y)} \tag{A-16}$$

We now transform to the film dielectric interface by taking $y = - \tau$

$$\eta \Big|_{y = -\tau} = - j \frac{(\omega/c)}{\gamma_{SF}} \frac{\frac{\gamma_o \gamma_{SF}}{(\omega/c)^2} - \tanh \gamma_{SF} \tau}{(1 - \frac{\gamma_o \gamma_{SF}}{(\omega/c)^2} \tanh \gamma_{SF} \tau)} \tag{A-17}$$

We simplify this greatly by noting that $C = (\frac{\gamma_o}{\omega/c})(\frac{\gamma_{SF}}{\omega/c})$ is much larger than 1. Since $\gamma_o^2 = \beta^2 - \frac{\omega^2}{c^2}$ by definition, the first factor must be greater than 1. The second, if we use A-8a and note that (c/ω) is the free space wavelength, becomes $(\text{wavelength}/\lambda_{In})$. Since the free space wavelength is of the order of centimeters, while λ_{In} is about 5×10^{-6} cm, this factor is very large. Since $\tanh \gamma_{SF} \tau$ is at most 1, we may neglect it in the numerator. In the denominator, however, we note that $\gamma_{SF} \tau = \tau / \lambda_{In}$, and that this will never be extremely small, since we are unable to make films for which $\tau \ll \lambda_{In}$ so that $\tanh \gamma_{SF} \tau$ will never be much smaller than 1. Hence we may neglect the first term. We have then

$$\eta\Big|_{y=-\tau} = -\,j\,\frac{(\omega/c)}{\gamma_{SF}}\coth\gamma_{SF}\tau \quad . \tag{A-18}$$

This approximation completely removes any effect of the volume above the film, since γ_o no longer appears. Thus the film may be covered with a dielectric layer (as we do) or placed near metallic objects such as the silvered dewar with negligible effect on propagation velocity v . In essence this occurs because nearly all the energy travels either in the superconductors or in the insulating layer.

We now repeat the calculations at the dielectric-substrate interface, which we now take to be $y = 0$. After equating impedances, we will transform the impedance in the dielectric to $y = d$, i.e., the other side of the interface for which equation A-18 is valid.

In the substrate we must choose

$$E_z = D\,e^{\gamma_{SS}y} \tag{A-19}$$

Hence

$$\eta = -\,j\,\frac{(\omega/c)}{\gamma_{SS}} \quad . \tag{A-19}$$

In the dielectric we have

$$E_z = F(\sinh\gamma_D y + G\cosh\gamma_D y)$$

Hence

$$\eta = j\,\frac{\gamma_D}{(\omega/c)K}\left(\frac{\tanh\gamma_D y + G}{1 + G\tanh\gamma_D y}\right) \tag{A-20}$$

Equating A-19 and A-20 we find

$G = -\frac{(\omega^2/c^2)K}{\gamma_{SS}\,\gamma_D}$ which is much less than 1. We then substitute into A-20, and transform η to the dielectric-film interface by setting $y = d$. We have

$$\eta = j\,\frac{\gamma_o}{(\omega/c)K}\;\frac{\tanh \gamma_D d - \frac{(\omega^2/c^2)K}{\gamma_{SS}\gamma_D}}{1 - \frac{(\omega^2/c^2)K}{\gamma_1\,\gamma_2}\tanh \gamma_D d} \quad . \tag{A-21}$$

We may again simplify by noting that $\frac{(\omega^2/c^2)K}{\gamma_{SS}\,\gamma_D}$ is very small compared to 1, since $(\omega/c)K/\gamma_D$ is less than 1 and $(\omega/c)/\gamma_{SS} =$ λ_{Ta} / Free Space Wavelength $\ll 1$ by arguments used before. Also $\gamma_D d$ is of the order of 1000Å/1 meter and hence is so small that $\tanh \gamma_D d \approx \gamma_D d$. We now have

$$\eta = j\,\frac{\gamma_D}{(\omega/c)K}\left(\gamma_D d - \frac{(\omega^2/c^2)K}{\gamma_{SS}\,\gamma_D}\right) \tag{A-22}$$

Equating A-22 and A-18 and solving for γ_D^2 we have

$$\gamma_D^2 = \frac{\omega^2}{c^2}K\left(\frac{1}{\gamma_{SS} d} + \frac{\coth \gamma_{SF}\tau}{\gamma_{SF} d}\right) \quad . \tag{A-23}$$

We now find $(c/v)^2$ by noting from the definition that

$$\begin{aligned}\beta^2 &= \frac{\omega^2}{c^2}K + \gamma_D^2 \\ &= \frac{\omega^2}{c^2}K\left[1 + \frac{1}{\gamma_{SS} d} + \frac{\coth \gamma_{SF}\tau}{\gamma_{SF} d}\right]\end{aligned} \tag{A-24}$$

or

$$\frac{c^2}{\omega^2/\beta^2} = \frac{c^2}{v^2} = \frac{K}{d}\left[d + \frac{1}{\gamma_{SS}} + \frac{\coth \gamma_{SF}\tau}{\gamma_{SF}}\right] \quad . \qquad \text{(A-25)}$$

We have made use of the relationship that the phase velocity $v = \omega/\beta$. We can put this in a more familiar form by noting from A-8c that

$$1/\gamma_{SS} = \lambda_{Ta} \qquad \text{and} \qquad 1/\gamma_{SF} = \lambda_{In} \,, \qquad \text{so}$$

$$\frac{c^2}{v^2} = \frac{K}{d}\left[d + \lambda_{Ta} + \lambda_{In} \coth \tau/\lambda_{In}\right] \quad . \qquad \text{(A-26)}$$

2. Non-Local Theories. We wish to find the surface impedance of the upper film of Figure 34 at the film-dielectric interface. We will match this with the surface impedance of the substrate transformed to the lower side of the same interface. This latter impedance was derived in the previous section.

We follow a method developed by Gould based on Schrieffer's derivation of magnetic susceptibility (10) of a thin superconducting film. Consider just the upper film, as shown in Figure 35. We assume a field $B_x = B_o$ at the lower surface. We also assume that the surface impedance is infinite and hence $B_x = 0$ at the upper surface, as in Part 1. Surface currents flow in the z-direction at and near the x-z plane which shield H_o from the interior of the metal. We calculate the vector potential A_z from which we obtain E_z and hence the surface impedance $\eta = E_z/cB_x$.

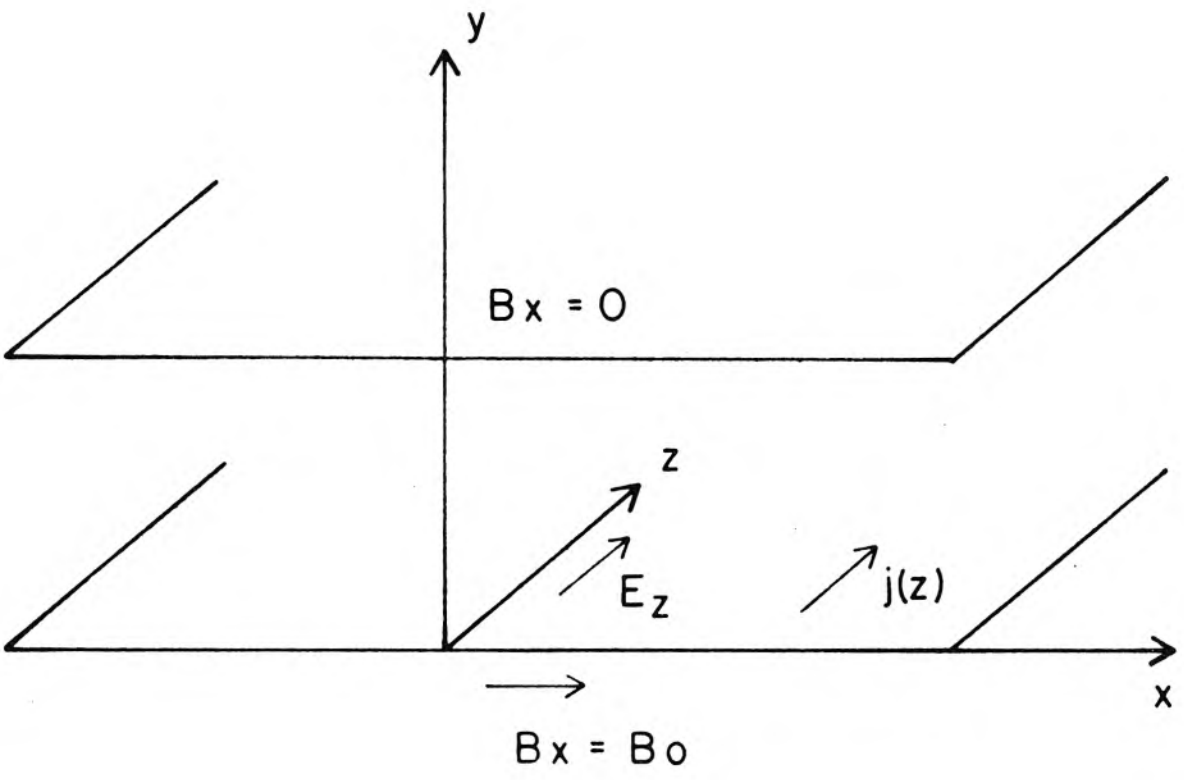

Figure 35. Boundary Conditions on Magnetic Field

We make two further assumptions; first that no free charge is present, which is strictly true only for the static case. Since the wavelength of our disturbances is of the order of centimeters as compared to film thicknesses of a few thousands of angstroms, the neglect in the variation of surface current density in the z-direction is justified. We must consider time dependence of $\bar{A}$, however, to compute $\bar{E} = -\frac{\partial \bar{A}}{\partial t}$, so strictly speaking we analyze the quasi-static case. In this case, it is convenient to choose a gauge in which $\nabla \cdot \bar{A} = 0$.

Secondly we assume that an electron striking a surface is reflected specularly (as from a mirror). Schrieffer considers the case of diffuse reflection for the Pippard case, but shows that the magnetic moment is not very sensitive to the choice. Because of mathematical difficulties he does not solve the case of diffuse reflection for the BCS theory.

To meet the boundary condition of specular reflection we must construct a solution in which the B, E and J fields in the z directions are symmetric about each boundary, but in the y direction are antisymmetric. Thus an electron approaching a boundary will be met by one with the same z velocity but opposite y velocity. Hence as the two cross the boundary an apparent specular reflection will take place.

We construct the periodic solution whose general form is shown in Figure 36b. This satisfies all boundary conditions, but requires B field discontinuities of amount $2B_o$ at $y = 0, \pm\tau, \pm 2\tau$, etc. These are obtained by allowing current sheets, J^* at these planes, as shown in Figure 36b. Application of Biot and Savart's law to a small loop in the x-z plane yields

$$J^* = 2B_o/\mu_o \cdot \qquad \text{(A-27)}$$

We now have a periodic problem to which we may apply Fourier analysis, using the k space relationships between current and vector potential described in Chapter II. We shall solve with a general kernel, then specialize.

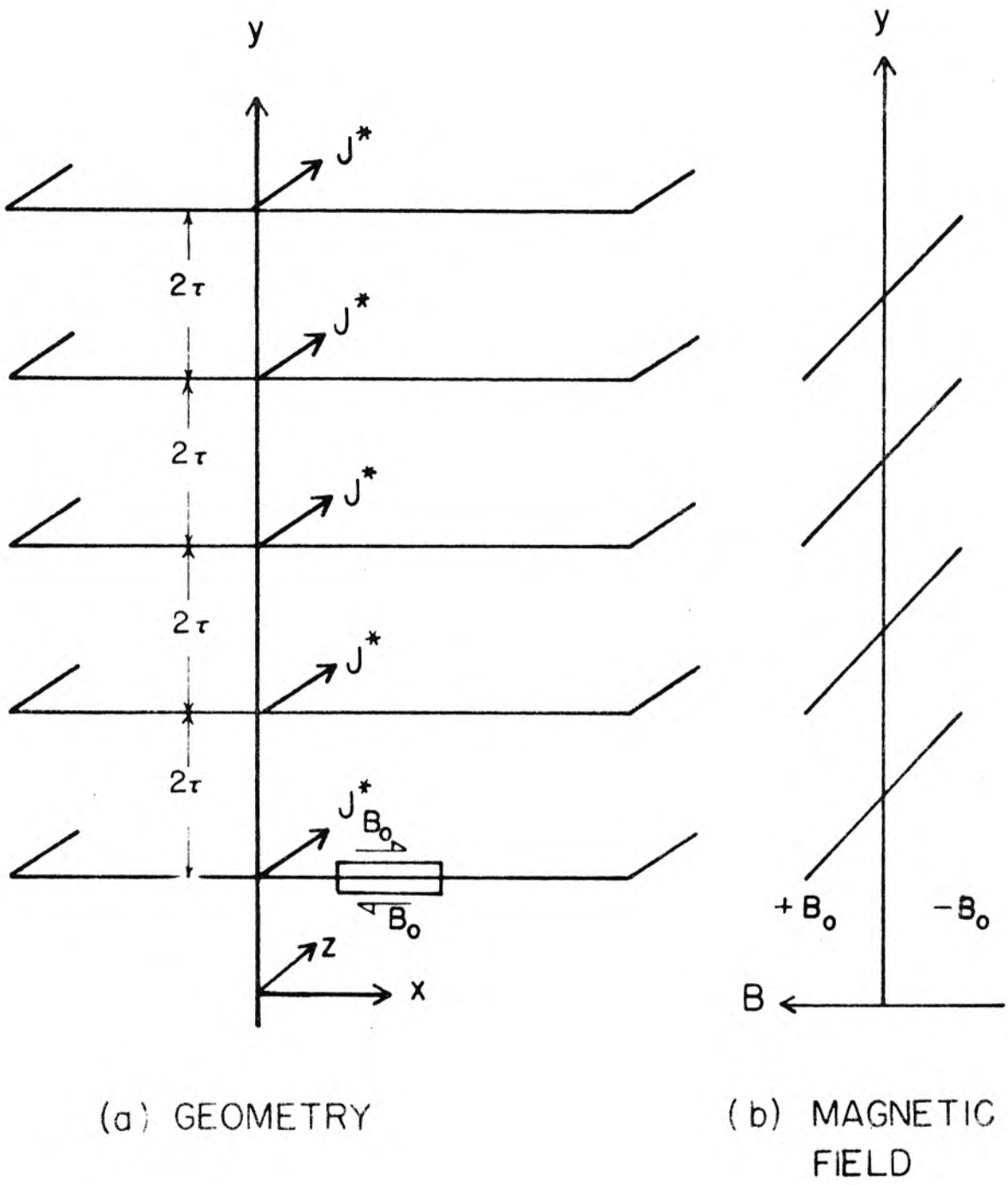

Figure 36 (a) Equivalent Current Sheets to Introduce Periodic Discontinuities in Magnetic Field

(b) General Form of Final Solution

We require the representation of the source current sheets in a Fourier series. Since the currents are symmetric about $y = 0$, and are δ functions of value $2B_o/\mu_o$, the space representation is

$$\bar{J}^*(y) = \bar{e}_z \frac{2B_o}{\mu_o} \sum_{n=-\infty}^{\infty} \delta(y - 2n\tau) \quad . \tag{A-28}$$

Using the usual integral expression for the coefficients of the Fourier series, we find that

$$\bar{J}^*(n) = \frac{2B_o}{\mu_o \tau} \qquad n \neq 0 \tag{A-29a}$$

$$\bar{J}^*(n) = \frac{B_o}{\mu_o \tau} \qquad n = 0 \quad . \tag{A-29b}$$

Thus the space representation is

$$\bar{J}^*(y) = \bar{e}_z \frac{B_o}{\mu_o \tau} \left[1 + 2 \sum_{n=1}^{\infty} \cos \frac{n\pi}{\tau} y \right] \tag{A-30}$$

The electrodynamic equation we wish to solve is

$$\nabla \times \bar{B} = \mu_o \bar{J}_{TOTAL} = \mu_o \left[\bar{J}_s + \bar{J}^* \right] \quad . \tag{A-31}$$

Since $\bar{B} = \nabla \times \bar{A}$ and $\nabla \cdot \bar{A} = 0$, we may use the vector identity $\nabla \times \nabla \times \bar{A} = \nabla (\nabla \cdot \bar{A}) - \nabla^2 \bar{A}$ to obtain

$$\nabla^2 \bar{A}(y) = - \mu_o \left[\bar{J}_s(y) + \bar{J}^*(y) \right] \quad . \tag{A-32}$$

We now Fourier transform this with respect to y, noting that for the quasi-static case we are considering all quantities as functions of y only, so

$$k^2 \bar{A}(\bar{k}) = \mu_o \left[\bar{J}_s(\bar{k}) + \bar{J}^*(\bar{k}) \right] \quad . \tag{A-33}$$

Since the problem is periodic, we must express $\bar{k}$ as the discrete variable $\bar{k}_n$

$$\bar{k}_n = \frac{n\pi}{\tau} \bar{e}_y \quad . \tag{A-34}$$

We now make use of equations A-29a and A-29b and also equation II-34 which is

$$\bar{J}_s(\bar{k}) = - \frac{1}{\mu_o} \bar{A}(\bar{k}) \, K(\bar{k}) \quad . \tag{II-34}$$

We have two equations for the components

$$k_n^2 \, \bar{A}(\bar{k}_n) = - \bar{A}(\bar{k}_n) \, K(\bar{k}_n) + \frac{2\bar{B}_o}{\tau} \tag{A-35}$$

$$0 = - \bar{A}(0) \, K(0) + \frac{\bar{B}_o}{\tau} \quad . \tag{A-36}$$

Solving these and forming the Fourier sum

$$A_z(y) = \frac{B_o}{\tau} \left[\frac{1}{K(0)} + 2 \sum_{n=1}^{\infty} \frac{\cos k_n y}{k_n^2 + K(k_n)} \right] \quad . \tag{A-37}$$

We are now able to compute the surface impedance, since in the gauge with $\nabla \cdot \bar{A} = 0$, $\bar{E} = - \frac{\partial \bar{A}}{\partial t} = -j\omega \bar{A}$. Using this and recalling that the surface impedance $\eta \equiv \frac{E_{TAN}}{CB_{TAN}}$ we have

$$\eta \Big|_o = - \frac{j(\omega/c)}{\tau} \left[\frac{1}{K(0)} + 2 \sum_{n=1}^{\infty} \frac{1}{k_n^2 + K(k_n)} \right] \tag{A-38}$$

Comparing the impedance at the same point for the localtheory, equation

A-18, with the final expression for $(c/v)^2$, equation A-25, we see that we might have written the latter as

$$\left(\frac{c}{v}\right)^2 = \frac{K}{d}\left[\, d + \lambda_{Ta} + j\,\frac{-\eta_{In}}{\omega/c}\,\right] . \qquad \text{(A-39)}$$

Hence we can define a length associated with the indium film

$$L = j\,\frac{\eta\big|_o}{\omega/c} = \frac{1}{\tau}\left[\frac{1}{K(0)} + 2\sum_{n=1}^{\infty}\frac{1}{k_n^2 + K(k_n)}\right]. \qquad \text{(A-40)}$$

We cannot express this in closed form so we must use a computer to calculate L for different kernels and for various values of τ.

For the Pippard theory we may express this in dimensionless form using the kernels from Schrieffer's paper (10)

$$\frac{L_{PIPPARD}}{\ell_p} = \frac{\ell_p}{\tau}\left[1 + 2\sum_{n=1}^{\infty}\frac{1}{(k_n\ell_p)^2 + \frac{3}{2}\,\frac{[(1+\xi k_n)^2]\tan^{-1}\xi k_n - \xi k_n}{\xi k_n}}\right] \qquad \text{(A-41)}$$

Here $k_n = \frac{n\pi}{\tau}$ as before and $\ell_p = \lambda_L\sqrt{\frac{\xi_o}{4\pi\xi}}$. For pure metals ξ reduces to ξ_o so that $\ell_p = \lambda/\sqrt{4\pi}$. For impure metals ξ becomes smaller as discussed by Pippard (6). Note that $k_n\ell_p = n\pi\ell_p/\tau$ and that the expression ξk_n may be written in the form $(\xi/\ell_p)(n\pi\,\frac{\ell_p}{\tau})$ so that the entire function depends on two dimensionless parameters ξ/ℓ_p associated with the range of integration and τ/ℓ_p, the normalized thickness of the film.

For the BCS theory we have

$$\frac{L_{BCS}}{\ell_B} = \frac{\ell_B}{\tau}\left[1 + 2\sum_{n=1}^{\infty} \frac{1}{(k_n \ell_B)^2 + \frac{\Delta k}{k_n}\, \ell n(1 + \frac{k_n}{\Delta k})}\right] \qquad \text{(A-42)}$$

Here $\ell_B = \sqrt{4/3}\,\lambda_L$. Again we may write $k_n \ell_B = \frac{n\pi \ell_B}{\tau}$ and $\frac{\Delta k}{k_n} = \Delta k \ell_B / \frac{n\pi \ell_B}{\tau}$ so the entire expression is a function of a dimensionless range parameter $\Delta k \ell_B$ and a normalized thickness τ/ℓ_B .

We have chosen to leave in ℓ_p and ℓ_B rather than reduce to λ_L because we wish to have these parameters free to adjust L to equal the best fit to our experimental data.

Graphs of $L_{PIPPARD}$ and L_{BCS} are given in Figures 5 and 6 for various values of ξ/ℓ_p and $\Delta k \ell_B$.

BIBLIOGRAPHY

1. Pippard, A. B., "The Surface Impedance of Superconductors and Normal Metals at High Frequencies, III The Relation between Impedance and Superconducting Penetration Depth", Proc. Roy. Soc. Lond. A191, 399-415 (1947).

2. Young, Swihart, Tansal and Meyers, "Use of Superconducting Transmission Line for Measuring Penetration Depths", Bull. Am. Phys. Soc. Ser. II 5, 163 (1960).

3. London, F., Superfluids, Vol. I, J. Wiley, New York (1950), p.27-34.

4. Trivelpiece, A. W. and R. W. Gould, "Space Charge Waves in Cylindrical Plasma Columns", Jour. App. Phys. 30, 1784-1793 (1959).

5. Bardeen, J., L. N. Cooper and J. R. Schrieffer, "Theory of Superconductivity", Phys. Rev. 108, 1175-1204 (1957).

6. Pippard, A. B., "An Experimental and Theoretical Study of the Relation between Magnetic Field and Current in a Superconductor", Proc. Roy Soc. Lond. A216, 547-568 (1953).

7. Shoenberg, D., Superconductivity, Cambridge University Press (1952), Chapters 5 and 6.

8. Meissner, W. and R. Ochsenfeld, "Ein neuer Effekt bei Eintritt der Supraleitfahigkeit", Naturwissenschafter 21, 787-788 (1933).

9. Glover, R. E. and M. Tinkam, "Conductivity of Superconducting Films for Photon Energies between 0.3 and 40 RT_c", Phys. Rev. 108, 243-256 (1957).

10. Schrieffer, J. R., "Evaluation of Some Non-Local Theories for a Thin Superconducting Film", Phys. Rev. 106, 47-50 (1957).

11. Schafroth, M. R. and J. M. Blatt, "Phenomenological Equations for Superconductors", Phys. Rev. 100, 1221-1222 (1955).

12. Toxen, A. M., "Size Effects in Thin Superconducting Indium Films", Phys. Rev. 123, 442-446 (1961).

13. Daunt, J. G., A. F. Miller, A. B. Pippard and D. Shoenberg, "Temperature Dependence of Penetration Depth of a Magnetic Field in Superconductors", Phys. Rev. 74, 842 (1948).

14. Desirant, M. and D. Shoenberg, "Penetration of Magnetic Field into Superconductors , I Measurements on Thin Cylinders", Proc. Phys. Soc. Lond. 60, 413-424 (1948)

15. Shoenberg, D., "Properties of Superconducting Colloids and Emulsions", Proc. Roy Soc. Lond. A175, 49-70 (1940).

16. Lock, J. M., "Penetration of Magnetic Fields into Superconductors, III Measurements on Thin Films of Tin, Lead and Indium", Proc. Roy Soc. Lond. A208, 391-408 (1951).

17. Bardeen, Cooper and Schrieffer, IBID, p. 1197.

18. "Reference Data for Radio Engineers", International Tel and Tel Company, Fourth Ed., New York, 574-582, (1956).

19. Sturge, M. D., "The Variation with Frequency of the Resistance of Superconducting Tin and Indium", Proc. Roy Soc. Lond. A246, 570-581 (1958).

20. Kaplan, R., A. H. Nethercot, H. A. Boorse, "Frequency Dependence of the Surface Resistance of Superconducting Tin in the Millimeter Wavelength Region", Phys. Rev. 116, 270-279 (1959).

21. Pippard, A. B., "The Surface Impedance of Superconductors and Normal Metals at High Frequencies, V Analysis of Experimental Results for Superconducting Tin", Proc. Roy. Soc. Lond. A203, 195-210 (1950).

22. Pippard, A. B., "The Surface Impedance of Superconductors and Normal Metals at High Frequencies, IV Impedance at 9400 mc/sec of Single Crystals of Normal and Superconducting Tin", Proc. Roy. Soc. Lond A203, 98-118 (1950).

23. Biondi, M. A. and M. P. Garfunkel, "Millimeter Wave Absorption in Superconducting Aluminum, I Temperature Dependence of the Energy Gap, Phys. Rev. 116, 853-861 (1959).

24. Mattis and Bardeen, "Theory of the Anomalous Skin Effect in Normal and Superconducting Metals", Phys. Rev. 111, 412-417 (1958).

25. Miller, P. B., "Surface Impedance of Superconductors", Phys. Rev. 118, 928-934 (1960).

26. Tegart, W. J. McG., "The Electrolytic and Chemical Polishing of Metals", Pergamon Press, New York (1959), page 68.

27. Vermilea, D. A., "The Kinetics and Structure of Anodic Oxide Films on Tantalum", ACTA Metallurgica 1, 282-294 (1953).

28. Charlesby A., and J. J. Polling, "The Optical Properties of Thin Oxide Films on Tantalum", Proc. Roy Soc. Lond. A227, 434-447 (1955).

29. MacSwan, A. M., "The Colour of Thin Oxide Films on Metals", Proc. Phys. Soc. Lond. 72, 742-748 (1958).

30. Tolansky, S., "Multiple Beam Interferometry of Surfaces and Films", Clarendon Press, Oxford (1958).

31. Sommers, H. S., "Two Types of Regulators and the Precision Control of Helium Bath Temperature", Rev. Sci. Inst. 25, 793-798 (1954).

32. Reeber, M. D., "Geometric Effects in the Superconducting Transition of Thin Films", IBM J. Res. and Devel. 3, 141-146 (1959).

33. Holland, L., Vacuum Deposition of Thin Films, J. Wiley, New York, (1958), page 205.

34. Bardeen, J. and J. R. Schrieffer, "Recent Developments in Superconductivity", Progress in Low Temperature Physics, C. J. Gorter, Ed., Interscience, New York (1961), page 170-287.

35. Caswell, H. L., "Effect of Residual Gases on Superconducting Characteristics of Tin Films", J. App. Phys. 32, 105-114 (1961).

36. Swihart, J. C., "Field Solution for a Thin-Film Superconducting Transmission Line", Jour. App. Physics 32, 461-469 (1961).

37. Budnick, J., "Some Studies of the Superconducting Transition in Purified Tantalum", Phys. Rev. 119, 1578-1586 (1960).

38. Jennings, L. D. and C. A. Swenson, "Effect of Pressure on the Superconducting Transition Temperatures of Sn, In, Ta, Tl and Hg," Phys. Rev. 112, 31-43 (1958).

39. Pippard, A. B., "Field Variation of the Superconducting Penetration Depth", Proc. Roy. Soc. Lond. A203, 210-223 (1950).

40. Christy, R. W.,"Formation of Thin Polymer Films by Electron Bombardment", Jour. App. Phys. 31, 1680-1683 (1960).

41. Seraphim, Budnick and Ittner, "Single Crystal Growth and Purifica- of Tantalum", Trans. Metal Soc. of AIME 218, 527-533 (1960).

42. Marchand, J. J. and A. Venema, "Note on Superconducting Tantalum Films", Phillips Res. Reports 14, 427-429 (1959).

43. Giaver, I. and K. Megerle, "Study of Superconductors by Electron Tunneling", Phys. Rev. 122, 1101-1111 (1961).

44. Ramo and Whinnery, Fields and Waves in Modern Radio, 2nd Ed., John Wiley and Sons, New York (1953), page 317-318.

45. Holland, IBID, p.212.

46. Sennet and Scott, "The Structure of Evaporated Metal Films and Their Optical Properties", J. Opt. Soc. Amer. 40, 203-211 (1950).

DISTRIBUTION LIST

Chief of Naval Research 2
Navy Department - CODE 427
Washington 25, D. C.

Director, Naval Research Lab.
Washington 25, D. C.
Attn: CODE 5240 1
CODE 7130 1
CODE 2000 6
CODE 5430 1

Commanding Officer 1
ONR Branch Office
1000 Geary Street
San Francisco, California

Scientific Liaison Officer 25
ONR, London
c/o Navy 100, Box 39, FPO
New York, New York

Commanding Officer 1
ONR Branch Office
1030 E. Green Street
Pasadena, California

Commanding Officer 1
ONR Branch Office
The John Crerar Library Bldg.
86 E. Randolph Street
Chicago 1, Illinois

Commanding Officer 1
ONR Branch Office
346 Broadway
New York 13, New York

Officer-in-Charge 3
Office of Naval Research
Navy 100, FPO
New York, New York

Chief, Bureau Aeronautics EL4 1
Navy Department EL43 1
Washington 25, D. C. EL45 1

Chief, Bureau of Ordnance
Navy Department Re 4 1
Washington 25, D. C. Re 9 1

Chief of Naval Operations Op20X 1
Navy Department Op421 1
Washington 25, D. C. Op 55 1

Director, Naval Ordnance Lab. 1
White Oak, Maryland

Director, Naval Electronics Lab 1
San Diego 52, California

Dept. of Electronics-Physics 1
U.S. Naval Post Grad. School
Monterey, California

Commander CODE 366 1
Naval Air Missile Test Center
Point Mugu, California

U.S. Naval Proving Ground 1
Attn: W. H. Benson
Dahlgren, Virginia

Commander 1
U.S.Naval Air Development Center
Johnsville, Pennsylvania

Thermionics Branch 5
Signal Corps Eng. Labs.
Evans Signal Lab, Bldg.42
Belmar, New Jersey

Commander 10
Armed Services Tech. Inform.
ATTN: TIPDR
Arlington Hall Station
Arlington 12, Virginia

Ballistics Research Labs 2
Aberdeen Proving Ground
Maryland
Attn: D.W.H. Delsasso

Chief, Ordnance Develop. Div. 2
Natl.Bureau of Standards
Connecticut Av, Van Ness St.NW
Washington 25, D. C.

Naval Research Laboratory 6
Washington 25, D. C.

Committee on Electronics 1
Research and Development Board
Department of Defense
Washington 25, D. C.

Director, Natl.Bureau of Stds. 1
Washington 25, D. C.
Attn: Div.14.0 CRPL, Librarian

Commanding Officer 1
Engineering Res. and Dev. Lab
Fort Belvoir, Virginia

Commanding Officer 1
Frankford Arsenal
Bridesburg, Philadelphia, Pa.

Air Research and Dev. Command 1
ATTN: RDSBTL(Hq.Tech.Library)
Andrews Air Force Base
Washington 25, D. C.

Commanding General WCLC 1
Wright Air Devel.Center WCLRC 1
Wright-Patterson AF Base, Ohio

Commanding General, CRRE 1
A.F. Cambridge Research Center
230 Albany Street
Cambridge 39, Massachusetts

Commanding General RCRW 1
Rome Air Development Center
Griffiss Air Force Base
Rome, New York

Chief, West Coast Office 1
Signal Corps Eng. Labs
75 So. Grand Avenue
Pasadena 2, California

Signal Corps Resident Engineer 1
Electronic Defense Laboratory
P.O. Box 205
Mountain View, California

Chief, Bureau of Ships 816 1
Department of the Navy 320 1
Washington, D. C. 340 1

Material Lab. Library 912B 1
New York Naval Shipyard
Brooklyn 1, New York

Office of Technical Services 1
Department of Commerce
Washington 25, D. C.

Director CR4582 1
Air University Library
Maxwell A.F. Base, Alabama

Chief, Western Division 1
Air Research and Devel.Command
Office of Scientific Research
P.O.Box 2035, Pasadena, Calif.

Technical Library 1
Research and Development Board
Pentagon Building
Washington 25, D. C.

Advisory Group on Electron Tubes 1
346 Broadway (8th Floor)
New York 13, New York

Dr. G. E. Barlow 1
Australian Joint Service Staff
Box 4837
Washington 6, D. C.

Microwave Library 1
W. W. Hansen Labs. of Physics
Stanford University
Stanford, California

Engineering Library 1
Stanford University
Stanford, California

Electronics Lab. Library 1
Stanford University
Stanford, California

Technical Library 1
General Electric Microwave Lab.
601 California Avenue
Palo Alto, California

General Electric Company 1
Electronic Components Div.
Power Tube Department
Microwave Lab at Stanford
Palo Alto, California

Dr. E. D. McArthur 1
Electron Tube Laboratory
General Electric Company
Schenectady, New York

University of Michigan 1
Electron Tube Laboratory
Ann Arbor, Michigan
Attn: J. Rowe

Johns Hopkins University 1
Radiation Laboratory
1315 St. Paul Street
Baltimore 2, Maryland
Attn: M.Poole, Librarian

Research Lab. of Electronics 1
Massachusetts Inst. of Tech.
Cambridge 39, Massachusetts

Sloane Physics Laboratory 1
Yale University
New Haven, Connecticut
Attn: R. Beringer

Mr. H. J. Reich 1
Department of Electrical Eng.
Yale University
New Haven, Connecticut

Laboratory for Insulation Res. 1
Massachusetts Inst. of Tech.
Cambridge 39, Massachusetts
Attn: A. von Hippel

Lincoln Laboratory 1
Massachusetts Inst. of Tech.
Cambridge 39, Massachusetts

Dr. J. M. Lafferty, Manager 1
Physical Studies
General Electric Company
P.O. Box 1088
Schenectady, New York

General Electric Company 1
One River Road
Schenectady 5, New York
Attn: Miss W. Crain, Librarian

Technical Report Collection 1
303A Pierce Hall
Harvard University
Cambridge 38, Massachusetts

Electron Tube Section 1
Electrical Engineering Dept.
University of Illinois
Champaign, Illinois

Chairman, Div.of Elec. Eng. 1
University of California
Berkeley 4, California

Radiation Laboratory 1
Tech. Information Division
University of California
Berkeley 4, California

Dr. A. W. Trivelpiece 1
Department of Elec. Eng.
University of California
Berkeley 4, California

Periodicals Librarian 1
General Library
California Inst. of Technology
Pasadena, California

Dr. Z. Kaprielian 1
Electrical Engineering Dept.
University of Southern Calif.
Los Angeles 7, California

Supervisor of Research Lab. 1
Electrical Engineering Bldg.
Purdue University
Lafayette, Indiana

Georgia Institute of Techn. 1
Atlanta, Georgia
ATTN: Librarian

W. E. Lear 1
University of Florida
Department of Electrical Eng.
Gainesville, Florida

Director Electronics Defense 1
Engineering Research Inst.
University of Michigan
Ann Arbor, Michigan

Cornell Aeronautical Lab 1
Cornell Research Foundation
Buffalo 21, New York

Director, Microwave Res.Inst. 1
Polytechnic Inst.of Brooklyn
55 Johnson Street
Brooklyn 1, New York

University of Washington
Department of Elec. Eng.
Seattle, Washington
ATTN: E. A. Harrison 1
A. V. Eastman 1

University of Colorado 1
Department of Elec. Eng.
Boulder, Colorado

University of Colorado 1
Engineering Experiment Sta.
Boulder, Colorado
ATTN: W. G. Worcester

Electrical Engineering Dept. 1
Princeton University
Princeton, New Jersey

Professor W. P. Dyke 1
Linfield College
McMinnville, Oregon

Research Lab.of Electronics 1
Chalmers Institute of Tech.
Gothenburg, Sweden
ATTN: Librarian

Columbia Radiation Lab. 1
538 W. 120th Street
New York 27, New York

Mr. John S. McCullough 1
Eitel-McCullough, Inc.
San Bruno, California

Cascade Research 1
5245 San Fernando Road
Los Angeles 39, California

Fred D. Wilimek 1
Varian Associates
611 Hansen Way
Palo Alto, California

John Dyer 1
Airborne Instrument Lab
Mineola, New York

Bell Telephone Laboratories 1
Murray Hill, New Jersey
ATTN: J. R. Pierce

Hughes Aircraft Company 1
Culver City, California
ATTN: Mr. Milek, Librarian

Hughes Aircraft Company 1
Microwave Laboratory
Culver City, California
ATTN: Dr. A. D. Berk

Bell Telephone Laboratories 1
Technical Information Library
463 W. Street
New York 14, New York

RCA Laboratories 1
Princeton, New Jersey
ATTN: Dr. W. M. Webster

Federal Telecommunic. Labs 1
500 Washington Avenue
Nutley, New Jersey
ATTN: W. Derrick
K. Wing 1

Countermeasures Laboratory 1
Gilfillan Brothers, Inc.
1815 Venice Boulevard
Los Angeles, California

The Rand Corporation 1
1700 Main Street
Santa Monica, California
ATTN: Librarian

Motorola Riverside Res. Lab. 1
8330 Indiana Avenue
Riverside, California
ATTN: Mr. John Byrne

Ramo-Wooldridge Corporation 1
Control Systems Division
P.O. Box 900B
Hawthorne, California
ATTN: Librarian

Microwave Physics Laboratory 1
Sylvania Electric Products
P. O. Box 1296
Mountain View, California

Dr. J. E. Shepherd 1
Sperry Gyroscope Company
Great Neck, New York

W. L. Maxson Corporation 1
460 West 34th Street
New York 1, New York
ATTN: M. Simpson

Bertram G. Ryland, Manager 1
Spencer Laboratory
Raytheon Manufacturing Co.
Burlington, Massachusetts

Westinghouse Electric Corp. 1
Electronic Tube Division
Elmira, New York
ATTN: Mr. S.S.King, Librarian

Mr. Gilbert Kelton 1
Security Officer
Philips Laboratories
Irvington-on-Hudson, New York

R. E. McGuire, Librarian 1
Boeing Airplane Company
P.O. Box 3707
Seattle 24, Washington

Dr. Donald W. Kerst 1
General Atomic
P. O. Box 608
San Diego, California

Image Instruments, Inc. 1
2300 Washington Street
Newton Lower Falls 62, Mass.

Sylvania Electric Prod. Inc. 1
Waltham, Massachusetts
ATTN: Charles A. Thornhill

Research Division Library 1
Raytheon Company
28 Seyon Street
Waltham 54, Massachusetts

ITT Laboratories 1
15151 Bledsoe Street
San Fernando, California

Technical Research Group Inc. 1
2 Aerial Way
Syosset, New York

American Systems Incorporated 1
3412 Century Boulevard
Inglewood, California
ATTN: M. D. Adcock

Microwave Physics Laboratory 1
Sylvania Electric Products
P.O. Box 1296
Mountain View, California

U. S. Atomic Energy Commission 1
Tech. Information Service Ext.
P.O. Box 62
Oak Ridge, Tennessee

Applied Research, RCA 1
Camden 2, New Jersey
ATTN: R. E. Skinner
Bldg.10-8, Sect.421

Bomac Laboratories, Inc. 1
Salem Road
Beverly, Massachusetts
ATTN: Arthur McCoubrey

Aerospace Corporation 1
Post Office Box 95085
Los Angeles 45, California
Attn: F. L. Vernon, Jr.